Time-Resolved Fluorescence and pH Sensing

Studies of Electropolymerised 5-Substituted Indoles

Alice E. Williams

Degree of Doctor of Philosophy

The University of Edinburgh

2005

Abstract

The electrochemical oxidation of 5-substituted indoles causes the formation of electroactive films constituting linked cyclic trimer units. The degree of linkage of these films can be controlled by changing the polymerisation conditions. The monomer, trimer and linked trimer, *i.e.* polymer, are all highly luminescent in solution. This thesis involves the study of electropolymerised samples of 5-cyanoindole and 5-bromoindole using Steady State and Time-Resolved Fluorescence spectroscopy, and potentiometric pH response experiments were carried out on poly-5-cyanoindole.

The potential of rotating disc electrodes modified with thick (1.37 μm) and thin (0.49 μm) films of 5-cyanoindole was found to vary linearly with electrolyte pH with a near-Nernstian slope, which is indicative of a promising pH sensing material. The response was independent of the direction of pH change and sustainable over a time period of at least a week. The rapidity of the responses of these films was studied and a theoretical analysis of the films' responses was developed. This was found to agree with the data collected for the thin film, and the thick film at low rotation speed. However, the assumptions of fast coat protonation kinetics made when carrying out this analysis did not hold true for the thick film. It was found that the pH response of the thin film was rapid, and therefore that the thin film showed promise as a good fast response pH sensor.

Steady State (SS) fluorescence emission spectra of electropolymerised 5-cyanoindole (5CnI) in ethanol at room temperature, excited at short wavelength, are dominated by emission from the trimer chromophore. Time Resolved Fluorescence measurements revealed that at short wavelengths the free trimer chromophore, lifetime 5.8 ns, was the only emitting species. At longer wavelengths further, shorter lifetimes were observed, corresponding to longer-than-trimer-conjugation length species with efficient non-radiative decay pathways.

In contrast to 5CnI, solutions of electropolymerised 5-bromoindole (5BrI) were found to show significant intensity of long wavelength emission due to polymeric species. Moreover, a marked difference was seen between the fluorescence spectra of higher and lower polymer samples.

A linkage-and-extraction method was used to obtain for the first time a pure sample of the 5BrI trimer. This enabled the determination of the fluorescence lifetime of the 5BrI free trimer, which was found to be 5.5 ns.

Time Resolved Fluorescence measurements on solutions of electropolymerised 5BrI prepared on a bare Pt electrode revealed the existence of a trimer species that was spectroscopically identical to the free trimer but displayed a much shorter lifetime, corresponding to a linked trimer unit with an efficient intra-chain energy transfer mechanism.

Time-Resolved Fluorescence measurements on solutions of poly-5BrI that had been prepared on an electrode that had been modified with a non-fluorescent, poly-5-nitroindole (5NI) template layer revealed the existence of a number of emitting species. These included the free trimer, which had a lifetime of 5.7 ns, quenched intrachain trimer species with lifetimes 200-300 ps, and several polymer species of different conjugation lengths. Intrachain electronic energy transfer was found to be an important non-radiative decay mechanism.

Declaration

I hereby declare that the work presented in this thesis is my own unless otherwise stated by reference.

Acknowledgements

Firstly, I would like to thank my supervisors Dr Andy Mount and Dr Anita Jones for their constant help and encouragement throughout the past four years. Without their support this work would never have been completed.

I would like to thank the EPSRC for funding.

Many other people helped me with the practical work, notably Steve Magennis and Jochen Arlt, who put in a great deal of time in helping me to perform experiments in COSMIC, and in helping to fix problems that arose, and Neil Speirs, who showed me how to perform steady state fluorescence experiments.

A special mention must go to Dr John Craven in the School of Geosciences, who helped me a great deal in polishing a particularly scratched reference electrode.

Many members of the Mount / Jones groups have given me a great deal of help, in particular Trish and Dave (old), who were always willing to answer my questions and help with computer problems. Being in this group has been an enjoyable experience, and thanks go to those who made it so, in and out of the group, especially Alex, Chris, Dave (young), Derek, Gaynor, Ian, Ken, Liz, Marica, Mike, Rob, Robin and Tom, who all share my enthusiasm for tea breaks, crosswords and the pub quiz. Emmelyn and Madelaine also shared this enthusiasm and gave me enormous support when things weren't at their best.

Derek, Kenny, Raymond and Tim in the stores were very helpful when it came to ordering items for research, and were wonderful colleagues during my employment there.

Thanks to the guys in KBH, especially Alan, Chris, Emma and Stuart, who made tea time and Friday beer a fun and friendly experience.

Many people outside work lent their support, and have helped to make things easier along the way. Thanks go to Kenny for hours of computer gaming fun and 'profound' chat; Ben, Eleanor, Nadine, and Rachel + Dave and for their constant support; and Dan + Sarah for letting me take refuge at their home in Cumbria when things were getting stressful. Jennifer and Benji, Penny and Tania, Lyndsey and Shirren, and Mary and Scout deserve great thanks for giving me the chance to horse-ride more regularly than I would ever have thought possible.

Finally, I would like to thank Mum, Dad, and the rest of the family for their unending encouragement and support over the past few years.

To Mum and Dad

Contents

Chapter 1

Introduction

1.1. Overview

1.1.1. Polymers

Research into polymeric materials is a field of enormous interest. Polymers have a vast number of actual and potential uses and are used in almost all areas of daily life as well as in technological applications. Their production is a major world-wide industry. Polymers consist of monomer units of one or more type that are linked together to form a chain. They can be found in nature, examples including proteins, cellulose, silk and natural rubber, or they can be synthesised very easily. They also have many desirable properties such as flexibility, strength, plasticity, elasticity and light weight[1]. Because of such characteristics they are attractive materials for a wide range of applications.

The development of synthetic polymers began in the mid to late nineteenth century. In the 1930s a range of polymers, including synthetic rubber, nylon and Teflon™, were being developed, and by the 1960s high-performance polymers, which could compete with the more traditional materials used in the automotive and aerospace industries, were being produced. By the late 1970s organic polymers that were able to conduct electricity had been discovered[1], leading the way to new, exciting materials for the electronics industry.

1.1.2. Conducting Polymers (CPs)

Organic polymers, both natural and synthetic, traditionally, have very poor electrical conductivity, and many synthetic polymers are used as electrical insulators. However, in 1977 it was discovered that acetylene could be polymerised to form an electronically conducting organic polymer (CP)[1,2] (figure 1.1)

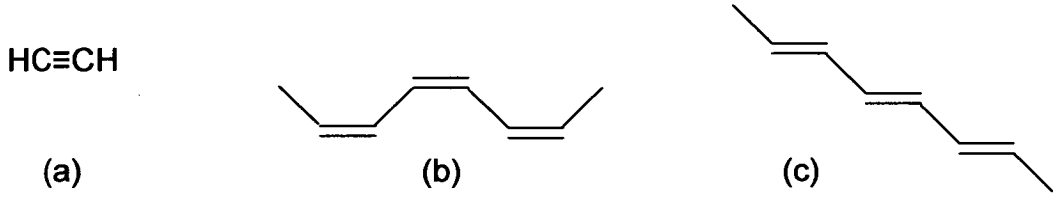

Figure 1.1: *(a) Acetylene monomer; (b)cis- and (c) trans- polyacetylene*

Polyacetylene exists in two forms, *cis-* and *trans-*[2] The *cis* form, which is less stable and has a lower conductivity (1.7×10^{-9} Scm^{-1} *cf.* 4.4×10^{-5} Scm^{-1}), can be converted to the *trans* form when heated to 200 °C. Although the conductivity of polyacetylene was relatively low, being in the semiconducting range[3], it was found to increase upon the addition of electron donating and electron withdrawing dopants[1,2,4]. For example doping with AsF_5 increases the conductivity to 400 Scm^{-1}, and doping with iodine increases its conductivity to 1,000 Scm^{-1}, both of which are in the metallic range[1,2]. CPs are of great commercial interest because of their mechanical properties. They have the desirable properties of flexibility, strength, plasticity, elasticity and light weight, and they are easy and relatively cheap to synthesise. Their many potential uses include electrodes and electrolytes in batteries, variable transmission windows, electrochromic devices, photovoltaic cells, light emitting diodes, semiconductors, polymer-based lasers, field effect transistors and sensors.

In spite of its many benefits, there are drawbacks to using polyacetylene in such devices. One major disadvantage is its chemical instability. It is sensitive to air and moisture, and upon oxidation polyacetylene loses its conductivity significantly and irreversibly. Because of this drawback much work has been carried out investigating many other organic polymers, which have much greater environmental stability than polyacetylene. Systems that have been shown to be conducting and have been studied extensively include polyheterocycles, polyphenylenes and polyanilines.

1.2. Conduction Mechanisms

Electroactive polymer films conduct both ions and electrons[5]. Polymers that conduct electrons share a common feature that makes them able to conduct: they all have an extended delocalised π-conjugated structure of double and single bonds along the polymer chain backbone through which electrons may be transported. However, the mechanism of conduction in CPs is under some debate. There are three general categories under which conducting polymers fall[5], these being redox polymers, electron conducting polymers and ion-exchange polymers. Ion-exchange polymers exchange charge-compensating counterions for electroactive ones. Redox polymers have localised electronic states (redox sites), and electronic conduction in this case is caused by electron hopping, the polymer going from the oxidised to the reduced state. Alternatively, there are the electronic conductors known as 'organic metals'. They can be considered to have delocalised metal-like band structures and their electronic conductivity is best described, like that of metals, in terms of band theory[6].

1.2.1. Band Theory

When atoms combine to form molecules, molecular orbitals are formed, each of which has a separate energy. When the number of atoms involved becomes very large, as for the case in solids, a band that appears to be a continuum forms, although there are still a finite number of separate orbitals of discrete energy[6,7]. In simple metals, represented in figure 1.2 (a), the energy levels overlap to form one continuous band, which will be only partially occupied by electrons, and there is no band gap between the occupied and vacant levels. Consequently only a small amount of energy is required to promote an electron from a filled energy level to a higher energy level. This promoted electron is delocalised and therefore facile electronic conduction can occur.

In materials that are classified as insulators or semiconductors there is a band gap between the filled valence band (VB) and vacant conduction band (CB). This is represented in figure 1.2 (b). In this case a certain energy will be required to promote an electron from the VB to the CB to allow conduction to occur. The size of this band gap defines the amount of energy required to promote the electron and, generally, conductivity increases as the band gap decreases. Typically, materials with a band gap of 2-3 eV are considered to be insulators. The electronic conductivities of most conducting polymers are in the semiconducting range, and can be increased to the metallic range upon doping. The semiconducting properties of CPs arise from the delocalised π-electron system along the polymer backbone; by judicious design of the chemical structure of the polymer backbone, the band gap may be lowered to as little as 0.5 to 1.0 eV[8]. The π (bonding) orbitals form a

delocalised valence band and the π* (antibonding) orbitals form a delocalised conduction band[9,10,11]. One electron is supplied from a p-orbital on each C, which completely fills the VB. Doping causes a change in the electronic population in the band. Dopants can be either electron-donating or electron-withdrawing species. If electron-donating dopants are used then a narrow band is formed just below the vacant conduction band of the semiconductor (figure 1.2 (c)). The electrons in this newly formed band can be promoted to the conduction band with relative ease, where they will be mobile and conduction will occur, giving rise to n-type semiconductivity. If electron withdrawing dopants are used a narrow electron accepting band is formed just above the valence band of the semiconductor (figure 1.2 (d)), which can accept electrons from the valence band, leaving behind positive 'holes', which are also mobile. This type of doped semiconductor is known as a p-type semiconductor. For redox active polymers, oxidation of the polymer is considered to act like p-doping in this model; reduction is the reversal of p-doping. This leads to the formation of polarons and bipolarons, charged species on the backbone. In essence, this can be considered as equivalent to redox-hopping.

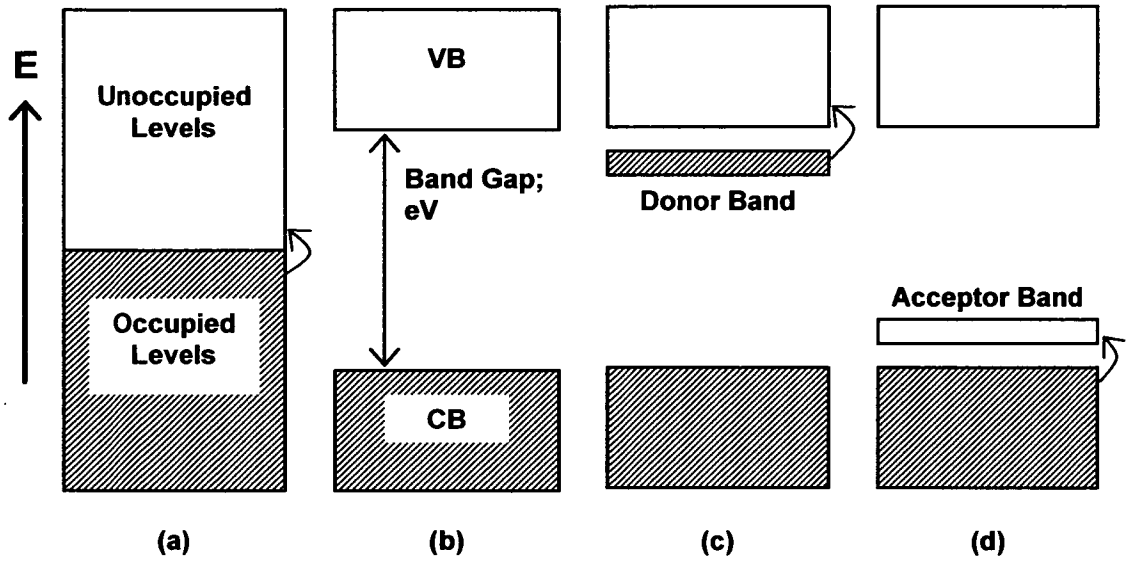

Figure 1.2 *Diagrammatic representation of the bands in (a) a metallic conductor, (b) an undoped semiconductor, (c) an n - doped semiconductor, (d) a p – doped semiconductor. Energy, E, in eV.*

1.3. Chemically Modified Electrodes (CMEs)

The inert electrode, for example Pt or C, is a powerful tool in analytical and synthetic applications[5]. It can be used as a source, or a sink, of electrons and the rate of electrons crossing the electrode / solution interface can be determined by the measurement of current and controlled by the voltage applied. This is described fully in chapter 2. However, the ability to control reactivity through changing the nature of the electrode surface would be very desirable. Indeed, the development of CMEs was instigated by this desire. Modification of the electrode surface can be used to cause the electrode to adopt the properties of the attached redox reagents rather than the underlying electrode and these properties can be tailored to control, for example, rates and selectivities of electrochemical reactions. The problems

caused by contamination of the electrode surface may also be overcome by surface modification.

Modifying a Pt, C or other electrode can be carried out in several different ways, and the chemical attached to the electrode surface is usually designed to be electroactive to enhance electron transfer, although this is not always the case. Methods of deposition of the surface species include drop- or spin-coating, which involves deposition and evaporation of solvent from a solution of preformed polymer, electrochemical precipitation of a preformed polymer or electrochemical polymerisation of an electroactive monomer. CMEs have uses in many different areas. They can be employed in the synthesis of electroactive polymers, in the studies of electron transfer kinetics, in photo-electrochemistry and in electrochemical sensing[12] of, for example, H^+ or metal ion concentration.

1.3.1. Synthesis of Conducting Polymer-Modified Electrodes

CMEs can be prepared by chemical or electrochemical oxidation, both of which have advantages and disadvantages. Chemically oxidised polymers are prepared and then spin-coated on to the electrode substrate. They are usually prepared using strong oxidising agents, or by exposing the monomer to catalysts[13]. They can be prepared on a large bulk ; however this technique is associated with a loss of precise control over synthesis.

Electrochemical oxidation of polymers can be accomplished using potential step techniques (chapter 2), whereby a solution of the electroactive monomer species in suitable electrolyte is subjected to a potential at which it becomes oxidised while rotating the electrode at a certain rotation speed, W. Experimental details of this technique are given in chapter 2. Electrochemical synthesis allows precise control of reaction conditions and *in-situ* analysis of the polymerisation process is achieved by monitoring the current produced with time. Once formed the polymer may be analysed or linked further by cyclic voltammetry (CV), typically driving the redox active polymer between the oxidised, conducting form and the reduced, insulating state.

1.3.1.1. Electrochemical Oxidation

The initial one-electron transfer step in the electrochemical oxidation reactions of monomers typically leads to the formation of a reactive radical cation[14]. From here a number of different pathways can occur. These are proton abstraction, nucleophilic substitution and radical cation recombination. The dominant pathway is dependent upon the relative rates of reaction, which depend upon the nature and stability of the radical cation, solvent interactions and the concentration of radicals and nucleophiles. Radical combination or coupling is the pathway that leads to formation of polymers, which are usually designed to be electroactive. This is typically favoured by high concentrations of radical cations, *i.e.* high potentials and high concentrations of monomers[15].

1.3.1.2. Electrochemical Properties

Conjugated polymers exhibit chemically reversible redox electrochemistry. They can generally be driven from the conducting to insulating state and back. In the oxidised (p-doped) state the films are conducting and when reduced they are semi-conducting or insulating. Generally it is hard to n-dope conducting polymers. Large amounts of charge are passed upon redox cycling of the polymers, and this electro-reversibility recommends them for use in electrochemical applications such as batteries or supercapacitors[16].

Upon oxidation the films swell as counteranions and solvent from the electrolyte become incorporated into the film. As the polymer structure is more open the ions can move through the film with relative ease. Upon reduction the ions are expelled back into the electrolyte. This often leads to differences in the kinetics of the oxidation and reduction reactions of the film, electrochemical reduction of the structurally more open oxidised film being more facile than the oxidation of the reduced film, which often produces asymmetry in the cyclic voltammetric response.

1.4. Polyheterocycles

Polymers consisting of heterocyclic monomer units offer advantages such as environmental stability and high conductivity. Much work has been carried out into the methods and mechanisms of electrochemical synthesis, properties and applications of many polyheterocyclic species, notably five-membered heterocycles such as pyrrole and thiophene (figure 1.3)[15,17,18,19].

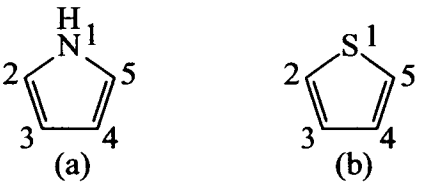

Figure 1.3: *Monomer units of (a) pyrrole and (b) thiophene*

Polypyrrole was first synthesised in the late 1970s[20,21,22]. Upon electrooxidation of pyrrole a radical cation is formed at the electrode surface. The concentration of this species at the electrode is high as the electron transfer reaction is much faster than the diffusion of fresh monomer from the bulk, and species close to the electrode surface will only exist as the radical cation. These cationic species can undergo a number of reactions, one of which is polymerisation. The cations, M, link to form carbon-carbon bonds[18], and a chain of monomer units linked via their 2 and 5 positions[17] is formed.

$$M^{\bullet+} + M^{\bullet+} \rightarrow M_2 + 2H^+ \xrightarrow{-e^-} M_2^{\bullet+} + M^{\bullet+} \rightarrow M_3 + 2H^+ \xrightarrow{-e^-} \rightarrow \rightarrow M_n + 2H^+$$

The polymer has a delocalised π-system along the polymer backbone, which allows the conduction of charge. This is shown in figure 1.4.

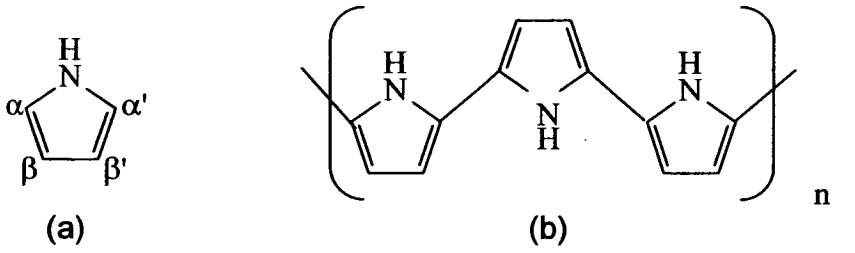

Figure 1.4: *(a) Pyrrole monomer and (b) Linked monomer units of Polypyrrole (Ppy). The coupling is thought to occur via the 2 and 5 positions*

The electropolymerisation and conductivity of these heterocycles were found to change when the heterocycle ring contained substituents[17,23,24]. When a substituent was present in the 2-position films were not seen to form, supporting the idea that the monomers couple in the 2-position, whereas in the 3-position, the formation of films changed depending on the electronic nature of the particular substituent.

Substituents affect the polymerisation by steric and/or electronic effects. The properties of the resulting polymer film may also be affected by the substituents[17]. For example, bulky substituents may cause a disruption in the planarity of the polymer backbone, resulting in loss of conjugation. This leads to a lowering of conductivity in the film. Conductivity may also be enhanced by appropriate substituents. Differently substituted polythiophenes show electroactivity at different voltages[17]. There are many other aromatic and heterocyclic molecules which, upon polymerisation, also form conducting polymers. Examples include carbazole[15], fluorene[15,25], furan[26], and para-phenylenevinylene (PPV) and indoles, which are given more attention later in this chapter.

1.5. Polyindoles

Indole (fig 1.5) was first polymerised by Tourillon *et al.* in 1982[3], and there has since been much interest surrounding the mechanism of its polymerisation.

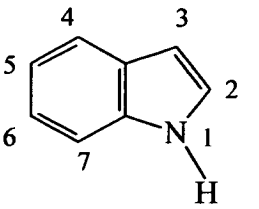

Figure 1.5: *Indole monomer unit*

Initially it was thought that indole would polymerise in a similar manner to pyrrole and thiophene, producing a linear polymer; however, the films showed behaviour that was inconsistent with other poly-heterocycles. Tourillon *et al* proposed that coupling of the monomer occurred *via* N-N linkage[3] as the initial films were non–conductive, and analysis by IR spectroscopy showed no N-H stretching band. This theory was backed up by the observation that when an N-substituted indole monomer, N-methylindole, was used a film was not formed. The proposed structure for the N-linkage is shown in figure 1.6. The second site of linkage, however, was not defined.

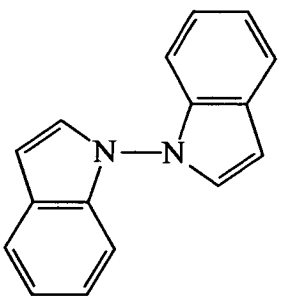

Figure 1.6: *Coupling of indole monomer via the ring nitrogens as proposed by Tourillon et al.*

Waltman *et al.* carried out work on the polymerisation of indole and, on the basis of high spin density, inferred that the linking of the monomer units was via the 2,3 positions[24] (figure 1.7) This hypothesis seemed to be backed up by the fact that a 1-, 2- or 3-substituted indole did not form a film.

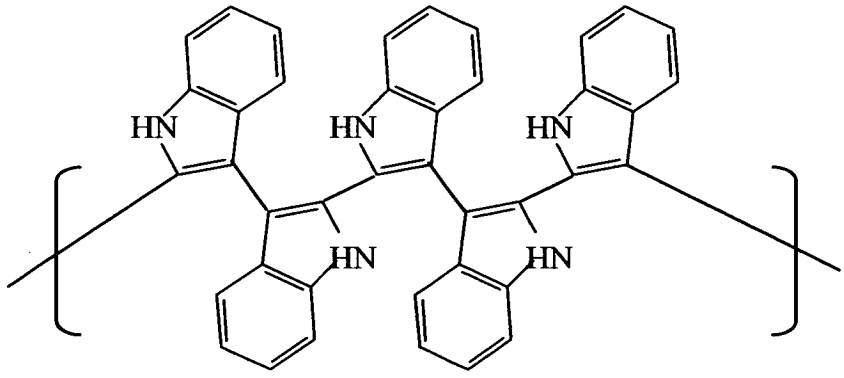

Figure 1.7: *The structure of polyindole proposed by Waltman et al*[21]

Other groups proposed different structures for different substituted polyindoles[27,28,29] and in 1994 Mount *et al.* proposed that indole-5-carboxylic acid and 5-cyanoindole monomer units actually form asymmetric trimers, which then go on to polymerise, linked via trimer N-atoms[30,31,32,33,34,35,36,37,38,39] (figure 1.8).

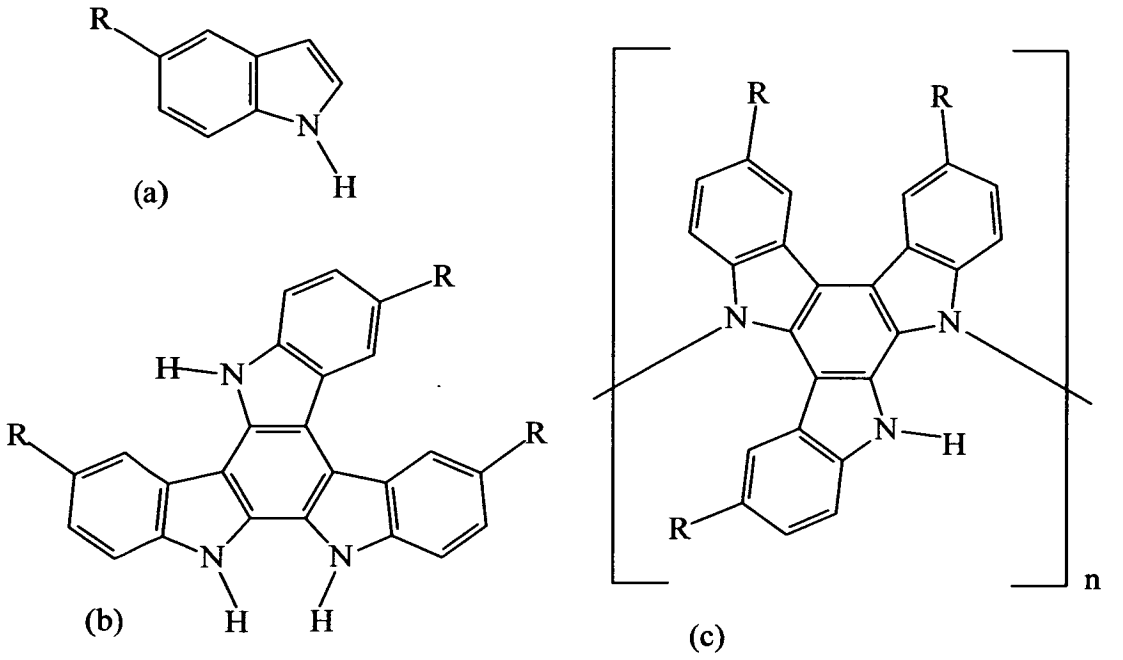

Figure 1.8: *(a) 5-substituted indole monomer where R = CN, COOH etc., (b) 5-substituted indole trimer as proposed by Mount et al., (c)possible site of linking of the indole trimer units*

They had shown that all the 5-substituted indole monomers presented in figure 1.9 form conducting polymer films. Work on indole-5-carboxylic acid and 5-cyanoindole showed that the electropolymerised films of these monomers comprised two different chemical species, which could be separated by differential solubility in dimethylformamide (DMF). These products were characterised by mass spectrometry, UV-visible spectrometry, fluorescence spectroscopy, IR spectroscopy and NMR spectroscopy[26], and it was shown that the DMF-soluble product was the free trimer and the DMSO soluble product was a polymer consisting of these linked trimer units. The trimers comprise three monomer units that are linked through their two and three positions (figure 1.8(b)). This corresponds with work carried out by previous groups, who proposed linkage through these positions[27,28,40,41,42,43,44,45]

The coupling chemistry of indole is very similar to that of pyrrole. The initial oxidation results in the formation of a radical cation, which then undergoes recombination to form a dimer. The dimer is then oxidised along with the monomer at the monomer oxidation potential. These cyclise upon oxidation to form an asymmetric cyclic trimer, which can then polymerise in its oxidised form, with linking occurring possibly via 2 of the N-atoms (figure 1.8 (c)). The equation for the electropolymerisation of the 5-substituted indoles studied has been shown to be[28,46]

$$3n\ \mathrm{In(aq)} \xrightarrow{-7ne,\ -6nH^{+}} n\mathrm{In_3}^{+}(s) \qquad \textbf{1.1}$$

$$n\mathrm{In_3}^{+}(s) \xrightarrow{-2ne,\ -2nH^{+}} -(\mathrm{In_3}^{+})_n-(s) \qquad \textbf{1.2}$$

Initially reaction (1.1) occurs close to the electrode in the diffusion layer and results in the precipitation of trimeric product on the electrode. This deposited electroactive layer then acts as a site for adsorption of monomer, oxidation and trimer formation, hence reaction (1.1) becomes a surface process. Therefore reaction (1.2) represents the linking of the trimer units that have been deposited on the electrode surface to form polymer[30]. Close to the electrode surface the film would be expected to be polymer-rich as these trimers have had the longest time to link as they are deposited first; at the film / solution interface the film would be expected to be trimer rich. As will be discussed in chapter 4 the monomer solution concentration and the rotation speed of the electrode are determining factors as to whether a trimer-rich or polymer-rich film is produced.

1.5.1. Substituted Indoles

Indoles with substituents attached have different oxidation potentials, and films with different electrochemical properties are formed. Polymer formation depends upon the stability of the radical cation formed, which depends on the electronic nature of the substituents, essentially the Hammett constant. Polymers were found to form if there was a substituent on the benzene ring of the monomer, even when bulky substituents were used, but not in the 2- and 3- positions of the heterocyclic ring (figure 1.5)[17], as in these cases cyclic trimer formation is blocked. Studies of 5-substituted indoles show that if electron–donating substituents are used the monomer radical cations tend to become stabilised leading to decreased radical coupling and decreased film formation, whereas electron–withdrawing substituents cause destabilisation leading to increased coupling. However a wide variety of substituted indoles form films, and judicious control of the radical cation concentration counteracts the differences in coupling rate constants, leading to appreciable coupling in all cases. As the Hammett substituent constant increases, so does the oxidation potential of the monomer (figure 1.9) and the redox potential of the resulting redox-active polymer. This allows control of the redox potential of the indole film.

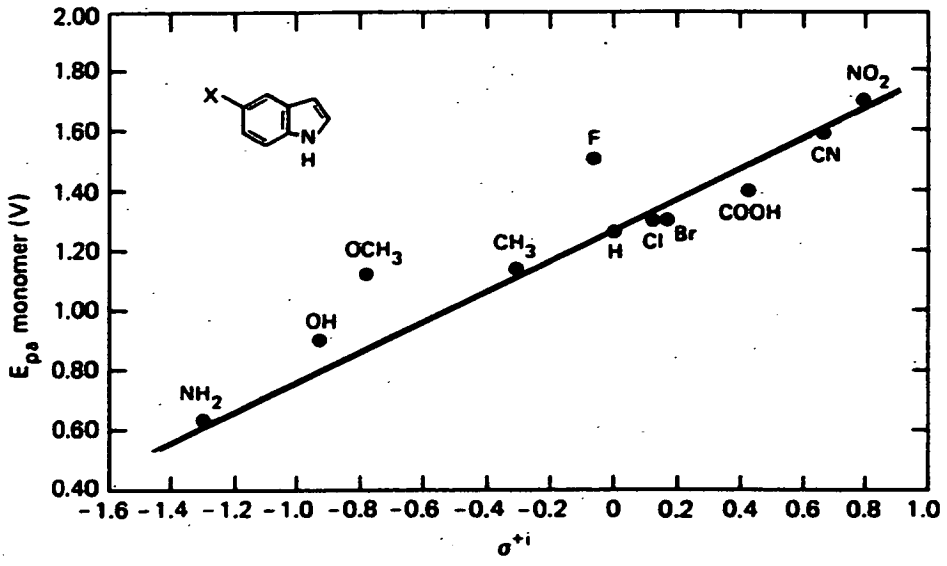

Figure 1.9: *Electrochemical peak oxidation (E_{pa}) of 5-substituted indole monomers versus their respective Hammett substituents (σ^{+i}).*

1.6. Photophysics of Conducting Polymers

The first organic conducting conjugated polymer to be synthesised, polyacetylene, showed only very weak photoluminescence. However there has been much development in the field of conjugated polymers that exhibit high photoluminescence quantum yields. One such system that has been studied in detail is poly-(p-phenylene vinylene) (PPV) and derivatives thereof. These systems were found to be electroluminescent; this means that they have enormous potential in the field of light emitting devices. PPV systems are organic conjugated polymer systems. They are conducting and have a high photoluminescence quantum yield[47]. Although these systems are largely produced by chemical rather than electrochemical methods, they provide a good model with which to compare the fluorescence behaviour of the poly-5-substituted indoles studied in this thesis.

1.6.1. Electroluminescence and Photoluminescence

Electroluminescence is the generation of light by radiative decay of an electron-hole excited state, which is formed after injection of charge carriers into the material of interest[8,9,10,48]. There are many applications for electroluminescent devices, principally in the areas of telecommunications and information displays. Early studies on organic semiconductors[26] showed that electroluminescence required injection of electrons and holes from opposite electrodes into the polymer chain, which would then recombine to form a localised electron-hole excited state (exciton), which then undergoes radiative decay. Effective luminescence requires a good balance of electron and hole currents, efficient capture of electrons and holes in the emissive layer and strong radiative transitions for singlet excitons. The mechanism for electroluminescence is given in section 1.7.1.

Conducting polymers would enable the manufacture of thin, flexible films that would be easy to produce over a large area, would cover a wide range of colours, and would be relatively inexpensive to manufacture, thus eliminating some of the problems associated with using inorganic materials. Luminescence from conjugated polymers was first observed in PPV[49,50,51,52] and since then much research has been carried out on different polymeric materials for application in LEDs.

Photoluminescence is the emission of light from a species that has undergone photoexcitation (chapter 2). Photoexcitation in a conjugated polymer causes an electron to be promoted from the highest occupied molecular orbital (HOMO) to the lowest unoccupied molecular orbital (LUMO). This generates a singlet excited state,

a singlet exciton. The polymer then gives up this excess energy by relaxation back to the ground state, a process that is accompanied by the emission of a photon. The light emitted is at a longer wavelength than the absorbed light; this is called the Stokes shift. The work carried out in this thesis is purely concerned with photoluminescence; specifically fluorescence. The theory behind fluorescence is described in chapter 2.

1.7. Fluorescence of Conducting Polymers

1.7.1. Conjugation Length and Fluorescence Emission Wavelength

The fluorescence of conducting polymers arises from the delocalised π-system along the conjugated carbon backbone (chapter 2). In an ideal CP the conjugation would be unbroken the entire length of the polymer strand; for a polymer of linked indole trimer units this can be represented as in figure 1.10.

-Tr-Tr-Tr-Tr-Tr-Tr-Tr-Tr-Tr-Tr-Tr-Tr-Tr-Tr-Tr-Tr-Tr-Tr-

Figure 1.10*Representation of ideal conjugated indole trimer units.*

In reality each polymer strand is coiled and the conjugated backbone is disrupted by chemical defects, and non-chemical defects such as kinks or twists[53]. Samples comprise many individual chains, each of which has many sections of different conjugation length, which are in different local environments. A 'real' polymer strand can be represented pictorially as in figure 1.11, consisting, in the case of the indole systems studied in this thesis, of chains of linked trimer units of different lengths of conjugation.

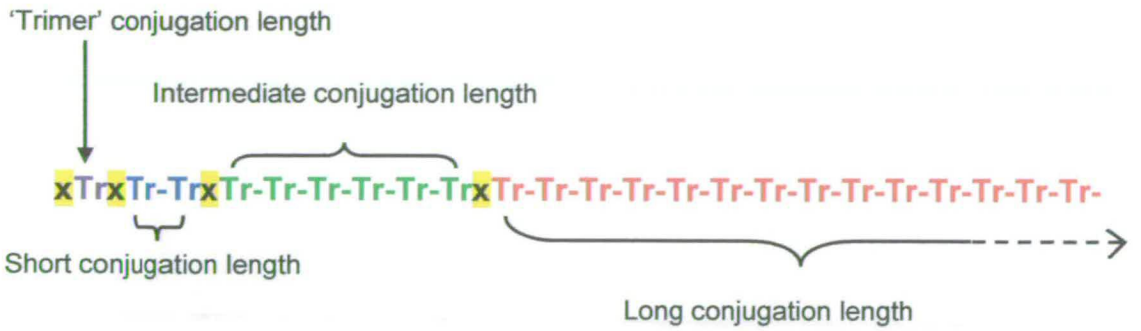

Figure1.11: *Representation of the different lengths of conjugation along the C backbone. x represents any defect along the conjugated C backbone.*

The defects along the C backbone break the conjugation, resulting in different conjugation length, quasi-independent fluorophores. Considering the simple 1D particle-in-a-box representation of electron delocalisation along the conjugated segments, the longer segments, having a low $\pi \rightarrow \pi^*$ energy gap, will have lower energy and will emit at longer wavelength than the shorter segments, which have a much higher energy gap.

With sufficient excitation energy, *i.e.* exciting at shorter wavelengths, excitons are generated on all the different length species within each polymer strand. (The excitation wavelengths used principally in this thesis are 360 nm and 450 nm.) These excitons are mobile and can migrate to longer, lower energy segments; therefore the species either emit or transfer energy to the lower energy neighbouring species, which may in turn emit or transfer energy in a similar mechanism. Exciting selectively at lower energy, excitons will only be generated on the longer conjugation length, lower energy sections, from which energy transfer to higher energy species cannot occur. Energy transfer pathways are represented schematically in figure 1.12.

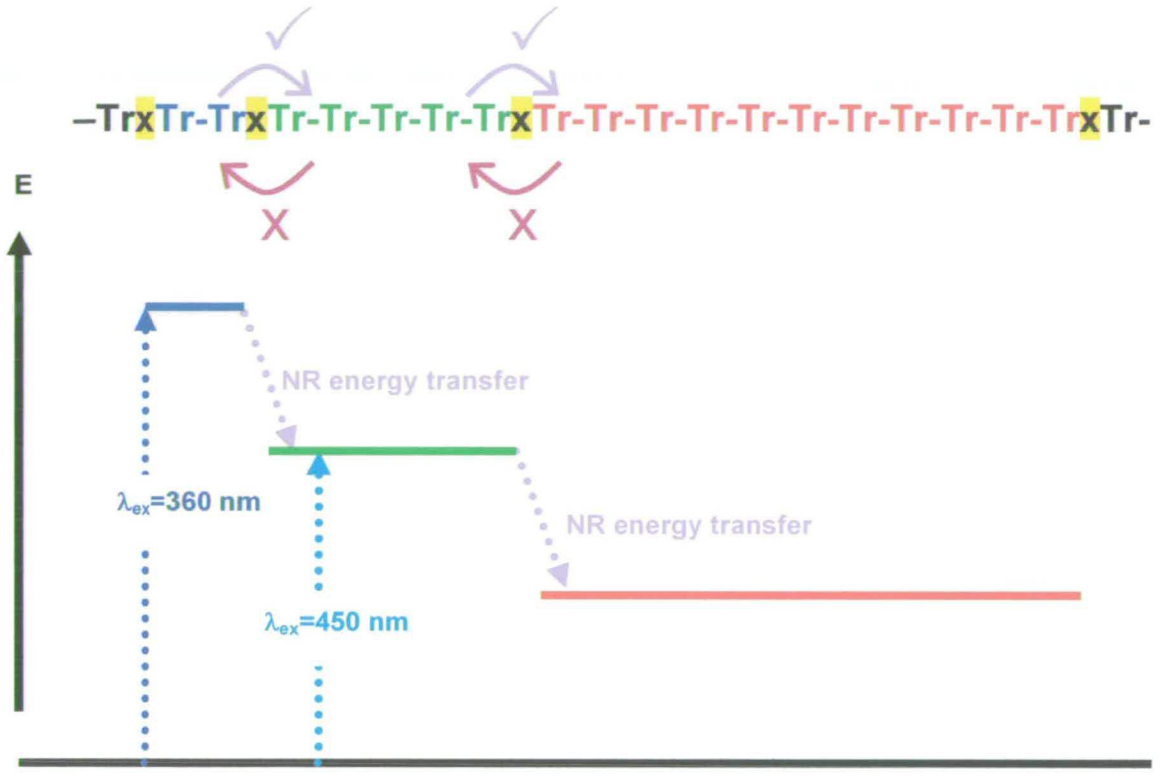

Figure 1.12: *Representation of the energy transfer mechanisms that are and are not possible. ✓=allowed; x=not allowed*

Within one sample there may be many chains of equal conjugation length, which are in different environments. For example, figure 1.13 illustrates a chain (green section) that is the shortest conjugation length, hence highest energy, species that can be excited at a specific excitation wavelength, in two possible situations.

-TrxTrxTrxTrxTrxTrxTrxTrxTr-Tr-Tr-Tr-Tr-TrxTrxTrxTrxTrxTrxTrxTrxTr-

(a)

-Tr-Tr-Tr-Tr-Tr-Tr-Tr-Tr-TrxTr-Tr-Tr-Tr-Tr-TrxTr-Tr-Tr-Tr-Tr-Tr-Tr-Tr-Tr-

(b)

Figure 1.13: *Representation of the same conjugation length species in 2 different environments. x represents any defect along the conjugated C backbone.*

Fig 1.13 (a) shows that the section of interest is surrounded by extended sections of non-conjugation. The green section would be unable to surrender its excess energy to these neighbouring segments, neither would it accept energy from a donor, hence would decay with a lifetime characteristic of this precise conjugation length. Fig 1.13(b), however, shows the same green length adjacent to two sections of lower energy, longer conjugation length (red), providing a non-radiative pathway to which the green section could surrender its excitation energy. This would manifest in a different, shorter lifetime from the situation represented in fig 1.13(a). The examples illustrated in figure 1.13 represent non-radiative, intramolecular energy transfer along the length of the polymer chain. Another possibility is illustrated in figure 1.14.

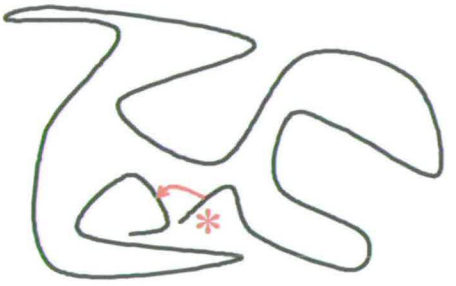

Figure 1.14: *A polymer strand undergoing pseudo inter-molecular transfer. * indicates excitation*

In solutions as dilute as these, the individual polymer chains would be rather diffuse and would be highly unlikely to come into contact with one another. However, the polymer chains may be long, coiled and 'tangled'. Figure 1.14 shows such a situation. The asterisk indicates the region of conjugation that is excited, with excess energy to give up. If this localised, owing to being adjacent to regions to which non-radiative transfer is not possible, and is in close proximity to another part of the

chain, pseudo intermolecular energy transfer may occur. This is in fact intramolecular energy transfer as the energy is being transferred within one polymer strand.

There has been much speculation over the nature of the excited state of photo-excited PPV. Samuel *et al* have conducted much research into the nature of photo-excitations in conjugated polymers[54,55,56], and the results indicate that there is generation of intra-chain excited states. Studies carried out on PPV showed that with an increase in conjugation length came an increase in emission wavelength and a decrease in fluorescence lifetime[57,58]. When excited at shorter wavelengths it was found that the decay was complicated and there was a broad distribution of fluorescence lifetimes, but at longer excitation wavelengths essentially a single lifetime was observed, or a narrow distribution of lifetimes. This was explained by the fact that the longer excitation wavelengths excited only the longer conjugation length species, which had little scope to surrender energy to lower energy species, whereas the shorter excitation wavelengths have many options for intrachain energy transfer. This is consistent with the explanation of the conjugation length and intrachain energy transfer mechanisms explained above.

1.7.2 Fluorescence of Poly-5-Substituted Indoles

The steady state fluorescence of 5-substituted indole monomers and electrochemically prepared polymers has been studied[59,60]. Of particular interest are poly-5-cyanoindole and poly-5-bromoindole, as they are the systems studied in this thesis. The steady-state fluorescence spectra of these systems show distinct regions

that can be attributed to the trimer and polymer species[59,60]. In ethanol the trimer is known to emit showing a characteristic 'double peak' due to vibronic structure with maxima at approximately 415 nm and 435 nm for both poly-5-bromoindole and 5-cyanoindole. 5-Bromoindole also shows broad, intense emission at wavelengths greater than 500 nm. The trimer and polymer steady state emission are both very different from that of the monomer, which emits at higher energy. Time-resolved fluorescence measurements have been carried out on both systems. Further details are given in chapters 6, 7 and 8.

1.8. Applications of Conducting Polymers

Organic based conducting polymers have a wide range of applications. These include electroluminescent devices and sensors. A brief overview of each is given in sections 1.8.1 and 1.8.2 respectively.

1.8.1. Electroluminescent Devices

Polymeric LEDs have attractive device characteristics, such as efficient light generation and low cost of manufacturing. There has also been a great deal of progress made in understanding the underlying science. Polymer LEDs consist of the conducting polymer sandwiched between two electrodes, one of which must be at least semi-transparent to allow the emission of light.

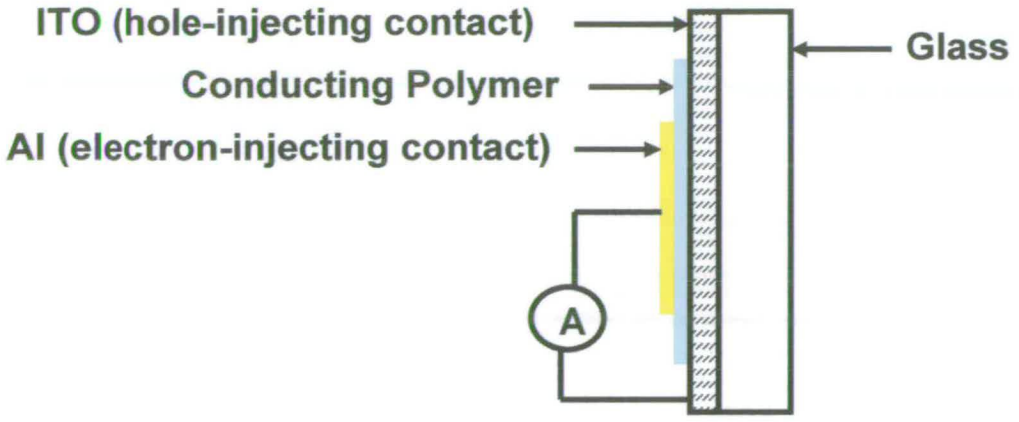

Figure 1.15: *Diagram of polymer LED with ITO as the hole-injecting contact and Al as the electron-injecting contact*[56].

The negative electrode is the electron-injecting contact, and for this a material with a low work function is used, such as Al, Mg/Ag alloy or amorphous silicon alloys. The positive, hole-injecting contact is constructed from a material with a high work function, for example Al with an oxidised layer, gold, or indium tin oxide (ITO)[26,61]. A potential is applied across the device and oppositely charged carriers are injected into the polymer layer. The electrons are injected into the conduction band of the polymer, the holes into the valance band, and are then swept through the device by the high electric field. Some of the electrons and holes will combine to form excitons, which then undergo radiative decay, which is seen as the emission of light. In the case of redox-active CPs the hole-injection is oxidation

$$M \rightarrow M^{+} + e^{-}$$

and electron injection is reduction

$$X + e^{-} \rightarrow X^{-}$$

The recombination reaction that leads to light emission is

$$M^{+} + X^{-} \rightarrow M + X + \text{energy } (h\nu).$$

Tuning the oxidation and reduction potentials of the emissive layer allows the amount of energy available as light to be controlled, enabling emission of light of a wide range of wavelengths, and hence colours.

1.8.2. Sensors

There has been much interest surrounding the use of CPs in sensing devices, in particular as pH sensors. Traditional glass pH electrodes are not accurate at extreme pH values, and the electrode requires special care and treatment before and after use. Also they are sensitive to extreme environment conditions, such as high pressure, and cannot be micro-fabricated. Many conducting polymers exhibit linear response in change in potential over a wide pH range when potentiometric methods, as described in chapters 2 and 5, are employed. Plotting potential *vs.* electrolyte pH should, for a good pH sensor, be linear with the theoretical gradient of -59 $mVpH^{-1}$. This is explained in detail in chapters 2 and 5. An example of a potential polymeric pH sensor is polypyrrole, which has been studied extensively[62,63,64,65,66,67,68,69,70,71,72].

In 1992 Bartlett and Farrington investigated the possibility of using 5-carboxyindole as a pH sensor[73]. It was found to be pH sensitive over the range pH 1 to 7, was found to be stable, and had rapid response to pH change. The films could also be stored dry and re-used. Later studies, however, have shown that the pH range over which the films are stable is less than this[37,38]. Poly-5-cyanoindole has also had a certain amount of work carried out on its applications as a pH sensor and it shows linear response over pH range 1 to 10[37]. The pH response for both these films is

attributed to the protonation and deprotonation of the labile free N-H group on the trimer unit. These phenomena are discussed in more depth in chapter 5.

1.9. Aims of This Work

The research reported in this thesis had two main aims. These were to investigate the potential of poly-5-cyanoindole as a practical pH sensor, and to investigate the intrachain fluorescence properties of poly-5-cyanoindole and poly-5-bromoindole in solution. Much work has been carried out previously on the electrochemical synthesis and characterisation of 5-substituted indole systems, so the electrochemical techniques were carried out only to synthesise the samples and check for reproducibility.

The initial work carried out on the poly-5-cyanoindole films as pH sensors was the determination of a reproducible, linear Nernstian gradient. Following this the response time of the films was investigated, and the mechanisms of coat response analysed. The experiments were carried out in conditions as realistic as possible; for example they were not carried out in a completely inert atmosphere.

Fluorescence experiments on both the poly-5-bromoindole and poly-5-cyanoindole systems were carried out to determine the fluorescence lifetime for the trimer species of each, and to investigate the differences in fluorescence lifetime characteristics between samples that were synthesised with different extents of polymerisation, and hence containing different proportions of trimer and polymer. Because poly-5-bromoindole undergoes relatively facile polymerisation, it had previously proved

impossible to isolate the free trimer of 5-bromoindole. In this work a special method for producing the isolated trimer was devised. Additionally, because the polymerisation of 5-bromoindole on Pt is known to be poorly reproducible, a method of improving the polymerisation by using a non-fluorescent template was employed.

1.10 References

1. C.K. Chiang, C.R. Fincher, Y.W. Park, H. Shirakawa, E.J. Louis, S.C. Gau, A.G. MacDiarmid, *Phys. Rev. Lett*, 1977, **39**, 1098
2. H. Shirakawa, E.J. Lewis, A.G. MacDiarmid, C.K. Chang and A.J. Heeger, *J.Chem.Soc.Chem.Comm*, 1977, 578-580
3. J. Tourillon and F. Garnier, *J. Electroanal. Chem.*, 1982, **135(1),** 173-178
4. C.K.Chiang, Y.W. Park and A.J. Heeger, *J. Chem. Phys.*,1978, **69(11),** 5098-5104
5. R.W. Murray, A.G. Ewing and R.A. Durst, *Anal. Chem.*, 1987, **59(5),** 379A-390A
6. P. W. Atkins, *Physical Chemistry,* 5th Edition, Oxford University Press, 1995
7. L. Smart and E. Moore, *Solid State Chemistry – An Introduction*, 2nd Ed., Stanley Thornes Ltd., 1998
8. J.R. Fried, *Polymer Science and technology*, Prentice-Hall, 1995
9. R.H. Friend, R.W. Gymer, A.B. Holmes, J.H. Burroughes, R.N. Marks, C. Taliani, D.D.C. R. Bradley, D.A. Dos Santos, J.L. Brédas, M. Logdlund and W.R. Salaneck, *Nature*, 1999, **397**, 121-128
10. M.M. DeSouza, *PhD Thesis*, 2000, Imperial College
11. R.H. Friend, D.C.C. Bradley, P.D. Townsend, *J. Phys. D.: Appl. Phys.*, 1987, **20**, 1367-1384
12. C.A. Widrig, M.D. Porter, M.D. Ryan, T.G. Strein, A.G. Ewing, ***Dynamic Electrochemistry: methodology and application***; *Analytical Chemistry*, 1990, **62(12)**, 1R-20R
13. P. Kovacic and A. Kyriakis, *J. Am. Chem. Soc.*, 1963, **85**, 454
14. R. Holze and C.H. Hamann, *Tetrahedron*, 1991, **47 (4/5)**, 737-746
15. R.J. Waltman and J. Bargon, *Can. J. Chem.*, 1986, **64**, 76-95
16. P.C. Pandey and R.J. Prakash, *J. Electrochem. Soc.*, 1998, **145 (3)**
17. P. Pfluger and G.B. Street, *J. Chem. Phys.*, 1984, **80(1),** 544
18. Andrieux, P. Claude, P. Audebert, P. Hapiot J.M. Saveant, *J. Phys. Chem.*, 1991, **95(24)**, 10158-64.
19. P. Aubert, *J. Phys. Chem.*, 1995, **99**, 11923-11929

20. K. Kanazawa, A.F. Diaz, R.H. Geiss, W.D. Gill, J.F. Kwak, J.A. Logan, J.F. Rabolt, G.B. Street, *J. Chem. Soc. Chem. Comm.*, 1979, 854
21. A.F. Diaz, K. Kanazawa, G.P. Gardini, *J. Chem. Soc. Chem. Comm.*, 1979, 635
22. K. Kanazawa, A.F. Diaz, W.D. Gill, P.M. Grant, G.B. Street, G.P. Gardini, J.F. Kwak, *Synth. Met.*, 1979/80, **1**, 329
23. R.J. Waltman, J. Bargon and A.F. Diaz, *J. Phys. Chem.*, 1983, **87**, 1459-1463
24. R.J. Waltman, A.F. Diaz and J. Bargon, *J. Phys. Chem.*, 1984, **88**, 4343-4346
25. R. J. Waltman, A.F. Diaz, J. Bargon, *J. Electrochem. Soc. Electrochem. Sci. and Tech.*, 1985, **123(3)**, 631
26. J.H. Burroughes, D.D.C. Bradley, A.R. Brown, R.N. Marks, K. Mackay, R.H. Friend, P.L. Burns and A.B. Holmes, *Nature*, 1990, **347**, 539
27. G. Zotti, *Chem. Mater.*, 1994, **6**, 1742-1748
28. A. Berlin and A. Canavesi, *Tetrahedron*, 1996, **52(23)**, 7947-7960
29. P.N. Bartlett and J. Farrington, *J. Electroanal. Chem.*, 1989, **261**, 471
30. J.G. Mackintosh and A.R. Mount, *J. Chem. Soc. Faraday Trans.*, 1994, **90(8)**, 1121-1125
31. J.G. Mackintosh, C.R. Redpath, A.C. Jones, P.R.R. Langridge-Smith, D.R. Reed, A.R. Mount, J. *Electroanal. Chem.*, 1994, **375**, 163
32. J.G. Mackintosh, A.R. Mount, D. Reed, *Magn. Reson. Chem.*, 1994, **32,** 559
33. J.G. Mackintosh, C.R. Redpath, A.C. Jones, P.R.R. Langridge-Smith, A.R. Mount, *J. Electroanal. Chem*, 1995, **388**, 179
34. J.G. Mackintosh, S.J. Wright, P.R.R. Langridge-Smith, A.R. Mount, *J. Chem. Soc., Faraday Trans.*, 1996, **92(20)**, 4109
35. A.R. Mount, A.D. Thomson, *J. Chem. Soc., Faraday Trans.*, 1998, **94(4)**, 553
36. P. Jennings, A.C. Jones, A.R. Mount, A.D. Thomson, *J. Chem. Soc., Faraday Trans.*, 1997, **93**, 3791
37. J.G. Mackintosh, *PhD Thesis*, 1995, The University of Edinburgh
38. A.D. Thomson, *PhD Thesis*, 1997, The University of Edinburgh
39. M. Robertson, *PhD Thesis*, 1998, The University of Edinburgh
40. E.B. Maarouf, D. Billaud, E. Hannecart, *Materials. Research Bull.*, 1994, **29(12)**, 637

41. D. Billaoud, E.B. Maarouf, E. Hannecart, *Materials Research Bull.*, 1994, **29(12)**, 1239

42. H. Talbi, E.B. Maarouf, B. Humbert, M. Alnot, J.J. Ehrhardt, J. Ghanbaja, D. Billaud, *J. Phys. Chem. Solids.*, 1996, **57(6-8)**, 1145

43. H. Talbi, B. Humbert, D. Billaud, *Synth. Met.*, 1997, **84**, 875

44. H. Talbi, G. Monard, M. Loos, D. Billaud, *J. Mol. Struc. (Theochem.)*, 1998, **434**, 129

45. S. W. Kong, K. M. Choi, K. H. Kim, *J. Phys. Chem. Solids.*, 1992, **53(5)**, 657

46. V. Bochi, A. Colombo and W. Porzio, *Synthetic Metals*, 1996, **80**, 309-313

47. R.H. Friend, D.D.C. Bradley, P.D. Townsend, *J. Phys. D. Appl. Phys.*, 1987, **20**, 1367

48. M. Pope, H.P. Kallmann and P. Magnanate, *J. Chem. Phys.*, 1963, **38**, 2042-2043

49. J.H. Burroughes, D.D.C. Bradley, A.R. Brown, R.N. Marks, K. Mackay, *Nature*, 1990, **347**, 539-41

50. K.S. Wong, D.D.C. Bradley, W. Hayes, J.F. Ryan, R.H. Friend, H. Lindenberger, S. Roth, *J. Phys. C: Solid State Phys.*, 1987, **20**, L187

51. N.C. Greenham, I.D.W. Samuel, G.R. Hayes, R.T. Philips, Y.A.R.R. Kessener, S.C.Moratti, A.B. Holmes and R.H. Friend, *Chem. Phys. Lett.*, 1995, **240**, 89-96

52. A.B. Holmes, D.D.C. Branley, A.R. Brown, P.L. Burn, J.H. Burroughes, R.H. Friend, N.C. Greenham, R.W. Gymer, D.A. Halliday, R.W. Jackson, A. Kraft, J.H.F. Martens, K. Pichler, and I.D.W. Samuel, *Synth. Met.*, 1993, **55-57**, 4031-4040

53. B.J. Schwartz, *Annual Review of Phys. Chem.*, 2003, 141-172

54. I.D.W. Samuel, G. Rumbles and C.J. Collison, *Am Phys. Soc. Phys Rev. B, Rapid Comm.*, 1995, **52(16)**, 573-576

55. I.D.W. Samuel, G. Rumbles, C.J. Collison, R.H. Friend, S.C. Moratti and A.B. Holmes, *Synthetic Metals*, 1997, **84**, 497-500

56. L. Magnani, G. Rumbles, I.D.W. Samuel, K. Murray, S.C. Moratti, A.B. Holmes, R.H. Friend, *Synth. Met.*, 1997, **84**, 899

57. I.D.W. Samuel, B. Crystall, G. Rumbles, P.L. Burn, A.B. Holmes, R.H. Friend, *Synth. Met.*, 1993, **54**, 281
58. I.D.W. Samuel, B. Crystall, G. Rumbles, P.L. Burn, A.B. Holmes, R.H. Friend, *Chem. Phys. Letts.*, 1993, **213(5,6)**, 472
59. P. Jennings, A.C. Jones and A.R. Mount, *J. Chem. Soc. Faraday Trans.*, 1998, **94**, 3619-3624
60. P. Jennings, *PhD Thesis*, 2000, The University of Edinburgh
61. 'Optically Patternable Light-Emitting Devices based on Conducting Polymers', *IEICE trans. Electron, 2000*, **E83-C (7)**
62. J.D. Kim, K.S. Lee and K.J. Kim, *J. Bull. Korean Chem. Soc.*, 1989, **10(1)**, 119
63. Y. Li and R. Qian, *Synthetic Metals*, 1989, **28**, C127-C132
64. G. Hailin and L. Yucheng, *Sensors and Actuators B*, 1994, **21**, 57-63
65. F. Yue, T.S. Ngin and G. Hailin, *Sensors and Actuators B*, 1996, **32**, 33-39
66. A. Michalska and K. Maksymiuk, *Electroanalysis*, 1998, **10(3)**, 177-180
67. K.K. Shiu, A.Y. Song and K.W. Lau, *J. Electroanal. Chem.*, 1999, **476**, 109-117
68. K. Maksymiuk, *Anal. Letters,* 2000, **33(7)**, 1339-1360
69. P. Qibing and Q. Renyuan, *Synthetic Metals*, 1991, **45**, 35-48
70. H. Muenstedt, *Polymer*, 1986, **27**, 899
71. G. Cheek, C.P. Wales and R.J. Nowak, *Anal. Chem.*, 1983, **55**, 380-381
72. A. Talaie, *Polymer*, 1997, **38(5)**, 1145
73. P.N. Bartlett and J. Farrington, *Bull. Electrochem*, 1992, **8(5)**, 208-211

Chapter 2

Theory

2.1. Electrochemistry

2.1.1. General

Electrochemistry provides a means of monitoring electron transfer reactions between an electrode and solution-phase or solid-phase reactant molecules adsorbed on the electrode. The overall rate of electrode reaction, measured by the current, is usually controlled by the slower of two processes. These are the surface electrochemical reaction and the rate of mass transport of material to the electrode from the bulk. The rate of mass transfer is often controlled, or enhanced, by diffusion or stirring.

Measuring electrode currents in relation to the potential applied can yield important information about the reaction being studied. In this thesis a three electrode system was used, comprising a working electrode, WE, where the reaction of interest occurs, a reference electrode, RE, which provides a reference potential against which the driving force of the WE reaction can be measured, and a counter electrode, CE, which completes the circuit, allowing the passage of current for the WE reaction. The current in this set up, therefore, flows between the working and counter electrodes and the potential of the WE is controlled relative to the RE, which is often placed close to the WE to minimise iR drop. Additionally, a background electrolyte that reduces the electrolyte resistance, R, and therefore further minimises iR drop, is added. The voltages in the system, represented in figure 2.1, can be described as

$$E = (\phi_m - \phi_s) + iR + (\phi_s - \phi_{REF}) \qquad \textbf{2.1}$$

where E = voltage applied between the electrodes, (ϕ_m - ϕ_s) = potential drop between WE (m) and solution (s) (the driving force for electrochemical reaction), iR = voltage drop in solution due to current, i, passing through the solution (resistance R) between the WE and the reference electrode (RE), and (ϕ_s - ϕ_{REF}) = potential drop at the RE (REF) / solution (s) interface. The last term is constant and dependent on the chemical composition of the reference electrode.

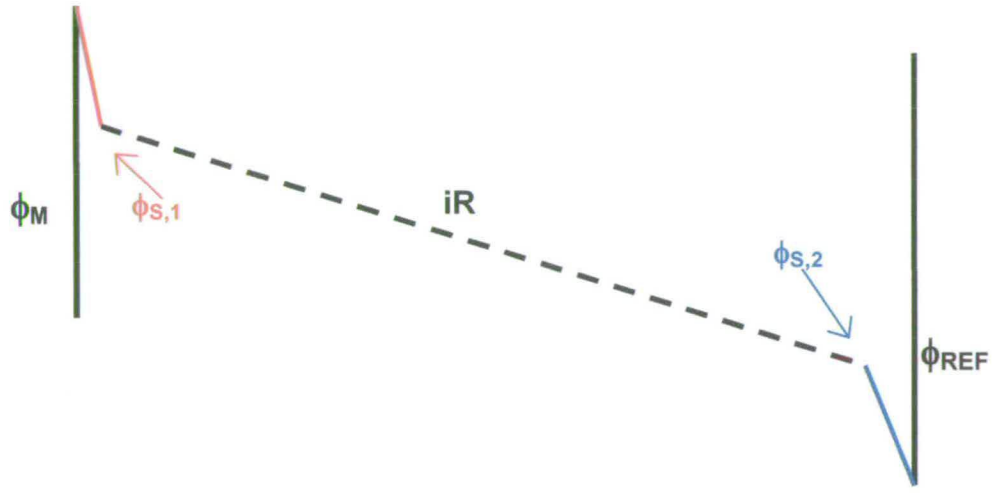

Figure 2.1: *ϕ_M=potential at the WE; ϕ_{REF}=potential at the RE; $\phi_{S,1}$=potential of the solution close to WE; $\phi_{S,2}$=potential of the solution close to RE; iR = drop in iR between WE and RE. The iR drop can be minimised with the use of an appropriate electrolyte, thereby reducing R so that $\phi_{S,1} \rightarrow \phi_{S,2}$*

Adding background electrolyte ensures that R is small, hence the iR term is negligible, and (ϕ_S - ϕ_{REF}) is fixed, so the reaction driving force at the working electrode (ϕ_M-ϕ_S) is solely dependent on E, as

$$E = (\phi_m - \phi_s) + constant \qquad \textbf{2.2}$$

However, for low electrolyte concentrations, or resistive solvents, iR is no longer negligible.

2.1.2. Potential Sweep Voltammetry

Potential Sweep Voltammetry (PSV) is a relatively cheap, simple technique from which a vast amount of information can be gained. This is carried out in a stagnant solution with a background electrolyte that contains an electroactive species, A, at much lower concentration than the electrolyte. This species can be reduced or oxidised upon the application of a potential that is either negative or positive with respect to the standard redox potential (E^{θ}), producing $A \rightarrow B^-$, or $A \rightarrow B^+$, respectively. Considering reduction, if a potential that is negative with respect to E^{θ} is applied, the electroactive species A can be reduced to species B^- with rate k_{red}:

$$A\,(aq) + e^-\,(m) \underset{k_{ox}}{\overset{k_{red}}{\rightleftharpoons}} B^-\,(aq) \qquad \textbf{2.3}$$

If a potential that is positive with respect to E^{θ} is employed, then the species B^- can be oxidised back to A with rate k_{ox}. In a stagnant solution, the movement of the species to the working electrode can be considered to be controlled only by diffusion. If E is swept from a potential more positive than E^{θ} to a potential more negative than E^{θ}, initially the concentration of the electroactive species A in the solution is equal to the bulk concentration, C_{∞}. During the potential sweep, as A becomes reduced to B^- at the electrode, the concentration of A in the solution close to the electrode decreases, and the concentration of B^- increases. Hence a boundary layer is formed near the electrode, with a concentration profile as shown in figure 2.2.

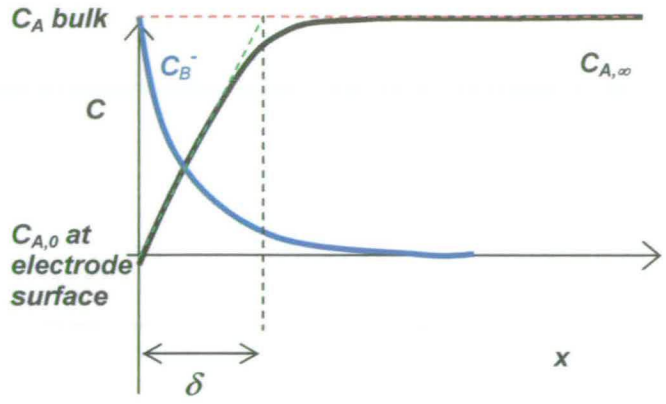

Figure 2.2: *Concentration profiles for A and B^- for potentials beyond E_P. x = distance from electrode surface, δ = diffusion layer thickness.*

Transport of A to the electrode surface from the bulk, and consequently rate of electrochemical reaction, is governed by the rate of diffusion, and the current passed is called the diffusion limited current. Such a system, represented in figure 2.2, can be modelled mathematically, and the current calculated using equation 2.4

$$i_L = -nFD(c_\infty - c_0) / \delta \qquad \textbf{2.4}$$

Where i_L = limiting current, n = number of electrons, F = the Faraday constant (96,500 C mol^{-1}), D = diffusion coefficient (cm^2s^{-1}), c_∞ = bulk concentration ($molcm^{-3}$), c_0 = concentration at the electrode surface ($molcm^{-3}$), δ = diffusion layer thickness (cm). In a stagnant solution δ increases with time. Initially during the potential sweep i rises as $c_\infty - c_0$ increases, then falls as δ increases.

2.1.2.1. Linear Sweep Voltammetry

The simplest of the potential sweep techniques is linear sweep voltammetry (LSV). The potential of the electrode is swept linearly with time at a sweep rate v (mVs^{-1}) from potential E_1, positive with respect to E^θ, at which species A cannot react, to

potential E_2, negative with respect to E^{θ}, at which electron transfer occurs very rapidly. A current is produced, which is plotted as a function of voltage (fig 2.3).

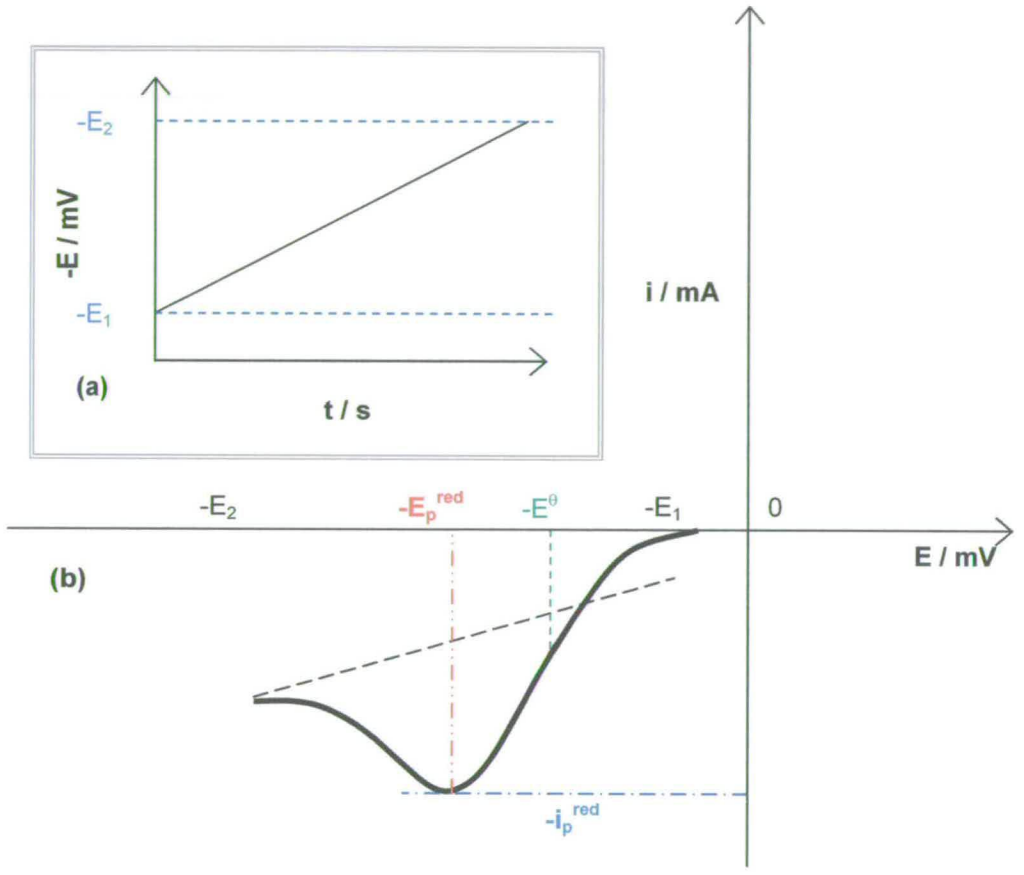

Figure 2.3: *(a) (inset) Potential profile and (b) Typical voltammogram for an LSV experiment*

The electrochemical rate constants for the reduction $A + e^- \rightarrow B^-$ and oxidation $B^- \rightarrow A + e^-$ are given by

$$k_{RED} = k^{\theta}\exp[(-\alpha_{RED}nF(E-E^{\theta})) / RT] \quad \textbf{2.5}$$

and

$$k_{OX} = k^{\theta}\exp[(-\alpha_{OX}nF(E-E^{\theta})) / RT] \quad \textbf{2.6}$$

respectively, where α_{ox} and α_{RED} are the mass transfer coefficients for oxidation and reduction respectively. Initially, at E_1, the voltage is insufficient to reduce A to B^- and so no current is observed. As E is made more negative and approaches E^θ reduction of the species A begins, k_{red} increases and a current is seen. On passing E^θ, as E becomes more negative, δ increases as species diffuse from progressively further away from the electrode. The surface concentration of A drops, therefore the flux to the surface, and current. Beyond E^θ the surface concentration drops to near zero, mass transfer of A to the surface reaches a maximum rate as the increase in $c_\infty - c_0$ equals the increase in δ, and then decreases as depletion occurs and δ increases (figure 2.3). This is seen as the current increases with E exponentially at first, the rate determining step (RDS) being electron transfer, then more slowly with the RDS being electron transfer and mass transport, until it reaches a peak, i_p, at potential E_p, after which it is seen to decrease, the RDS being mass transport.

2.1.2.2. Cyclic Voltammetry

Cyclic Voltammetry is an extension of LSV, whereby upon reaching the reducing potential E_2, which is negative with respect to E^θ, the potential is swept back to E_1, positive with respect to E^θ, at the same rate, v. Potential–time profiles and corresponding voltammograms for typical CV experiments are shown in figure 2.4 (a) and (b) respectively.

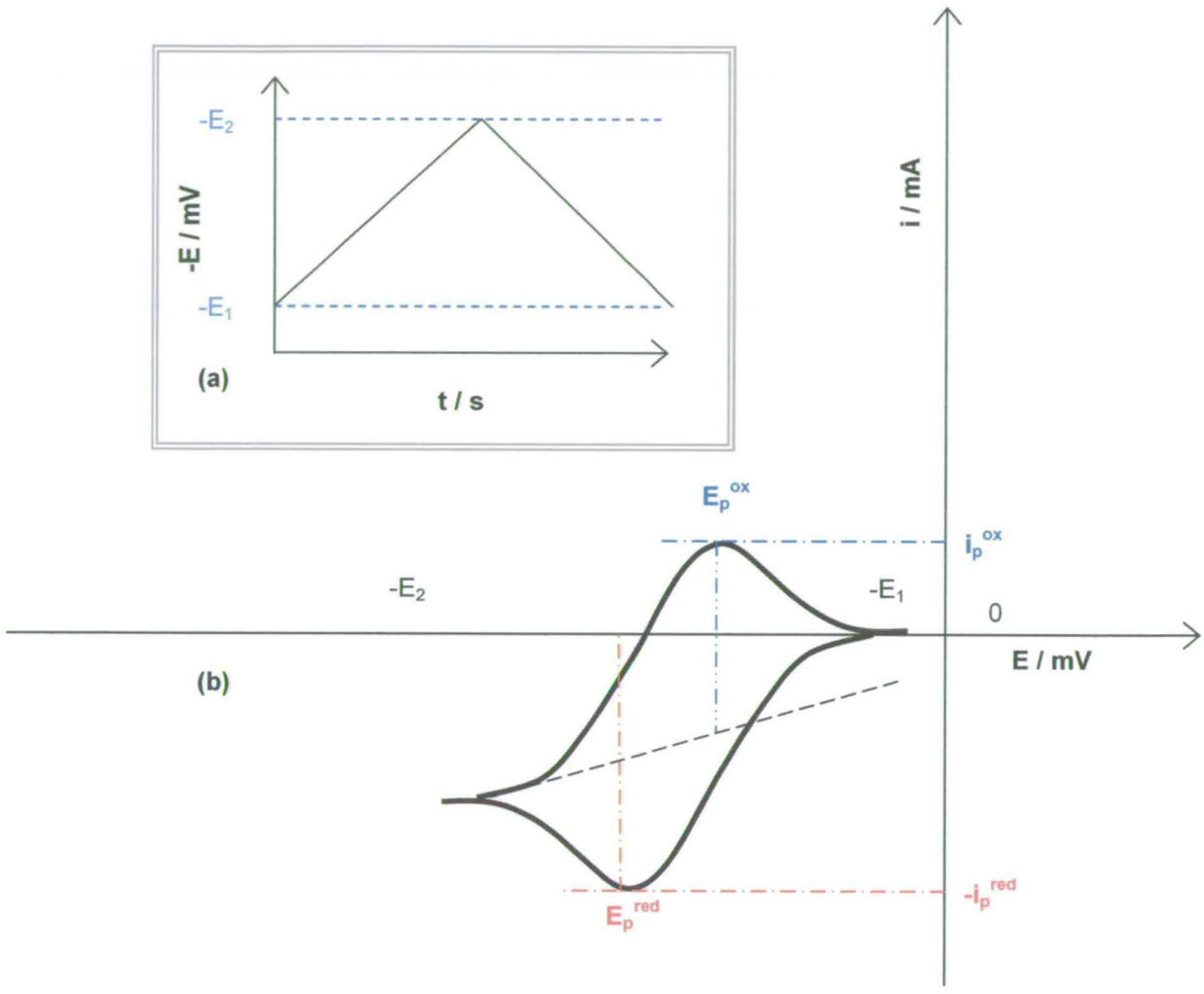

Figure 2.4: *(a) (inset) Potential profile and (b) Typical voltammogram for an CV experiment*

Initially, when the concentration of A^- in the diffusion layer is high, the current is seen to increase rapidly, but as all the A^- in the diffusion layer is oxidised back to A the current drops to zero. Either a single CV can be recorded (figure 2.4(b)), or multiple scans, the potential sweeping from E_1 to E_2 and back being repeated producing multiple voltammograms in the same plot. Only at the start of the first cycle can it be ensured that $\delta=0$ and $c_\infty=c_0$, hence kinetic information can be gathered only during this cycle.

From the cyclic voltammogram obtained it can be deduced whether the reaction observed is electrochemically and chemically reversible or irreversible and the charge passed can be estimated from the area beneath the plot. For example, for the reaction

$$B^- \rightarrow A + ne, \qquad \textbf{2.7}$$

assuming equilibrium, the relationship between the potential, E, of the working electrode and the surface concentrations of A and B^- is given by the Nernst equation

$$E = E^{\theta} + \frac{RT}{nF} \ln \frac{C_{B^-}}{C_A} \qquad \textbf{2.8}$$

where R is the gas constant, T is the temperature, F is the Faraday constant, and C_B^- and C_A are the concentrations of the oxidised and reduced species at the electrode surface respectively. For an electrochemically reversible reaction the electrode kinetics are fast; in this case $|E_p-E_{p/2}|$ is equal to $\frac{56.5}{n}$ mV at 25 °C. The CV of a reversible reaction will have $E_p^{red}=E_{p/2}^{ox}$ and $E_p^{ox}=E_{p/2}^{red}$. For a reversible system E_p is independent of scan rate.

For an irreversible reaction the electrode kinetics are slow. A high overpotential is required to induce current flow therefore the increase in current with potential is slower than for a reversible reaction. E_p will be shifted to a more positive potential than for the reversible reaction at the same scan rate, and increasing the scan rate pushes E_p to increasingly positive potential.

For both irreversible and reversible reactions where the redox active species is in solution $i_p \propto v^{1/2}$, as the reaction is under diffusion control; however in cases where a

film is formed on the electrode this will only hold true as long as the whole film is not oxidised or reduced on each sweep; in this case $i_p \propto v$.

2.1.3. Hydrodynamic Systems

The theory in previous sections covers stagnant systems, where the rate of reaction is controlled by diffusion. Hydrodynamic systems induce forced convection of the reaction solution, which can be controlled precisely, into the system, enabling controlled transport of the electroactive species to the electrode surface. There are many techniques for inducing convection, which fall under two broad categories. These are systems whereby the solution is forced to flow past a stationary electrode and systems where the electrode is in motion. The system employed in this work, the rotating disc electrode (RDE), falls under the latter category.

Hydrodynamic systems have advantages over stationary systems in that steady states can be achieved relatively quickly. The currents produced are also rather larger than those observed under diffusion alone. This is because the diffusion layer thickness, x_D, is typically smaller than δ and depends on the rate of convection. The main advantage for these systems, however, is that the constant flow of the species to the electrode allows control of surface concentrations, and therefore control of the polymerisation process.

2.1.3.1. Rotating Disc Electrode

A Rotating Disc Electrode (RDE) is a common example of a hydrodynamic electrode whereby the electrode moves. It is cylindrically symmetrical and consists of a Pt disc (diameter approximately 5 mm) embedded centrally in a large cylindrical insulating mantle (figure 2.5).

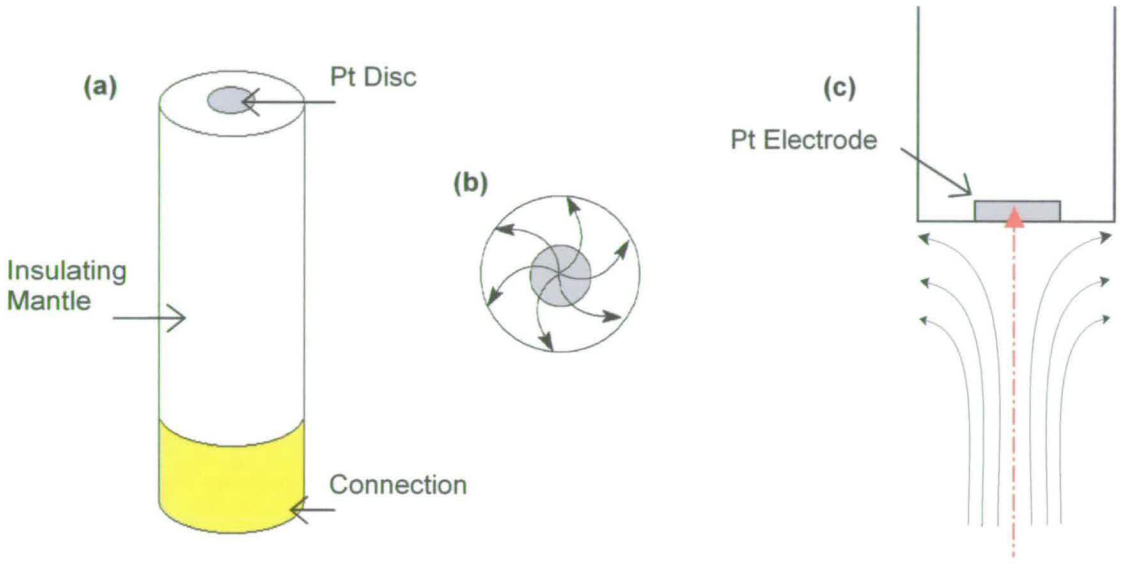

Figure 2.5: *(a) Rotating disc electrode (b) Flow over the electrode surface, end-on view (c) Direction of motion of electroactive species to and flow pattern over the electrode surface*

It is introduced into the solution of interest and is rotated at a constant speed, W (Hz). This rotation induces convection. The solution is thrown out from the surface of the electrode radially, and this in turn causes fresh electroactive species to be drawn to the electrode perpendicular to the electrode surface, the resulting flow pattern being illustrated in figure 2.5 (b) and (c), which sustains a constant supply of the electroactive species at the electrode surface. This movement of fresh electroactive species perpendicular to the electrode surface results in the concentration profile shown in figure 2.6.

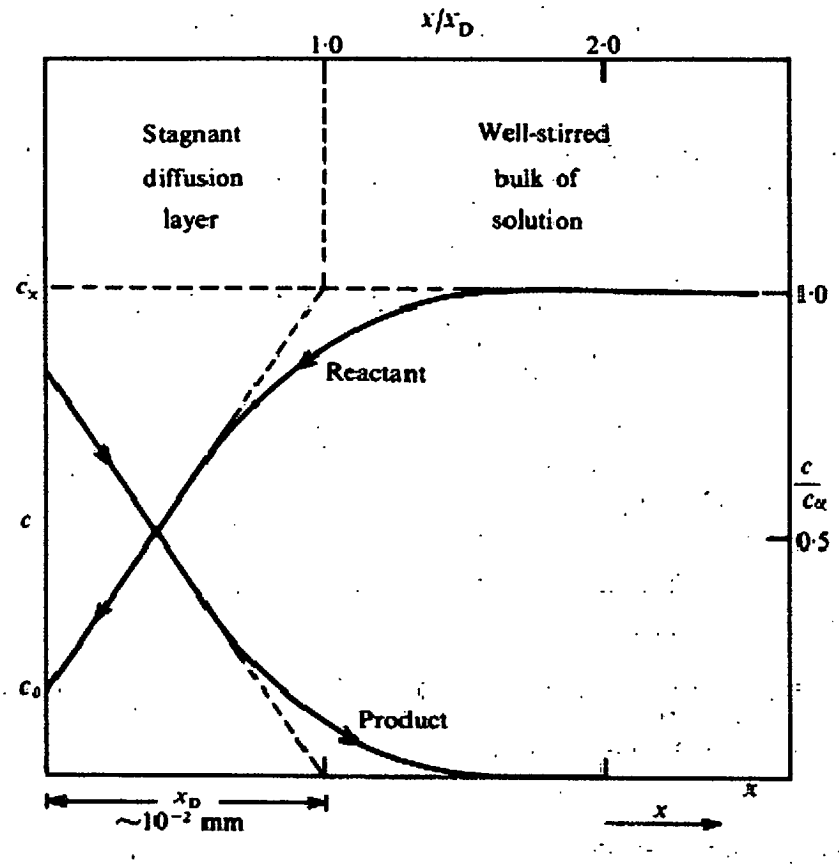

Figure 2.6: *Concentration profile at the RDE*

Inside the diffusion layer, which is close to the electrode and has a thickness x_D, the solution can be considered to be stagnant in the direction perpendicular to the electrode and transport to the electrode occurs in this direction by diffusion only. The thickness of the diffusion layer varies with the rotation speed, W (Hz), of the electrode.

The equation relating x_D to W is

$$x_D = 0.643D^{1/3}\nu^{1/6}W^{-1/2} \qquad \textbf{2.9}$$

where D = diffusion coefficient of the species (cm^2s^{-1}) and ν = kinematic viscosity (= viscosity / density; cm^2s^{-1}) of the solvent. Therefore, increasing W decreases the thickness of the diffusion layer, as shown in figure 2.7.

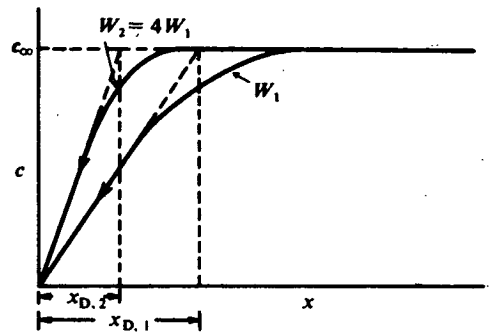

Figure 2.7: *Depletion of diffusion layer as W increases*

In the case of totally mass-transport limited conditions, and where the concentration of reactant at the electrode is zero, the Levich equation (eq 2.4) relates the mass transport limited current, i_L, to the rotation speed, W. In such a situation the electrode reaction is relatively fast and not rate determining (eq. (2.10)):

$$|i_L| = 1.554nFAC_R^{\infty}\nu^{-1/6}D_R^{2/3}W^{1/2} \qquad \textbf{2.10}$$

C^{∞}_R and D_R are the bulk concentration and diffusion coefficients of reactant R, n is the number of electrons involved in the reaction, and A is the area of the electrode surface. Plotting i_L against $W^{1/2}$ gives a straight line through the origin if the system being studied has no mass transport independent surface steps. The gradient of the

plot, which is proportional to $nD_R^{2/3}$, allows the calculation of the number of electrons that were involved in the reaction, n, or the diffusion coefficient, D.

If, however, the reaction being studied has a finite mass transport–independent step at the electrode surface, for example slow electron transfer with rate constant k' that is comparable to or less than the rate constant for mass transport k_{MT} this expression will not hold true. Such a situation can be described as

$$C_\infty \xrightarrow{k_{MT}} C_0 \underset{-ne^- /+ne^-}{\overset{k'_{ox}/k'_{red}}{\longrightarrow}} \text{product} \qquad 2.11$$

In general the kinetics of the reaction can be described by the Koutecky-Levich equation (2.12)

$$\left|\frac{1}{i}\right| = \left(\frac{1}{nFAc^{\infty}{}_R}\right)\left[\frac{0.6435\nu^{1/6}}{D_R{}^{2/3}W^{1/2}} + \frac{1}{k}\right] \qquad 2.12$$

where i is the observed current, k is k_{ox} or k_{red} as appropriate. A plot of $\left|\frac{1}{i_{obs}}\right|$ *vs.* $\frac{1}{W^{1/2}}$, termed a Koutecky-Levich plot, should show a linear relationship, with the gradient being the inverse of the Levich gradient. The intercept yields $k_{ox/red}$ at the given potential.

2.1.4. Potential Step Chronoamperometry (PSC)

This type of experiment is, like LSV and CV, carried out using a 3–electrode system. However instead of sweeping the potential between a lower (E_1) and an upper (E_2) limit, graduating from no reaction to reaction, the potential is stepped from E_1 to E_2 (figure 2.2 (a)), usually causing 'instantaneous' complete conversion of A to B^- at the electrode, when $E_2 << E^\theta$ such that $C_{A,0}=0$. For a stagnant solution, after the step the concentration gradients are large as the electroactive material has not yet depleted, and this leads to large currents being observed. However, with time the diffusion layer thickness increases as depletion occurs, and this is seen as a fall in the observed current. However, using a RDE the diffusion layer is constantly being replenished with monomer from the bulk. If the rotation speed is constant, the concentration of the monomer at the electrode surface becomes constant; therefore the current reaches a steady state (figure 2.8).

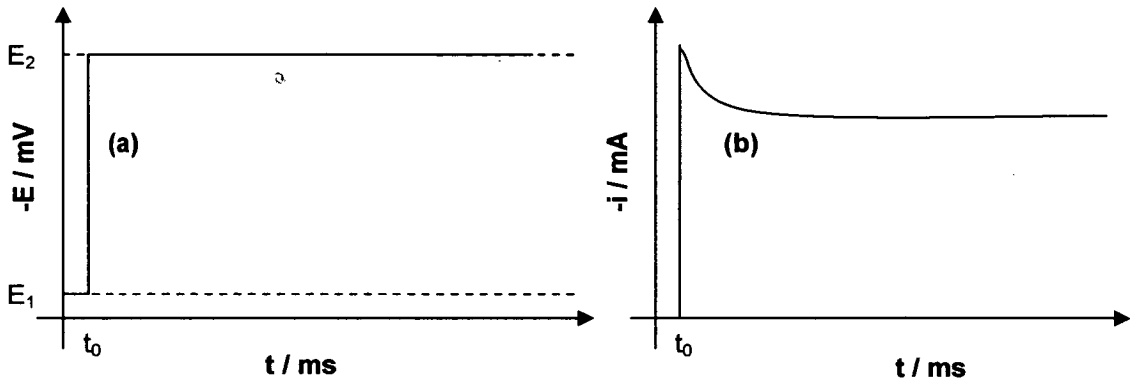

Figure 2.8: *(a) Potential / time profile and (b) current / time response for PSC experiments*

The initial spike corresponds to the oxidation of the monomer and the time to set up the diffusion-layer, x_D, and reach steady-state conditions. The steady-state current's magnitude is determined by the rate of transport of the reactant A to the electrode

surface. The theoretical current response is given as a function of time by the Cottrell equation, eq. (2.13):

$$|i| = \frac{nFAD_A^{1/2}[A]_{bulk}}{\pi^{1/2}t^{1/2}} \quad \textbf{2.13}$$

Where |i| = the modulus of the current, n = number of electrons, F = Faraday constant (96,500 C mol^{-1}), A = area of electrode, D_A = Diffusion coefficient of reactive species A (cm^2s^{-1}), $[A]_{bulk}$ = concentration of reactive species A in bulk solution ($molcm^{-3}$), t = time (s).

Where a film is formed on the electrode surface, such as is the case in this thesis, the steady – state current will only be maintained if the film is highly conducting, as otherwise, iR drop in the film will decrease the surface potential as the film grows thicker, therefore reducing i with respect to time.

2.1.5. pH Response Experiments

pH response experiments are carried out using potentiometric techniques. Such studies are performed using zero – current galvanometry, the change in electrode potential being measured as a function of pH change. As no current flows there is no overall reaction of the species in solution and the concentration of species at the surface of the electrode is equal to the bulk concentration. The process under observation in this thesis is protonation / deprotonation at the electrode. This is a process to which the Nernst equation can be applied if it is assumed that the reaction is reversible and reaches equilibrium (equation 2.15). Hence for the equilibrium 2.14

$$A + ne^- \rightleftharpoons B^{n-} \quad \textbf{2.14}$$

the Nernst equation can be written as

$$E = E^{o} + \frac{RT}{nF} \ln \frac{a_{A,0}}{a_{B,0}} \qquad \textbf{2.15}$$

where a is the activity of a given species. In the situation where the reduced species BH_m undergoes deprotonation or oxidation to give A the general equation for the reaction can be written as

$$BH_m \rightleftharpoons A^{(m-n)-} + mH^{+} + ne^{-} \qquad \textbf{2.16}$$

Deriving the Nernst equation leads to expression 2.17, with BH_m written as B for simplicity

$$\begin{aligned} E &= E^{o} + \frac{RT}{nF} \ln a \frac{B\, a_{H^{+}}{}^{m}}{a_A} \\ &= E^{o} + \frac{RT}{nF} \ln a \frac{B}{a_A} + \frac{RT}{nF} \ln a_{H^{+}}{}^{m} \\ &= E^{o} + \frac{RT}{nF} \ln a \frac{B}{a_A} - 2.303 \frac{mRT}{nF} pH \end{aligned} \qquad \textbf{2.17}$$

As zero current is being passed, the species in the solution are not reacting so the ratio a_B/a_A does not change. This means that the term

$$E^o + \frac{RT}{nF} \ln \frac{a_B}{a_A} \qquad \textbf{2.18}$$

is a constant, E′. Also the term 2.303RT/F = 59 mV at 298 K. Substituting these into equation 2.17 produces

$$E = E' - 59 \frac{m}{n} pH \qquad \textbf{2.19}$$

A plot of E/mV vs pH should therefore give a straight line with gradient = -59m/n at 298 K. This allows the determination of m/n from the gradient of the graph.

In practice, for many pH sensitive redox films the gradient is observed to be less than m/n; this has been attributed to film inhomogeneity and / or interactions between redox centres in the film, which cause a variation in the redox potentials of the redox centres. In this case, the gradient is usually found to be $59\beta\frac{m}{n}$, with $\beta<1$. The closeness of β to unity can be used to assess both the film's suitability as a pH sensor and the validity of the assumption of ideality.

2.2. Photophysics

2.2.1. Quantum Mechanics and the Nature of Matter

In matter energy levels are quantized; they are confined to distinct values particular to the system. This means that a system's energy cannot be varied arbitrarily. A molecule possesses vibrational, rotational and electronic internal energies, which exist in discrete energy states. Rotational and vibrational energy levels are much closer together in energy than the electronic energy levels, which require much higher energy (shorter wavelength) radiation to ensure excitation. Excitation occurs when a species in a lower energy state absorbs a quantum of energy and becomes vibrationally, rotationally or electronically excited to a higher energy state. Conversely, emission may occur if the species, in a higher energy state initially, surrenders its excess energy and undergoes a transition to a lower energy state. This de-excitation can occur via radiative, *e.g.* luminescence, or non-radiative processes. The processes of interest in photophysics are illustrated in figure 2.9.

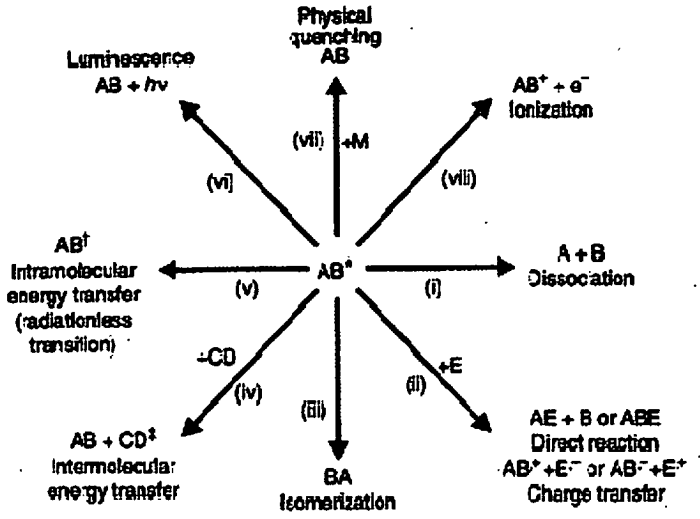

Figure 2.9: *Several Routes to Electronic Loss ofExcitation*

Molecules can be excited by irradiation with a source of light, or they can gain energy from chemical reactions. However, the work in this thesis is solely concerned with photo-excitation and subsequent de-excitation by luminescence.

Photo-excitation of a species is possible owing to the nature of light, which consists of oscillating perpendicular electronic and magnetic fields. The electric field can interact with the electrons in the species to be excited; if the light is of sufficient energy then electronic excitation occurs. Photons can only interact with molecules one at a time. The energy of the photons for a particular wavelength of light is fixed, the intensity of the light describing only the number of photons per unit time. Hence

increasing the intensity of radiation increases the number of species excited, not the energy available to each individual species.

Any transition occurring between two states of a molecule has a defined energy; hence only specific energies can be absorbed or emitted. Electronic excitation of species M to M* by irradiation with light, for example, will occur if the energy of the radiation to which M is being subjected, hν, is equivalent to the separation between its electronic energy levels, thus

$$M + h\nu \rightarrow M^*$$

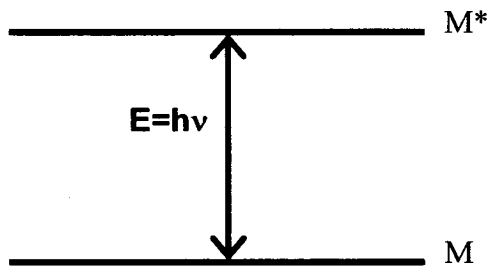

Figure 2.10: *Representation of electronic excitation of molecule in its ground state M to its excited state M* where the energy separation, E, between the 2 states is equal to hν*

where h=Planck's constant, ν=frequency of incident radiation, M*=electronically excited species. Therefore, when using light as an excitation source it is essential to choose the correct wavelength to achieve excitation to a higher energy level. Typically the energy of radiation in the visible to ultraviolet region is adequate for electronic excitation; infrared radiation generally induces only rotational or vibrational excitation. The best excitation sources are monochromatic so the effect of the wavelength on the nature and rate of reaction can be assessed accurately; this can be achieved by using lasers, monochromators, colour filters or interference filters.

2.2.2. Photophysics of Indoles

Monomers, trimers and polymerised films of indole and its substituted derivatives, owing to their highly conjugated nature, are known to be highly luminescent, enabling extensive characterisation using fluorescence spectroscopy. The photophysical properties of such molecules arise from the delocalisation of the bonding between the carbon atoms in the six-membered carbon ring.

When a carbon-carbon double bond absorbs a quantum of light, a π electron is excited into an antibonding π^* orbital. Such transitions are known as $\pi^* \leftarrow \pi$ transitions and have energy of approximately 7 eV for an unconjugated double bond, corresponding to an absorption band at 180 nm (in the ultraviolet). As conjugation increases, the molecular orbitals lie closer together in energy and the $\pi^* \leftarrow \pi$ transition moves to longer wavelength. In a system that has extensive conjugation, such as poly-indoles, the energy of the transition is sufficiently low that it lies in the visible region.

2.2.3. Electronic Excitation

If a molecule absorbs a photon of energy greater than or equal to the separation of its electronic energy levels, it will undergo electronic excitation, from a lower energy level, E_1 to a higher energy level, E_2 (figure 2.11). To describe electronic excitation, and the absorption and emission of radiation, quantitatively, the domain of wave mechanics must be introduced. This theory concerns the concepts of amplitude and wavefunction, and gives rise to the quantum numbers that define the electronic state of a species. The feasibility of an interaction of a species with electromagnetic

radiation can be determined by the spin, orbital momentum and symmetry properties of the wavefunctions of the lower (initial) and upper (final) electronic states.

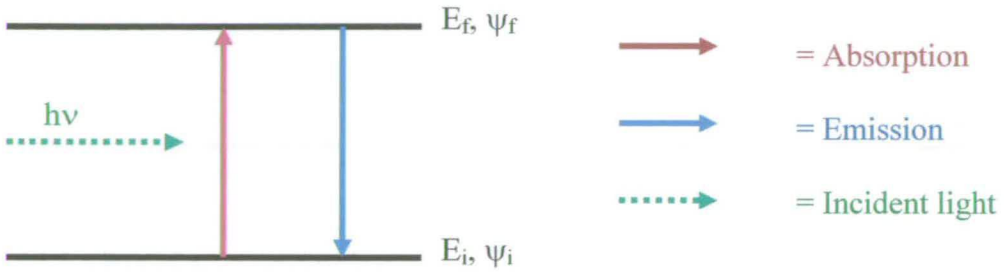

Figure 2.11: *Representation of electronic excitation from the initial (Ei) to the final (Ef) electronic state by absorption of radiation, and subsequent emission back to the lower state.* ψ_i*=wavefunction of the initial state (absorption; would be final state for emission),* ψ_f*=wavefunction of the final state (absorption; would be final state for emission).*

2.2.3.1. Spin Multiplicity

Electrons possess spin angular momentum and orbital angular momentum, both of which are vector quantities. A single electron has a spin moment **s**=½. The spin coupling, *i.e.* vector summation of spin moments of each individual electron in a species, gives the overall spin **S**. For an electron pair the spins are anti-parallel, therefore **S**=0. More commonly used than **S** is the term spin multiplicity, defined as 2**S**+1. In a system where all electrons are paired 2**S**+1=1 and the species is described as a singlet. If there are two unpaired electrons with parallel spins then **S**=1, hence 2**S**+1=3 and the system is described as a triplet. The ground singlet state can be denoted S_0, the first excited singlet state S_1, the second S_2 and so forth. The triplet states can be described in a similar manner, *i.e.* the first excited triplet state T_1, the second T_2 etcetera, T_0 being omitted as there is no triplet ground state; the ground states of most chemical species, moreover the species studied in this thesis, are singlets. Transitions, either radiative or radiationless, between terms of the same

multiplicity are spin-allowed, and transitions between terms of different multiplicity are spin-forbidden.

2.2.3.2. Wavefunctions and The Schrödinger Equation

A wavefunction $\psi(x,y,z,t)$, which is a function of position and time, describes the amplitude of an electron wave. Rather than saying that the particle is actually at a specific place at a specific time, its position is described as the probability of finding the particle there, and is given by $\psi^*\psi$, where ψ^* is the complex conjugate of ψ. Hence, where $d\tau$ is the volume element,

$$\int \psi^* \psi \, d\tau = 1 \quad \textbf{2.17}$$

as the probability of finding the electron in all space is unity. Assuming that this probability is independent of time

$$\delta(\int \psi^* \psi \, d\tau) / \delta t = 0 \quad \textbf{2.18}$$

2.2.3.3. Einstein Coefficients

Spectral lines occur with a variety of intensities, and sometimes lines may not appear when they are predicted to do so. The intensities of spectral lines depend on the population of the molecular states, and also on the strength of the interaction with the electromagnetic field. Considering transitions between two states m and n in the presence of an electromagnetic field (figure 12) there are three processes occurring, each having a different rate. These are stimulated absorption, stimulated emission and spontaneous emission. The Einstein Coefficients ascertain the probability of absorption and emission processes and characterise the rates of these processes. For

stimulated absorption, stimulated emission and spontaneous emission the Einstein coefficients are B_{mn}, B_{nm} and A_{nm} respectively.

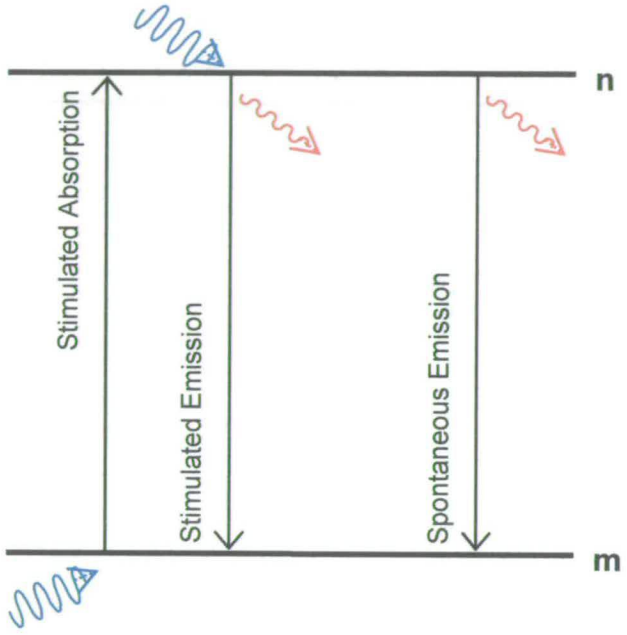

Figure 2.12: *Illustration of the Stimulated Absorption and Emission, and Spontaneous Emission of a molecule between two states m and n. Blue wavy lines represent incident radiation; red wavy lines represent emitted radiation*

Stimulated absorption is driven by oscillations of the electromagnetic field at the transition frequency, and results in a transition from the lower energy state to the higher energy state. For an absorption leading to a transition between two states m and n, the total rate of change of the population of state n, N_n is given by

$$\frac{dN_n}{dt} = N_m B_{mn} \rho(\nu) \qquad \textbf{2.19}$$

where N_m = population of state m, $\rho(\nu)$ = energy density of radiation at the frequency of the transition / $Jm^{-3}Hz^{-1}$. B_{mn} can be thought of as an empirical parameter that characterises the transition: if B_{mn} is large then the sample will be strongly absorbing.

2.2.3.4. Transition Moments

If a molecule is to interact with an electromagnetic field and absorb or create a photon of frequency ν it must possess a dipole oscillating at the same frequency. The dipole need only exist transiently. The transient dipole for absorption and emission spectra can be expressed quantum mechanically in terms of the transition dipole moment. For a transition as illustrated in figure 2.12 This can be defined as

$$\mu_{fi} = \int \psi_f^* \, \mu \, \psi_i \, d\tau \qquad \textbf{2.20}$$

where μ is the electric dipole operator. The size of the transition dipole can be thought of as a measure of the charge redistribution that accompanies a transition, and a transition will generate or absorb photons strongly only if the accompanying charge redistribution is dipolar. The coefficient of stimulated absorption (and emission), and therefore the intensity of the transition, is proportional to the square of the transition dipole moment

$$B_{mn} = \frac{\left|\mu_{fi}\right|^2}{6\varepsilon_0 \, \mathrm{h}^2} \qquad \textbf{2.21}$$

hence for the transition to contribute to the spectrum, then $\mu_{fi} \neq 0$.

2.2.3.5. Vibronic States and the Franck-Condon Principle

Although this absorption process results in electronic excitation, this is not the only process occurring. Electronic transitions are always accompanied by vibrational and rotational transitions. The differences between rotational energy levels are two orders of magnitude smaller than those for vibrational energy levels, and are not resolved at room temperature in the solution phase (although population of rotational levels induces broadening of the spectrum). Hence electronic transitions can be thought of as being accompanied by vibrational transitions, and are termed vibronic transitions (figure 2.13).

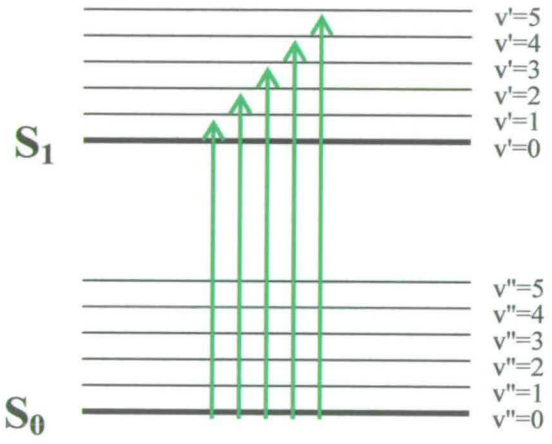

Figure 2.13: *Representation of vibronic progression between the S_0 and S_1 electronic states*

The Franck-Condon Principle states that because nuclei are so much more massive than electrons, electronic transitions can take place very much faster than the nuclei can respond. Hence, the nuclear conformation readjusts after the electronic transition has occurred, not during the transition.

Initially the molecule is in the lowest vibrational state of its lowest electronic state, and the nuclei are at their equilibrium separation, R_e. The electronic transition is most likely to occur when the nuclei have this separation as the vibrational wavefunction has a maximum at this position. After the electronic transition has occurred the nuclei are still at R_e, but the forces to which they have been subjected cause vibration, therefore the transition has occurred to both an electronically and a vibrationally excited state; a vibronic transition. As the nuclear framework stays the same throughout it is a 'vertical transition' that is occurring, *i.e.* an electronic transition that occurs without change of nuclear geometry. This vertical transition cuts through several vibrational levels of the upper electronic state and terminates in the vibrational state in which the nuclei have the most probable separation R_e.

In cases where the nuclear geometry of the excited state is not radically different from that of the ground state, *i.e.* the ground and excited state equilibrium bond lengths (R_e) are equivalent, (figure 2.14) it is most probable that a 0 – 0 transition will occur, hence an intense 0 – 0 band is observed with other transitions being very weak.

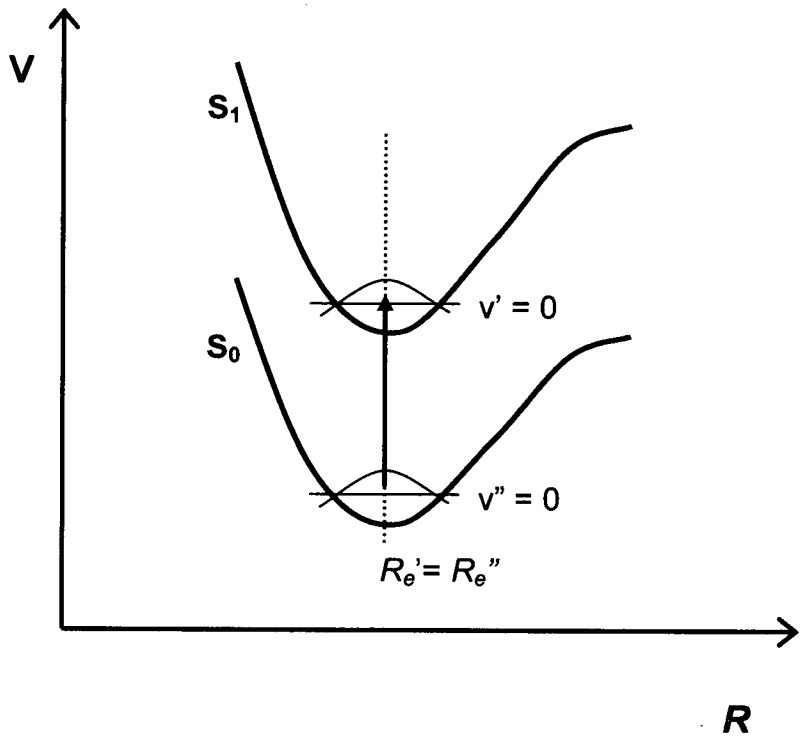

Figure 2.14: *Potential energy diagram representing excitation between two states with similar nuclear geometry; R_e'=R_e". V = potential energy, R = Internuclear Distance. The most intense transition is the 0-0 transition.*

Usually, however, the ground state and excited state of the molecule do not have the same nuclear geometry, and the equilibrium bond lengths will not be the same in both states. In the case where $R_e' > R_e''$, the most probable transition is no longer the 0 – 0 transition. There may be significant overlap with several vibrational levels in the electronic excited state (the example in figure 2.15 illustrating the most overlap with the state v'=3) and several bands will be seen on the resulting spectrum.

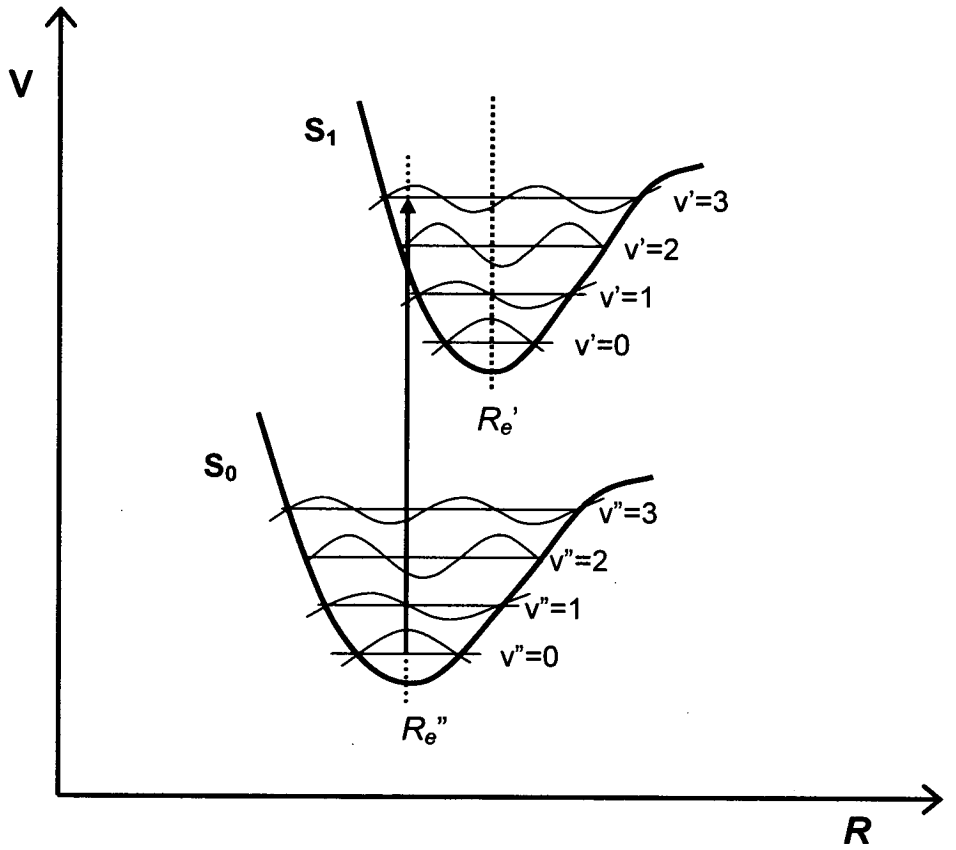

Figure 2.15: *Potential energy diagram representing excitation between two states with dissimilar nuclear geometry; $R_e' > R_e''$.*

It is in such cases that vibrational progressions are seen, with an increase in vibrational structure observed as the relative displacement of the potential energy curves increases.

2.2.4. De-excitation Processes

2.2.4.1. Radiative Decay

An electronically excited molecule is unstable and will readily surrender its excess energy. There are many processes by which this may occur, several of which are illustrated in figure 2.9. In this thesis the process primarily of interest is fluorescence. However, decay of an excited species is the result of several processes, which are listed with the corresponding first order rate constants.

Fluorescence	$^1M^* \rightarrow M + h\nu$	k_r
Intersystem Crossing	$^1M^* \rightarrow {}^3M$	k_{ISC}
Internal Conversion	$^1M^* \rightarrow {}^1M$	k_{IC}
Dissociation	$^1M^* \rightarrow$ products	k_D
Quenching	$^1M^* + Q \rightarrow {}^1M + Q$	k_Q

The general process of radiative de-excitation, *i.e.* fluorescence, of an excited molecule M* as it decays back to the ground state can be written as

$$M^* \rightarrow M + h\nu \quad \textbf{2.22}$$

where $h\nu$ is the quantum of electromagnetic radiation emitted equal to the energy separation between the ground and excited electronic energy levels.

This process occurs with first-order kinetics such that

$$-\frac{d}{dt}\left[M^*\right]=k_r\left[M^*\right] \qquad \textbf{2.23}$$

Equation 2.23 can be integrated to show that M* decays exponentially to zero from initial concentration $[M^*]_0$ at t=0. Accordingly

$$\left[M^*\right]=\left[M^*\right]_0 e^{-tk_r} \qquad \textbf{2.24}$$

The radiative rate of decay is characterised by the lifetime, the natural lifetime of a radiative process being defined as

$$\tau_r^0=\frac{1}{k_r} \qquad \textbf{2.25}$$

Bearing in mind that the de-excitation process is the consequence of several processes, the fluorescence decay time, τ_F, can be expressed as

$$\tau_f=\frac{1}{k_r+k_{ISC}+k_{IC}+k_D+k_Q} \qquad \textbf{2.26}$$

As the concentration of molecules falls to 1/e of its initial value in a time $t=\tau_r^0$ (equation 2.25) the exponential decay of emission intensity, I(t), is

$$I_{(t)}=k_r\left[M^*\right]=k_r\left[M^*\right]_0 e^{-tk_r}=I_{(0)}\,e^{-k_r t}$$

and can be expressed in terms of τ_f as follows

$$I_t = I_0 e^{\frac{-t}{\tau_f}} \qquad \textbf{2.27}$$

The overall quantum yield, Φ, is the number of reactant molecules that react, in the case of fluorescence this is photon emission, per photon absorbed, and can be expressed in terms of the rate constants for all the processes occurring as follows

$$\Phi_f = \frac{k_r}{k_r + k_{ISC} + k_{IC} + k_D + k_Q}$$

$$= k_r \tau_f \qquad \textbf{2.28}$$

2.2.5. Internal Conversion and Intersystem Crossing

Internal Conversion (IC) and Intersystem Crossing (ISC) are two types of non-radiative (NR) decay of excited states that are of consequence when the principal de-excitation processes of interest are radiative. They occur without emission of a photon, and are ways in which a molecule converts between isoenergetic vibronic levels in different electronic states. During the process of internal conversion, spin multiplicity is conserved, the conversion being between *e.g.* $S_1 \rightarrow S_0$. An internal conversion occurs most readily where the two potential energy curves intersect as the nuclear geometries at this point are equivalent. During intersystem crossing there is a spontaneous change from one spin quantum number to another, and the conversion occurs between *e.g.* $S_1 \rightarrow T_1$. The singlet and triplet excited states have the same geometry at the point where their potential energy curves intersect. Therefore, if there is a process by which the two electron spins may be unpaired, converting the ↑↓ system to↑↑, intersystem crossing to a triplet state may occur. Singlet-triplet

transitions can occur in the presence of a moderately heavy atom, whereby spin-orbit coupling is large. Both systems, IC and ISC, are represented in figure 2.16.

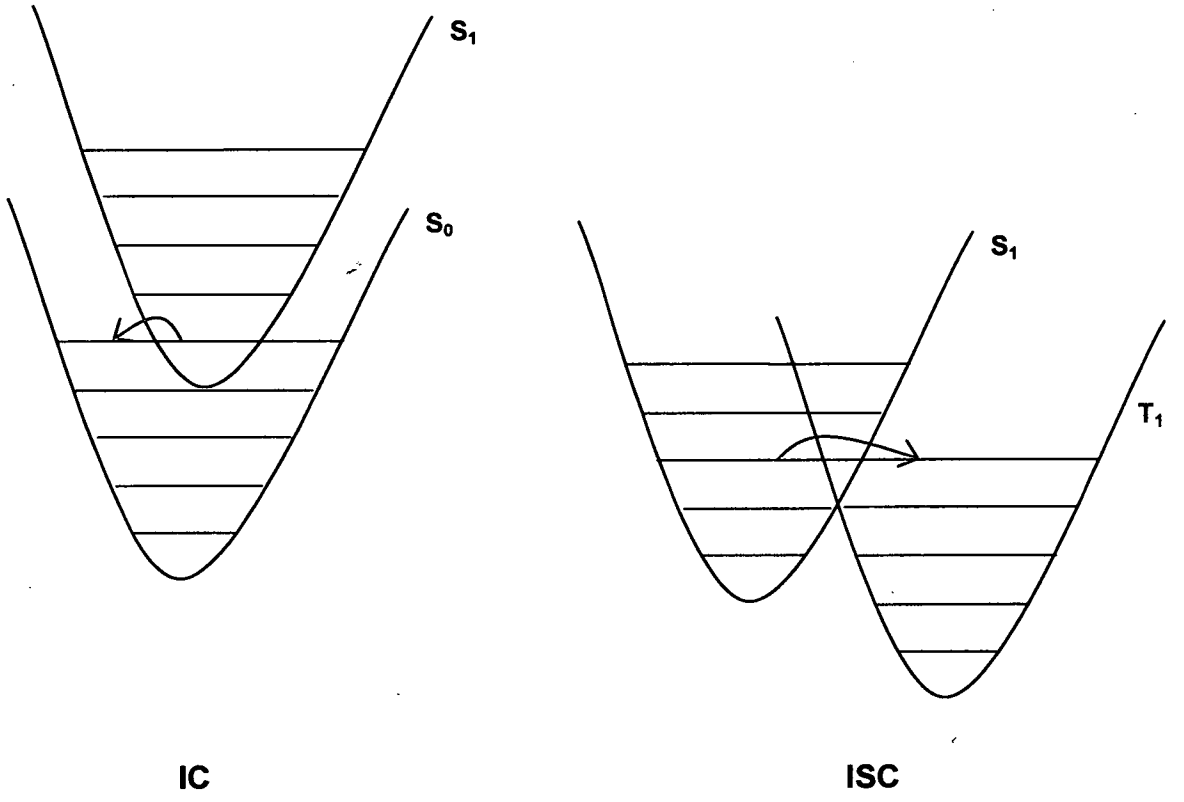

Figure 2.16: *Representation of Internal Conversion (IC) from S_1 to S_o and Intersystem Crossing (ISC) from S_1 to T_1*

2.2.6. Fluorescence

Luminescence, the process of most interest in photophysics, is the loss of excitation energy from the optically excited molecule that is seen as the emission of light, and falls into two categories: fluorescence and phosphorescence. Fluorescence results from a spin-allowed, singlet-singlet transition and phosphorescence is the result of the spin-forbidden triplet-singlet transition. The processes are illustrated in the Jablonski diagram, figure 2.17.

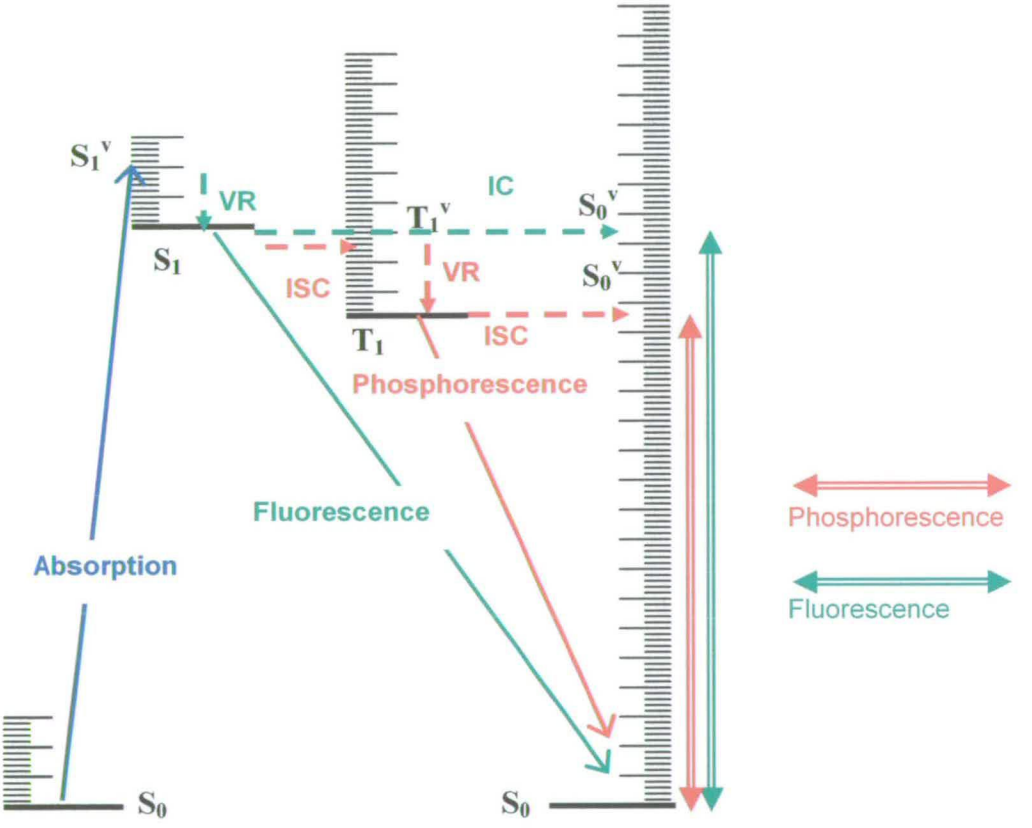

Figure 2.17: *Jablonski Diagram representing absorption and the emission processes of fluorescence and phosphorescence. IC = Internal Conversion, ISC = Intersystem Crossing, VR = vibrational relaxation. Superscript v denotes the vibrationally excited state*

In this thesis the process of interest is fluorescence.

Initially the molecule is in an excited electronic state, and there will also be occupation of different vibrational levels within the state. The molecule gives up some of its excess energy by collision with surrounding molecules, for example solvent molecules. This leads to radiationless decay as the molecule descends, or relaxes down, the vibrational energy levels in a process known as Vibrational Relaxation (VR) (figure 2.17).

The energy difference needed to lower the molecule to the ground state S_0 from S_1 may, however, be too large for the surrounding solvent molecules to accept. This leads to emission from the ground vibrational level of the S_1 state as the excess energy is emitted as light. In accordance with the Franck – Condon principle the transition to the GS is vertical, *i.e.* no nuclear reorientation occurs during light emission.

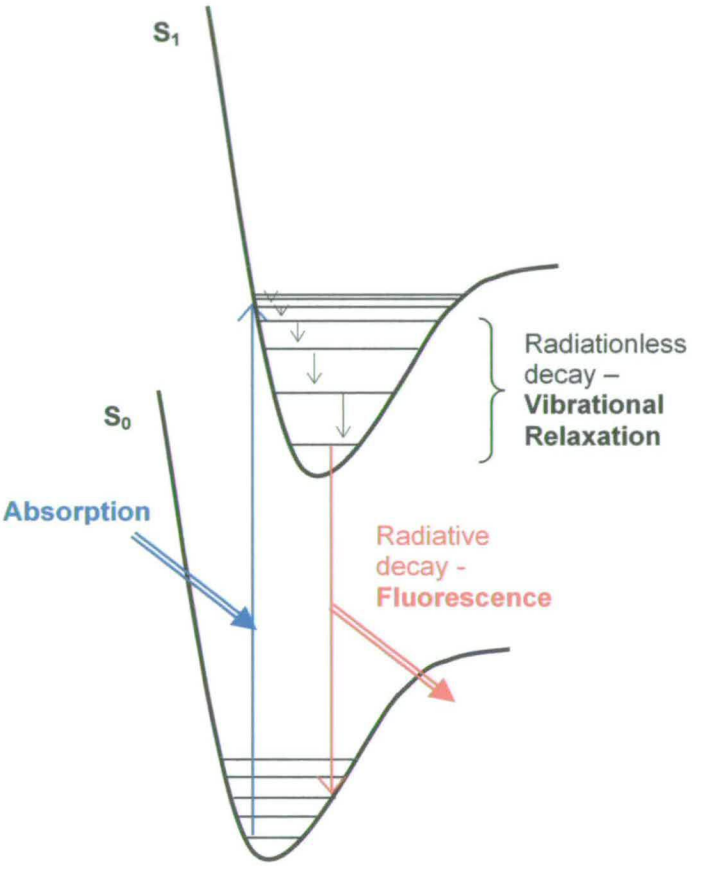

Figure 2.18. *The sequence of steps leading to fluorescence*

2.2.6.1. Steady-State Fluorescence Spectroscopy

In Steady-State (SS) fluorescence spectroscopy two kinds of experiment are typically carried out. These are emission acquisition and excitation acquisition. In the former the molecule is excited by light of fixed wavelength. The intensity of light emitted by the molecules is measured over a chosen emission wavelength range, resulting in a fluorescence emission spectrum. This shows lines due to the emission from the ground vibrational level of the S_1 state to various vibrational levels in S_0. That is, the vibrational interval is characteristic of the ground state. The latter experiment involves exciting the molecule with light of varying wavelengths and measuring the intensity of emitted light at a fixed wavelength. This absorption, or excitation, is from the v"=0 level in S_0 to different v' levels within S_1, and the resulting spectrum gives vibrational information for the excited state. These processes are illustrated in figure 2.19.

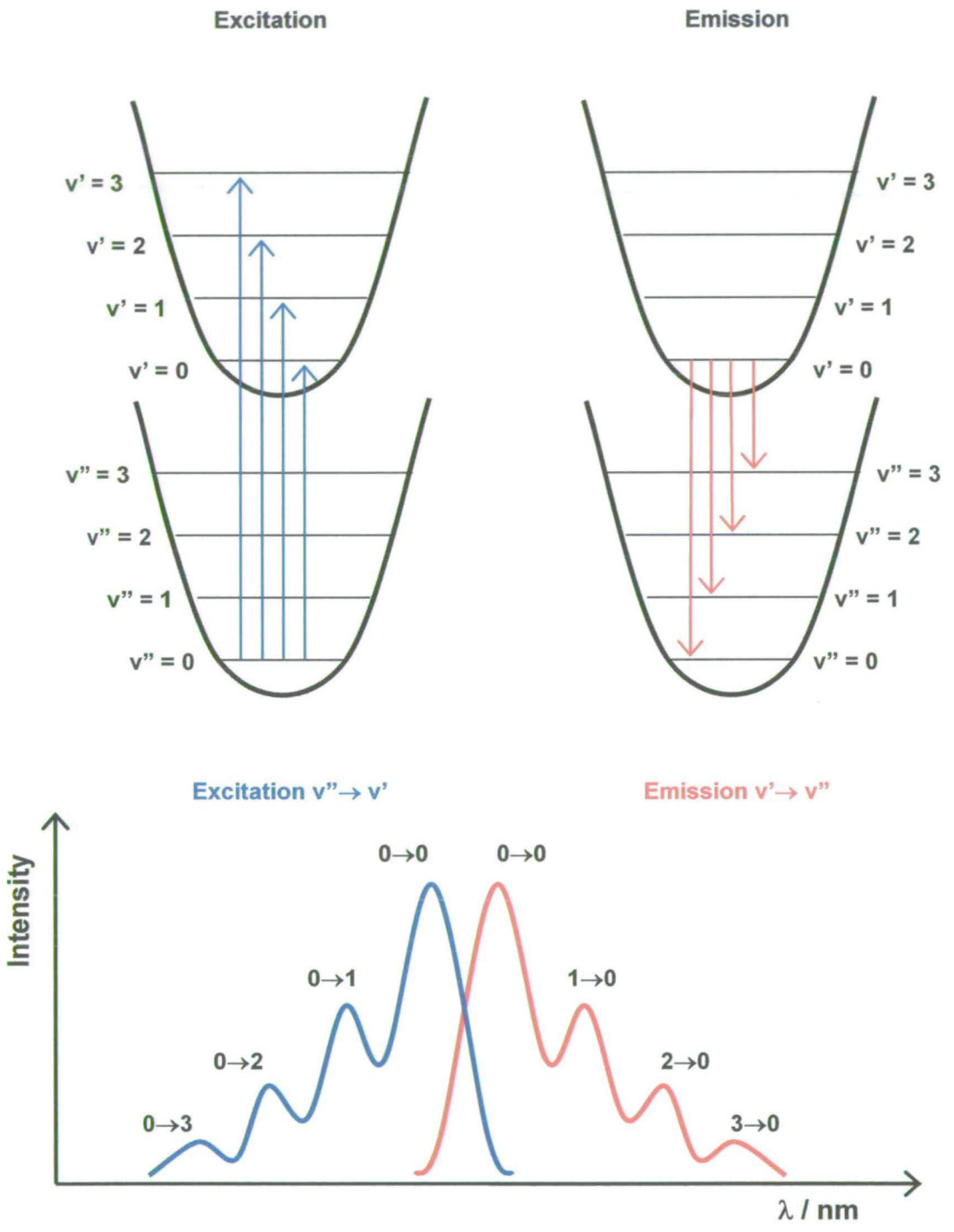

***Figure 2.19**: Representation of the transitions giving rise to the bands in fluorescence excitation and emission spectra*

It would be expected for the 0-0 transitions for both experiments to be coincident. However, in solution this is not always the case as the molecules interact with surrounding solvent molecules. Therefore the emission spectrum 0-0 transition occurs at lower frequency (longer wavelength) than the absorption spectrum. The intensity of the luminescence is also dependent on the solvent's ability to accept the extra energy.

Because fluorescence is a radiative transition between energy states of the same spin multiplicity, the transition is usually strongly allowed, and fluorescence lifetimes are generally in the picosecond to nanosecond range.

2.2.7. Time Correlated Single Photon Counting

Time Correlated Single Photon Counting (TCSPC) experiments can yield much information that cannot be gained from SS spectra alone. Whilst SS emission and excitation experiments give a profile of the overall fluorescence of a system, no information regarding the particular fluorophores can be obtained. Using TCSPC enables determination of the fluorescence lifetimes, the contribution of each component to the emitting population, and the contribution of each component to the SS emission.

TCSPC is a technique whereby a sample is excited by a laser pulse at λ_{ex} and the emitted photons are counted. One event, *i.e.* emitted photon, is counted per excitation pulse. Many excitations are performed, usually in excess of 10,000 counts are recorded, and a histogram of events versus time channels is built up. The count

rate is limited to less than 1% of the repetition rate to ensure that no more than one photon arrives at the detector per excitation pulse. This histogram of photon arrival times represents the intensity decay of the sample. In general, if the plot of log counts *vs.* time is linear, the component contains a single exponential whereas if it is non-linear it contains multiple components. The decay data can be fitted to a single, or multi-exponential function to yield the lifetimes.

Figure 2.20 Shows an instrument schematic of the system employed throughout this work.

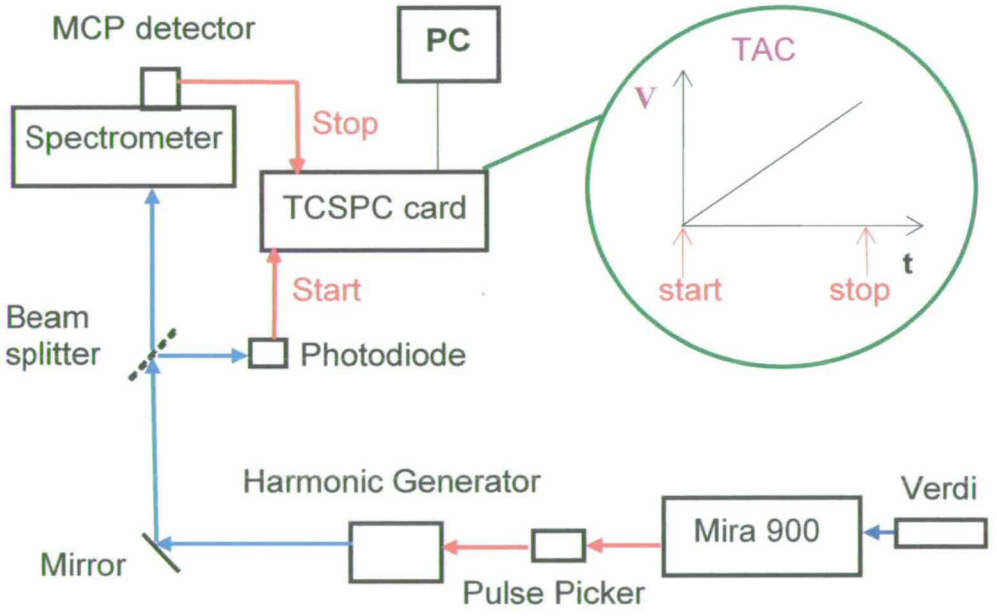

Figure 2.20: *Schematic diagram of the TCSPC set-up*

A non-tunable diode laser is used to pump the tunable, pulsed titanium:sapphire (Ti:sapphire) laser, which has a repetition rate of 76 MHz and a pulse width of 100-200 fs. As this is too rapid a repetition rate to obtain useful decays a pulse picker is used, which selects one out of sixteen pulses, hence reducing the repetition rate to

4 MHz. The Ti:sapphire laser is tunable over the wavelength range 720 to 1000 nm, and shorter wavelengths were obtained by frequency doubling or tripling the Ti:sapphire output to obtain the excitation wavelength required.

This excitation pulse passes through a beam splitter, part of the pulse being directed to the sample, part being reflected onto a photodiode, which produces a 'start' signal, triggering the voltage ramp of a time to amplitude converter (TAC).

The start signal and sample excitation occur simultaneously. The excitation pulse is vertically polarised. The emission from the sample passes through a polariser set at at 54.7 ° from the vertical, the magic angle, and the passes through a monochromator. A stop signal is triggered upon the detection of the first photon emitted from the sample. The detector is a microchannel plate photomultiplier tube (MCP PMT), which has a high time resolution. From here the photon passes to a constant fraction discriminator (CFD) and on to the TAC, whereupon the stop signal is triggered. The TAC provides an output pulse with a voltage proportional to the time between the start and stop signals and this voltage is converted to a time channel using an analogue-to-digital converter. This device can be considered analogous to a very fast stopwatch, and is capable of measuring events on a sub-nanosecond timescale.

2.2.7.1. Instrument Response Function and Convolution

Three curves are typically associated with an intensity decay; these are in terms of discrete times (t_k) as the photons are collected into channels, each of which has a

known time (t_k) and width (Δt). The three curves are the measured data $N(t_k)$, the Instrument Response Function (IRF) $L(t_k)$ and the calculated decay $n_c(t_k)$. The IRF is the response of the instrument to a zero-lifetime sample. This is narrow (FWHM 50 ps) and is collected using a dilute scattering solution and no emission filter, and it represents the shortest time profile that can be measured by the instrument. The data collected from the fluorescent sample is the intensity decay, $[N(t_k)]$. The calculated data, $[N_c(t_k)]$, is known as the fitted function. The fitted function represents a convolution of the IRF with the sample decay histogram. The decay time is the value of τ that provides the best match between the measured data and the fitted function.

The excitation of the sample does not occur on an infinitely small time scale. Molecules that are excited at the start of the pulse are decaying while others are being excited by photons in the tail of the pulse, and this leads to the phenomenon known as convolution. If there was δ-function excitation, and a δ-function for the instrument response then the Impulse Response Function $I(t)$ is what would be observed. However, due to the non-existence of such systems, the excitation pulses are considered to be a series of δ-functions of different amplitudes, each of which excites an impulse response from the sample with intensity proportional to the height of the δ-function. The measured data, $N(t_k)$, is the sum of all these decays, which start with different amplitudes at different times.

Consider an impulse response that is started at $t = t_k$, there being no emission before excitation (*i.e.* $t>t_k$). If each δ-function excites an impulse response at t_k then

$$I_k(t) = L(t_k)I(t-t_k)\Delta t \qquad \textbf{2.29}$$

Summing all the impulse responses created by the individual δ-function excitation pulses until t_k yields the measured decay $N(t_k)$,

$$N(t_k) = \sum_{t=0}^{t=t_k} L(t_k)I(t-t_k)\Delta t \qquad \textbf{2.30}$$

and where values of Δt are small, equation 2.30 can be expressed as an integral thus

$$N(t) = \int_0^{t'} L(t')I(t-t')dt' \qquad \textbf{2.31}$$

which describes the experimentally measured intensity at time t as the sum of the intensities expected for all the δ-function excitation pulses that occur until time t. New intensity decays are created in the sample as long as there is non-zero intensity in $L(t_k)$. In determining the lifetime, or lifetimes, of the sample it is necessary to determine the impulse response function $I(t-t')$ that best matches the experimental data.

2.2.8. Fluorescence Lifetimes

The decay of intensity of fluorescent emission is characterised by the radiative lifetime, τ, which is the time taken for the intensity to decay to 1/e of the initial intensity immediately after excitation. If a fluorophore is excited with an infinitely sharp pulse of light, the excited state becomes populated, and the initial population of

fluorophores in the excited state is n_0. The excited state decays with a rate k_r+k_{nr} according to

$$\frac{dn(t)}{dt} = -(k_r+k_{nr}) n(t) \quad \textbf{2.32}$$

where $n(t)$ is the number of excited molecules at time t following excitation, k_r is the emissive rate and k_{nr} is the non-radiative decay rate. Emission being a random event, every excited fluorophore has the same probability of emitting in a given time period. This results in an exponential decay of the excited state population,

$$n(t) = n_0 \exp(-t/\tau) \quad \textbf{2.33}$$

Rather than observing the number of excited molecules, a fluorescence intensity, which is proportional to $n(t)$, is measured. Equation 2.33 can be integrated and written in terms of the time-dependent intensity $I(t)$. For a single exponential decay this is expressed as

$$I(t) = I_0 \exp(-t/\tau) \quad \textbf{2.34}$$

I_0 being the intensity at t=0.

The lifetime, τ, is the inverse of the total decay rate, that is the sum of the rates that depopulate the excited state, hence

$$\tau = (k_r+k_{nr})^{-1} \quad \textbf{2.35}$$

In systems where many fluorophores are present the same premise can be employed, with the intensity being assumed to decay as the sum of the individual single exponential decays as follows

$$I(t) = \sum_{i=1}^{n} A_i \exp(-t/\tau_i) \qquad \textbf{2.36}$$

where τ_i are the decay times, and n is the number of decay times, and A_i are the amplitudes of the components at t=0, commonly referred to as the A-factors.

At t=0, $\exp(-t/\tau_i) = 1$; therefore the intensity I(0) will be the sum of the A-factors (plus a background value). The A_i values can be considered to represent the excited state population of the sample before any radiative or non-radiative interactions have occurred, and hence indicate the proportion of each component constituting the emitting population at a particular excitation wavelength. Multiplying the A-factor by the corresponding lifetime, $A_i\tau_i$, gives the percentage contribution of each particular component to the steady state fluorescence spectrum.

It is not possible to measure the exact number of fluorescing species in a sample, and the data fitting procedure produces the most probable values of A_i and τ_i for the data set. It is common practice to begin by using as few lifetimes as possible, adding more to improve the fit as needed. Adding more exponents will usually result in a better fit, so care and judgment need to be exercised. The fitting process is illustrated in appendix 1.

2.2.8.1. Quality of Fit Assessment

The goal, when fitting the data, is to obtain parameter values that provide the closest match between the data $N(t_k)$ and the calculated decay $N_c(t_k)$ using assumed parameter values. The goodness-of-fit parameter, χ^2, can be expressed as

$$\chi^2 = \sum_{k=1}^{n} \frac{1}{\sigma_k^2}\left[N(t_k) - N_c(t_k)\right]^2 \qquad \textbf{2.37}$$

where n=the number of channels, or data points for a particular analysis, and σ_k is the standard deviation (SD) for each point. From Poisson statistics it is known that σ_k=the square root of the number of photon counts,

$$\sigma_k = \left[N(t_k)\right]^{1/2} \qquad \textbf{2.38}$$

hence

$$\chi^2 = \sum_{k=1}^{n} \frac{\left[N(t_k) - N_c(t_k)\right]^2}{N(t_k)} \qquad \textbf{2.39}$$

For multiexponential decays the values of α_i and τ_i are varied until χ^2 is a minimum, which occurs when $N(t_k)$ and $N_c(t_k)$ are most closely matched. In this case, the quality of fit is assessed by the value of the reduced χ^2, as follows

$$\chi_R^2 = \frac{\chi^2}{\nu} \qquad \textbf{2.40}$$

where χ_R^2= reduced χ^2, ν=number of degrees of freedom. For a good fit, $\chi_R^2 \approx 1$.

2.2.8.2 Global Analysis

Global analysis involves simultaneously fitting several decays to one set of lifetimes. In this case decays that were recorded over different emission wavelengths but that were excited at the same excitation wavelength were fitted globally. Global fitting is a useful tool because, in a system with many components, if there seems to be some fluctuation in the lifetimes when fitting individually, globally fitting the lifetimes to one set of parameters will reveal whether the fluctuations are real or just down to different distributions.

The lifetimes obtained are global, but the α_i values vary with emission wavelength because of the different emitting populations at each emission wavelength. If across a particular wavelength region the same distribution of components is contributing to the emission then a global set of lifetimes will be obtained. The α_i values will differ because of their different contributions to the emitting population at different emission wavelengths. The χ_R^2 values are generally higher for globally than individually fitted data.

If a sample's decays do fit globally to one set of lifetimes then the variation in the A-factors, which give the contribution of each sample to the emitting population, and the percentage contributions to the steady state emission can be examined. This yields important information about the emitting species within the sample; for example, in a conjugated polymer system information about the relative conjugation lengths of the emitting species can be obtained.

2.3. Bibliography

The following texts were used in the writing of this chapter:

A. J. Bard and L. R. Faulkner, *Electrochemical Methods – Fundamentals and Applications, John Wiley & Sons,* 1980

A. C. Fisher, *Electrode Dynamics, Oxford Chemistry Primers, Oxford University Press,* 1996

P. W. Atkins, *Physical Chemistry fifth edition, Oxford University Press,* 1995

J. M. Hollas, *Modern Spectroscopy third edition, John Wiley & Sons,* 1996

J. R. Lakowicz, *Principles of Fluorescence Spectroscopy second edition, Plenum Publishers,* 1999

C. E. Wayne and R. P. Wayne, *Photochemistry, Oxford Chemistry Primers, Oxford University Press,* 1996

J. A. Barltrop and J. D. Coyle, *Excited States in Organic Chemistry, John Wiley & Sons,* 1975

A. I. M. Rae, *Quantum Mechanics third edition, Institute of Physics Publishing,* 1992

P. W. Atkins, *Molecular Quantum Mechanics – An Introduction to Quantum Chemistry, parts I-III, Clarendon Press,* 1970

D. V. O'Connor and D. Phillips, *Time-Correlated Single Photon Counting, London: Academic Press, 1984*

Chapter 3

Experimental

3.1. Materials

3.1.1. Monomers and Electrolytes

5-Cyanoindole (5CnI) (99%), Silver perchlorate ($AgClO_4$), (99%), Lithium perchlorate ($LiClO_4$), (99.99%), and 5-Bromoindole (5BrI) (99%) were obtained from Aldrich. NaCl (Analytical Reagent Grade) was obtained from Fisher. These chemicals were used as received. 5-Nitroindole (5NI), (99%) was obtained from Aldrich and was recrystallised from deionised water and dried in a vacuum oven at 70 °C for two days.

3.1.2. Solvents

Acetonitrile (MeCN) (HPLC grade, Fisher) and ethanol (EtOH) (spectrophotometric grade, Aldrich) were used as received. All water was doubly deionised by means of a Millipore water system.

3.2. Electrodes

For non-aqueous systems experiments were carried out in background electrolyte of 0.1M $LiClO_4$ / MeCN (for Potential Step Chronoamperometry (PSC) and Cyclic Voltammetry (CV) studies) using a three - electrode system comprising a Pt rotating disc electrode (area 0.387 cm^2, Oxford Electrodes Ltd.) as the Working Electrode (WE), a Pt gauze (area 2 cm^2) as the Counter Electrode (CE) and Ag / Ag^+ (+0.437 V w.r.t. Saturated Calomel Electrode; +0.681 V w.r.t. normal hydrogen electrode) as the Reference Electrode (RE). The WE was hand–polished using 3 μm alpha-

alumina (Buehler) in a water slurry on a soft cloth. The CE was cleaned by rinsing in acetone and burning in a Bunsen flame. The reference electrode was made in–house and consisted of a silver wire (1 mm diameter, 99.9%, Acros) dipping into a solution of 10 mM $AgClO_4$ / background electrolyte contained in a glass tube, separated from the bulk by a VYCOR frit. The electrolyte solution was degassed with N_2 for all experiments.

Experiments on aqueous systems (pH and metal ion response experiments) were carried out using a three–electrode system with the polymer–modified electrode as the WE, Potassium Chloride (KCl) SCE as the RE and the Pt gauze, as before, as CE. The electrolyte was 0.1 M NaCl / H_2O.

3.3. Apparatus

3.3.1. Electrochemistry

A modular potentiostat / galvanostat with a combined waveform generator and voltage source (Oxford Electrodes Ltd.) was used to carry out all electrochemical experiments. The rotating disc electrode was controlled using a motor controller (Oxford Electrodes Ltd.). Data collection was carried out on a PC using an Intelligent Instruments PC data acquisition card, the Visual Designer data control system (Burr-Brown) and an in-house software control program.

3.3.2. Spectroscopy

3.3.2.1. UV-Vis

UV-vis spectra were measured on a Unicam spectrometer using a matched pair of 1 cm pathlength fused silica cuvettes.

3.3.2.2. Steady State Fluorescence

Steady State (SS) fluorescence spectra were recorded on a Jobin Yvon Spex Fluromax Spectrofluorometer, using a 150 W continuous ozone-free xenon lamp as the excitation source. The data acquisition and manipulation were carried out on Instruments S.A. Datamax software on a PC. Fused silica cuvettes, 1 cm pathlength, were used for all measurements. A schematic diagram of the spectrofluorometer is shown in figure 3.1.

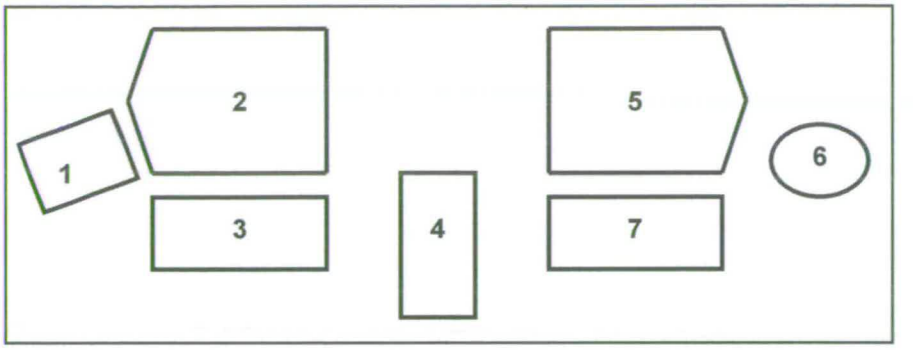

1 Illuminator
2 Excitation spectrometer
3 Sample compartment coupling optics
4 Sample compartment
5 Emission spectrometer
6 Emission detector
7 Electronic components

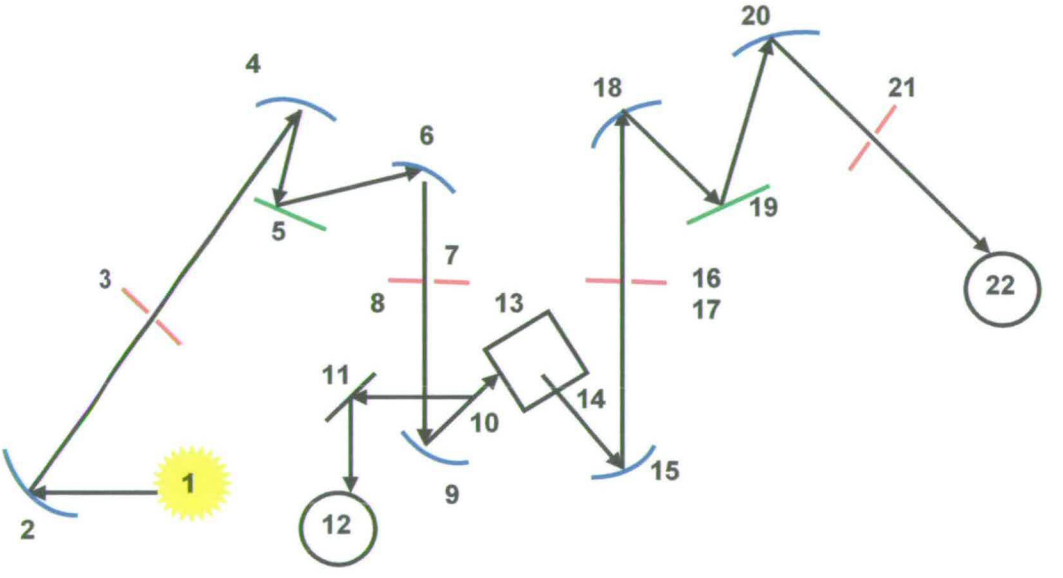

1 150 W ozone free lamp
2 Collection mirror (excitation spectrometer)
3 Entrance slit (excitation spectrometer)
4 Collection mirror (excitation spectrometer)
5 Grating
6 Focussing mirror (excitation spectrometer)
7 Excitation slit (excitation spectrometer)
8 Excitation shutter
9 Collection mirror (excitation spectrometer)
10 Beam splitter
11 Deflection mirror
12 Photodiode reference collector
13 Sample position
14 Window
15 Sample collection mirror
16 Emission shutter
17 Entrance slit
18 Collection mirror
19 Grating (1200 gr / mm)
20 Focussing mirror
21 Exit slit (emission spectrometer)
22 Emission detector

Figure 3.1: *Schematic diagram of the components of the spectrometer*

3.3.2.3. Time Correlated Single Photon Counting

Time correlated single photon counting (TCSPC) experiments were performed at the Collaborative Optical Spectroscopy, Micromanipulation and Imaging Centre (COSMIC) at the University of Edinburgh. The technique used is outlined in full in chapter 2. Samples were excited using a mode-locked Ti-Sapphire laser. Decays were recorded on an Edinburgh Instruments F900 TCSPC spectrometer incorporating a Hammamatsu R3809U-50 series microchannel plate. Fused silica cuvettes, 1 cm pathlength, (Starna) were used for all measurements. The data was acquired on a PC using Edinburgh Instruments F900 software, and data analysis was carried out on a PC using Edinburgh Instruments F900 software (for individual fits) and Edinburgh Instruments Level 2 software (for global fits).

3.4. Methods

3.4.1. Electrochemical Synthesis

Monomer solutions of different concentrations (20–10 mM) in background electrolyte (100 mM $LiClO_4$ / MeCN) were prepared and degassed by bubbling through with N_2 for 10 minutes prior to oxidation. Films were formed by Potential Step Chronoamperometry (section 1.3), stepping the potential past the oxidation potential of the particular monomer. The concentration of the solution and rotation speed of the RDE were controlled according to whether polymer– or trimer– rich films were required. A current / time transient was obtained for each polymerisation, from which the amount of charge in the film could be determined. Once prepared the films were rotated in background electrolyte to remove any remaining monomer

solution before further studies were carried out. Details for each specific sample are given in chapter 4.

3.4.2. Cyclic Voltammetry

The films were cycled in background $LiClO_4$/MeCN electrolyte to encourage linkage in certain films. The potential was swept between a lower and an upper limit at a scan rate, v. The data were logged on a PC with relevant software (section 3.2) and the current obtained was plotted as a function of the voltage, giving a cyclic voltammogram.

3.4.3. pH Response

Response of the films to changes in pH were carried out using galvanostatic circuitry at zero currents (Oxford Electrodes). Typically, the electrolyte was 0.1 M NaCl / H_2O. The electrode was rotated at 2 Hz to ensure thorough mixing of the electrolyte. The pH probe used was a standard glass pH electrode (Mettler Toledo Delta 320 Inlab® 405 combination pH; pH 0-14, 80 °C, 120 mm). Time response experiments were monitored on a PC with relevant software (section 3.2).

3.4.4. Fluorescence

3.4.4.1. Steady-State Fluorescence

Films produced were washed in background electrolyte and were typically dissolved into 10 ml EtOH. Further details are given in chapter 4. The fluorescence spectra were recorded on a Spex Fluoromax Spectrofluorimeter (section 3.3.2.2), using a

150 W Xe lamp. Emission and excitation spectra of the films were recorded, as well as a reading of the pure solvent for comparison. Emission spectra were recorded at the UV-vis absorption maximum initially, and then at further judiciously chosen wavelengths. Excitation spectra were recorded at fluorescence emission maxima.

3.4.4.2. Time Correlated Single Photon Counting

The samples of polymer films dissolved in EtOH were excited at λ_{ex}=360 nm or 450 nm depending on whether trimer or polymer excitation was required. Decays were recorded at wavelengths across the emission region of interest. See results chapters for further details. The TCSPC experimental set up is described in chapter 2 And 3.3.2.3.

Chapter 4

Preparation of Samples

4.1. Introduction

4.1.1. Polymerisation Conditions

The systematic electrochemical study of the polymerisation of 5-substituted indoles (and indole monomers substituted in certain other positions) in $LiClO_4$ / acetonitrile has been carried out previously[1,2,3,4,5,6,7,8,9] and it is known that these monomers can be polymerised reproducibly for a wide range of substituents, as discussed in chapter 1. As described in chapter 2, electropolymerisation of the monomer is carried out at or well past its peak oxidation potential to ensure mass transport control of the polymerisation process, maximising the concentration of indole radical cations at the electrode surface, to ensure maximum and reproducible coupling rate. The oxidation potentials of the monomers used throughout this thesis are shown in table 4.1.

Monomer	Oxidation Potential / V
5-cyanoindole	+1.64
5-bromoindole	+1.10
5-nitroindole	+1.70

Table 4.1: *Oxidation potentials of the 5-substituted indoles used with respect to Ag/Ag^+ (0.05 M)*

It is known that, when carrying out electrooxidation at a rotating disc electrode, indole radical cations form initially. These then cyclise to form the asymmetric indole trimer in the diffusion layer close to the electrode surface, as discussed in chapter 1.

$$3In \rightarrow (In)^{+}_{3} + 6H^{+} + 7e^{-} \qquad \textbf{4.1}$$

Deposition of the trimer onto the electrode surface follows, upon which further monomer can adsorb and oxidise, and hence further trimer units can be formed. Thus polymerisation is initially in solution (when increasing the rotation speed, W, decreases polymerisation efficiency) but then occurs via an adsorptive mechanism, where increasing W increases the amount of monomer arriving at the electrode, and hence increases the degree of polymerisation. In this regime, Koutecky-Levich behaviour is observed for polymerisation currents *vs.* concentration and $W^{-1/2}$ (figure 4.1, for 5-cyanoindole)[3].

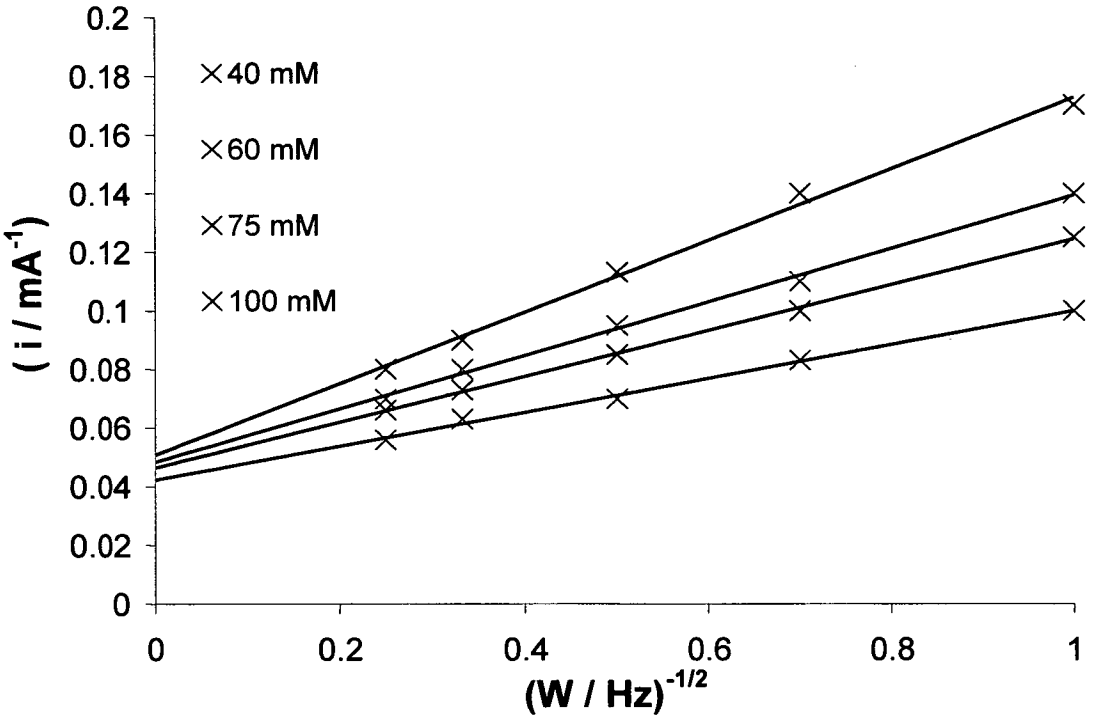

Figure 4.1: *Koutecky-Levich plots for the electropolymerisation of 5-cyanoindole from different monomer solution concentrations; data collected after the onset of steady-state currents*[3]

This means that control of W and concentration, C, enables precise and reproducible control over the coat composition. During the course of the polymerisation, in addition to new trimer units forming on the electrode surface, the trimer units already present can oxidise and link up with neighbouring trimer species. The extent of this linkage can be controlled by changing the polymerisation conditions, specifically the starting monomer concentration and the disc rotation speed. Using a relatively high starting monomer concentration (≥50 mM) and high disc rotation speed (*e.g.* 9 Hz) trimer-rich films are produced; conversely if a low starting monomer concentration (≤20 mM) and disc rotation speed (*e.g.* 1 Hz) are used then the rate of new trimer deposition is relatively low and there is more extensive linkage of the trimer units, hence polymer-rich films are formed.

Cyclic voltammetry (CV) was performed on the electropolymerised 5-cyanoindole and 5-bromoindole films to verify that the work carried out was consistent with previous work. Additionally, in the case of 5-bromoindole, it was used to cause extensive linkage in the film prepared for the free trimer fluorescence experiments as part of the linkage-and-extraction technique (chapter 7).

4.2. 5-Cyanoindole

Much work has been carried out on the electropolymerisation of 5-cyanoindole (figure 4.2)[3]. At an RDE it polymerises reproducibly, which allows facile control of the polymerisation process. During polymerisation, once the diffusion layer has been established and the electrode initially coated with film, (the time for which has been

shown to be proportional to $\frac{1}{W}$ (chapter 2)) steady-state currents are always produced. Typical i/t transients for the electropolymerisation from the same concentration monomer solution at different rotation speeds are shown in figure 4.2.

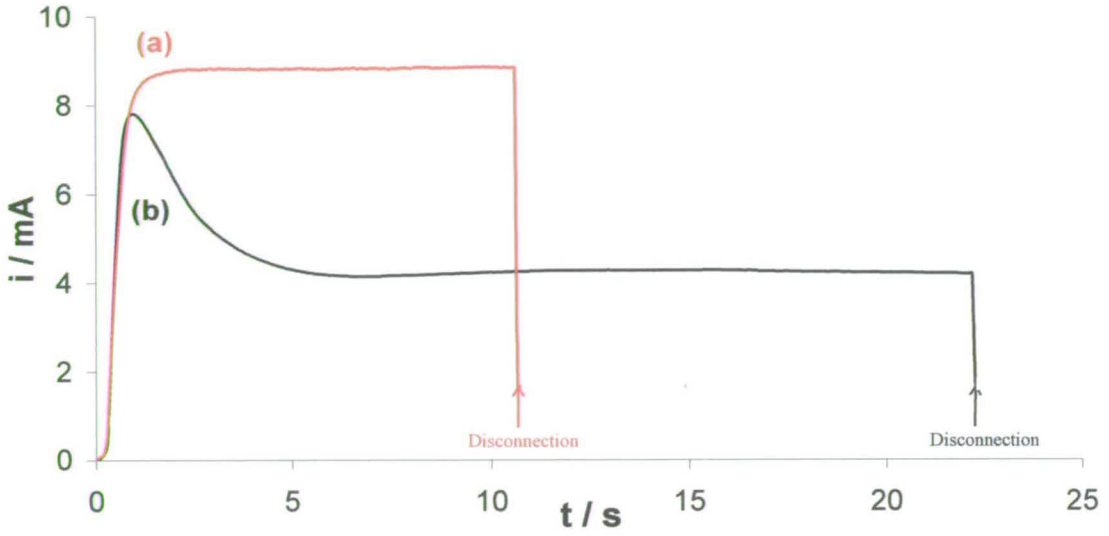

Figure 4.2: *Current / time polymerisation transients for 5-cyanoindole films polymerised from the same 20 mM monomer solution. (a) W=9 Hz (b) W=1 Hz*

It can be seen that higher rotation speed means that a higher steady-state polymerisation current is passed, consistent with the Koutecky-Levich behaviour seen previously[3]. Additionally using higher concentration monomer solution produces higher steady state currents for a given rotation speed. The currents observed are also in accord with those seen previously.

Cyclic voltammetry on the deposited films in background electrolyte also showed behaviour consistent with previous observations. For example, a poly-5CnI film prepared from 20 mM monomer solution at 1 Hz was cycled repeatedly at 50 mVs^{-1} in $LiClO_4$ / acetonitrile background electrolyte (figure 4.3).

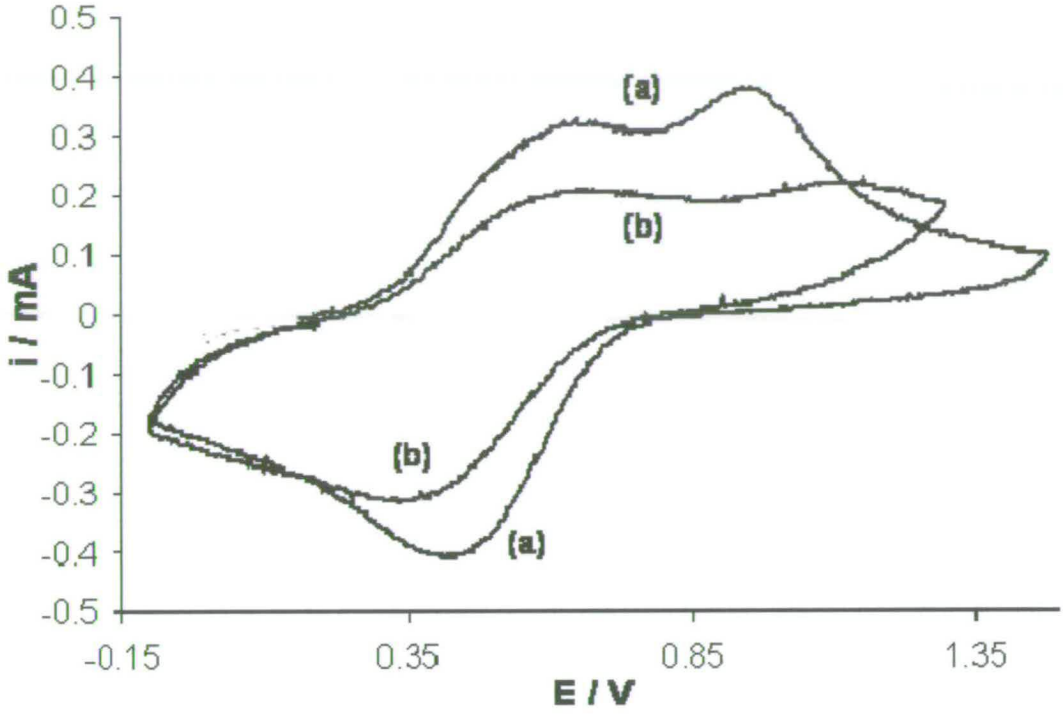

Figure 4.3: *Typical CV for a film of poly-5CnI on a Pt electrode in background electrolyte, sweep rate 50 mVs^{-1}. (a) First cycle (b) second cycle.*

Consistent with previous observations, if the cyclic voltammetry is performed up to around 0.8 V then only one set of redox peaks is seen, which can be attributed to the one electron redox reaction of the trimer centres in the film; this cycling can be carried on indefinitely with little change in peak positions or heights. However, cycling to higher potentials, as is the case here, causes a second irreversible oxidation peak to appear. Upon further cycling, and hence oxidation, the magnitude of this peak successively decreases. This is attributable to the irreversible intertrimer linkage reaction

$$nTr^{+} \rightarrow -[Tr]-_{n} + 2e^{-} + 2H^{+} \quad \textbf{4.2}$$

Thus the behaviour of 5-cyanoindole is consistent with results observed previously. For all experiments, integration of the currents with respect to time yields the charge passed, and hence the amount of material present. For example, integration of the polymerisation current with respect to time enables the polymerisation charge to be determined (see chapter 5) and assuming essentially 100% film formation, 1 redox electron would be expected for every 7 electrons passed during polymerisation if the coat remains unlinked, and for 1 for every 9 electrons in a totally linked film. Integration of polymerisation charge with respect to the redox charge under the CVs showed these results to be consistent with previous observations[1-9]. Furthermore, in this case, the total polymerisation charge, Q, (or redox charge) can simply be used to determine the total number of moles of indole monomer (or trimer) on the electrode interface, through

$$Q = nFm \qquad \textbf{4.3}$$

where n is the number of moles of electrons passed during reaction, and m is the number of moles of redox active species. Therefore, although a great deal of electrochemical characterisation has been carried out on these films to ensure reproducibility, as the film response is consistent with previous observations, it is only necessary to give the synthesis conditions, which can be used to determine film structure, and polymerisation charge, which determines the film thickness for subsequent data.

4.2.1. pH Response Samples

The samples for the work in chapter 5 were produced under the same electropolymerisation conditions to ensure that the same type of film was produced. However the polymerisation procedure was carried out for different lengths of time to produce both thick (1.37 μm) and thin (0.49 μm) films. In both cases samples were produced from a 50 mM solution of the monomer in $LiClO_4$ / acetonitrile electrolyte at W=2 Hz; the polymerisation times for thick and thin films were 12 s and 5 s, and the charges passed were 89 mC and 32 mC respectively. The films were rinsed to remove monomer and were transferred from the $LiClO_4$ / MeCN electrolyte to the NaCl(aq) electrolyte immediately after the preparation was finished; *i.e.* in their oxidised form without CV cycling so that they correspond as closely as possible to their as formed state.

4.2.2. Time Correlated Single Photon Counting Samples

The samples of poly-5-cyanoindole for higher / lower polymer comparison were prepared under the conditions shown in table 4.2.

Sample	Concentration / mM	W / Hz
Higher trimer	20	9
Higher polymer	20	1

Table 4.2: *The conditions used for sample preparation showing concentration of the original monomer solution used and disc rotation speed (W)*

The samples, once they had been prepared, were rinsed in MeCN to remove any monomer. The higher trimer and higher polymer samples were rinsed in MeCN to remove monomer and were then removed from the electrode entirely, and were dissolved in EtOH. Further details of the experimental procedure are given in chapter 6.

4.3. 5-Bromoindole

In contrast, the polymerisation of 5-bromoindole is less reproducible than that of 5-cyanoindole. Additionally the polymerised product can be seen to be much more soluble than the 5-cyanoindole with brown products being seen to dissolve from the electrode surface during polymerisation. This is consistent with a lesser degree of linkage, as typically the lesser the extent of the polymerisation the greater the solubility. On bare Pt, especially when using low monomer concentrations in an attempt to produce extensive film linkage during polymerisation, it was found that the current of the film dropped off, not reaching a steady state, and occasionally fell to zero. The currents obtained were also not as high as those obtained for the polymerisation of 5CnI under similar conditions. Figure 4.4 shows typical current / time transients for two poly-5BrI samples: a sample produced at high W and high concentration, and a sample produced at low W and low concentration.

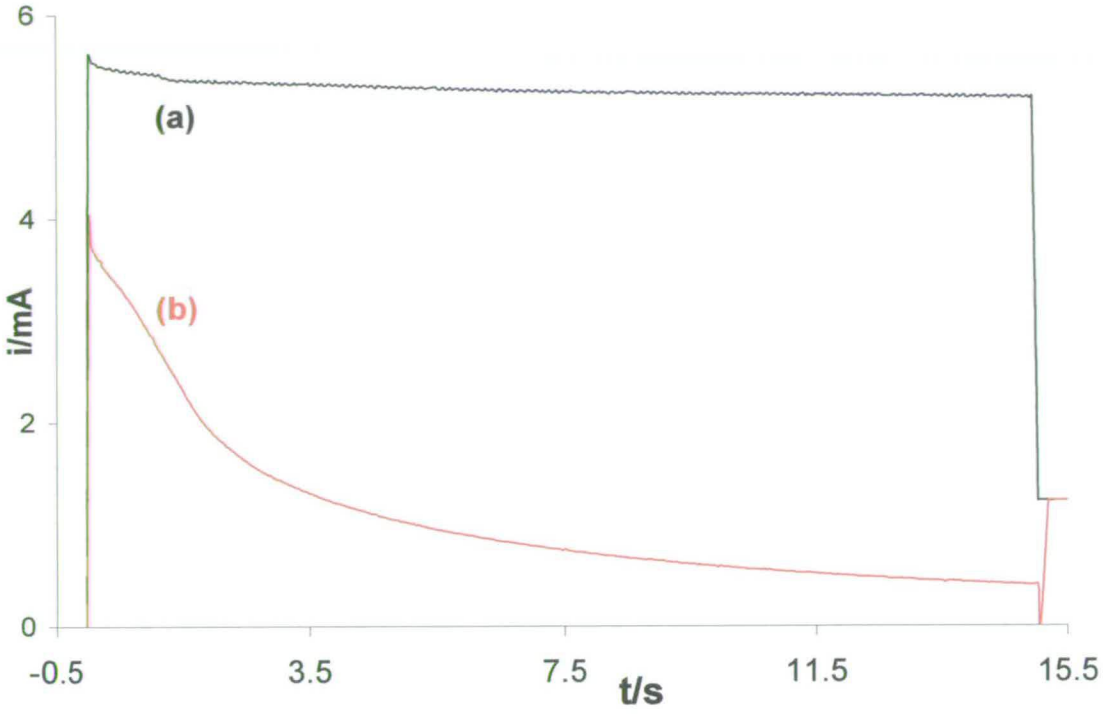

Figure 4.4: *Current / time transients for the polymerisation of 5BrI on polished Pt. (a) W=9 Hz, C=200 mM; (b) W=1 Hz, C=10 mM*

It is evident from the current / time transient of the low C, low W sample (figure 4.4 (b) that no steady state value is obtained, and the current falls steadily; additionally, although the current obtained for the high C, high W film figure 4.4 (a) is a steady-state value, it was not very reproducible. It is known that for some films using a template greatly improves the polymerisation[5] currents and reproducibility. This is attributed to the difficulty in initially forming a polymer layer when using pure monomer. However, polymerisation on a template avoids this; hence polymerisations were carried out on a template of electropolymerised poly-5NI (figure 4.5) to assess whether this is the case for 5-bromoindole, and allows polymerisation to immediately occur from the adsorptive mechanism which applies once a film has been formed.

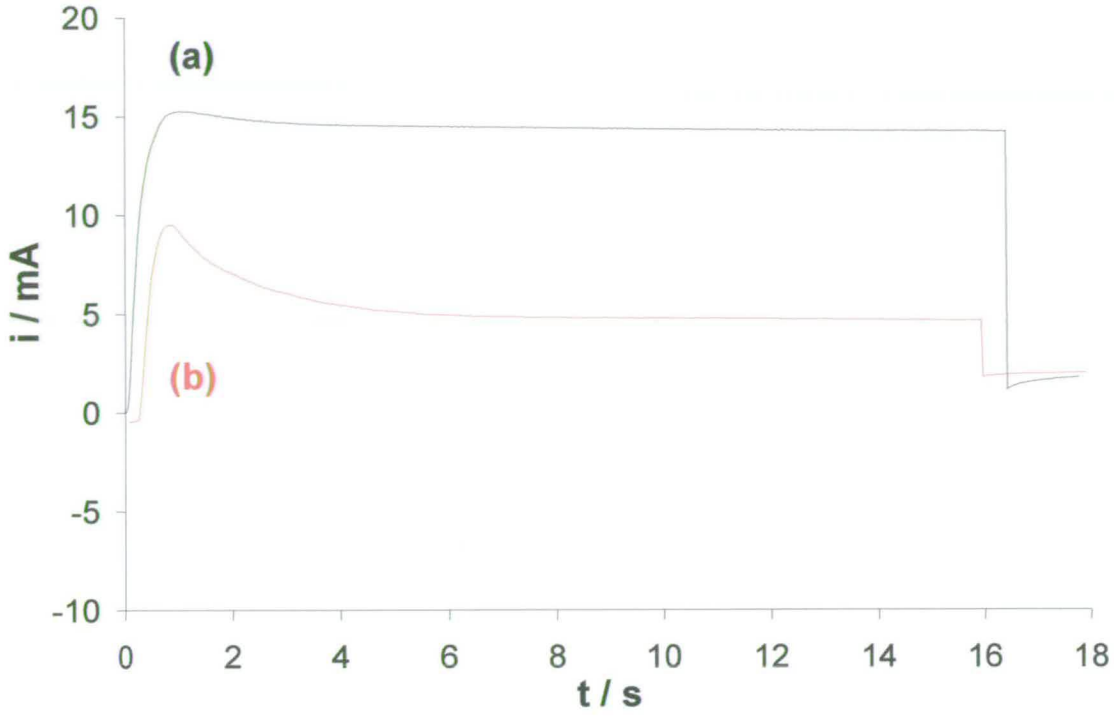

Figure 4.5: *Polymerisation of 5BrI on a poly-5NI template. (a)W=9 Hz, C=200 mM; (b) W=9 Hz, C=10 mM*

Typical data for these experiments are shown in figure 4.5. It can be seen, when comparing this with the previous figure, that the currents are higher and both reach a steady-state value. More importantly, the results are reproducible. Thus polymerisation of 5-bromoindole using a template produces the best film structure. However, the complication of the presence of additional indole trimers from the template film can be a disadvantage, particularly when carrying out fluorescence lifetime measurements of the polymer films. This is because, although 5-NI has been shown not to be fluorescent, it is likely that 5-NI may be an efficient fluorescence quencher, and may complicate the analysis of 5-bromoindole trimer fluorescence lifetimes (chapter 9).

Even allowing for the variation in absolute polymerisation currents found for 5-bromoindole on bare Pt, it is clear that there is a systematic dependence of the polymerisation current on rotation speed, with larger currents being observed at higher rotation speeds and monomer concentrations. Hence, the data are consistent with the variation in the polymerisation currents observed being due to variations in the integrity of the initially deposited 5-bromoindole film, and that once this is deposited across most of the electrode surface, a similar adsorption and deposition reaction is occurring as with 5-cyanoindole. Thus, high rotation speeds and high concentrations should still favour trimer-rich films, and low W and low C should still favour trimer linkage, *i.e.* the formation of polymer-rich films. Further details regarding the polymerisation conditions of all the 5-bromoindole samples are given in chapters 7, 8 and 9.

4.4. References

1. J.G. Mackintosh and A.R. Mount, *J. Chem. Soc. Faraday. Trans.*, 1994, **90(8)**, 1121-1125
2. J. G. Mackintosh C.R. Redpath, A.C. Jones, P.R.R. Langridge-Smith, D. Reed and A.R. Mount, *J. Electroanal. Chem.*, 1994, **375**, 163
3. J. G. Mackintosh, C.R. Redpath, A.C. Jones, P.R.R. Langridge-Smith, A.R. Mount, *J. Electroanal. Chem.*, 1995, **388**, 179-185
4. A.R. Mount, A.D. Thomson, *J. Chem. Soc., Faraday. Trans.*, 1998, **94(4)**, 553
5. P. Jennings, A.C. Jones, A.R. Mount A.D. Thomson, *J. Chem. Soc., Faraday Trans.*, 1997, **93(21)**, 3791-3797
6. J.G. Mackintosh, *PhD Thesis*, 1995, The University of Edinburgh
7. A.D. Thomson, *PhD Thesis*, 1998, The University of Edinburgh
8. M. Robertson, *PhD Thesis*, 1997, The University of Edinburgh
9. P. Jennings, *PhD Thesis*, 1999, The University of Edinburgh

Chapter 5

Poly-5-Cyanoindole as a pH Sensing Film

5.1. Introduction

Pt electrodes, modified with a conducting polymer layer, can be used to monitor the changes in the local pH of an electrolyte. There has been extensive research on the role of polypyrrole as an ion sensor. Polypyrrole films have been shown to undergo reversible changes in conductivity, and resistivity,[1] when treated with strong acids and bases. However, the work in this thesis is carried out on poly-5-cyanoindole (poly-5CnI) and uses potentiometric techniques, the benefits of which are described in section 5.2.2. Through early potentiometric studies on polypyrrole films, it was found that for a thin film (<2 μm) a linear gradient of -52.9 $mVpH^{-1}$ was obtained, but that this gradient decreased for thicker films (4-20 μm)[2]. Additionally, thin films showed good reversibility and linearity, with no significant hysteresis, and no dependence of the response on the direction of pH change. Thicker films, however, showed non-linearity and irreversibility[2]. It was initially thought that it was the NH units constituting the polymer chain that underwent protonation and deprotonation resulting in the pH response seen[2]; however more recent studies have shown that, whilst this protonation / deprotonation may contribute somewhat to the system's pH response, the pH response of polypyrrole films depends largely on the doping anion system present to balance coat electroneutrality[3,4].

Polyindoles, in contrast, have been investigated significantly. Initial work has been carried out on polyindole systems, primarily on poly-5carboxyindole[5,6] and poly-5cyanoindole[5]. The voltage response with change in electrolyte pH for both systems has been attributed to the protonation / deprotonation of the ring NH[7]. Poly-indole-5-carboxylic acid shows two distinct regions of similar gradient: approximately pH 2-6 and 9-10 for an uncycled film and approximately pH 3-5 and 9-10 for a cycled film. The gradient in the intermediate region (6-9 and 5-10 respectively) has been attributed to the fact that there are carboxylic acid moieties on the trimer units, which become deprotonated around pH=5 for the oxidised but not for the reduced form. It has been shown that addition of Pb^{2+} or Cu^{2+}, which complexes with carboxylate and precludes deprotonation, negates this phenomenon, and produces a linear E / pH response over a much wider pH range.

In contrast, poly-5cyanoindole has been shown to give a linear response over the pH range 2-10 with a gradient of -57 $mVpH^{-1}$ at 298 K. This is extremely close to the expected Nernstian gradient for a 1 proton, 1 electron reaction, and suggests little film inhomogeneity as $\beta \rightarrow 1$ (section 2.1.5). In this chapter the viability of poly-5cyanoindole as a practical pH sensor is therefore investigated, in particular the time-dependent response.

5.2. Experimental Procedure

5.2.1. Sample Preparation

Poly-5cyanoindole chemically modified electrodes (CMEs) were prepared by polymerising a layer of the selected monomer electrochemically (chapter 3). Samples were prepared to produce relatively thick and relatively thin films. In both cases samples were produced from a 50 mM solution of the monomer in $LiClO_4$ / acetonitrile electrolyte at W=2 Hz; the polymerisation times for thick and thin films were 10-12 s and 5 s respectively. After formation, the modified electrodes were rotated in 0.1 M $LiClO_4$ / acetonitrile background electrolyte for several minutes to remove unpolymerised monomer, and then were transferred from this electrolyte to 0.1 M NaCl aqueous electrolyte, in which the pH response experiments were conducted. If the changeover between the different solvent types was rapid, this resulted in the destruction of the film upon the electrode surface. This can be attributed to the considerable osmotic pressure, which indicates a rapid ingress of water[5]. To avoid this transfer was carried out thus: the polymer-modified electrode was placed in 20 ml of 0.1 M $LiClO_4$ / acetonitrile background electrolyte, and 1 L of 0.1 M NaCl (aq) was added dropwise over a period of several hours. 20 ml of this mixed-electrolyte solution was then retained and a further 1 L of 0.1 M NaCl (aq) electrolyte was added dropwise over several hours. Finally the CME was transferred to a pure 0.1 M NaCl (aq) electrolyte.

5.2.2. pH Response Experiments

The pH response studies of the modified electrodes were carried out using zero-current galvanometry (section 3.4.3). This ensures that no overall reaction takes place at the electrode, and the voltage change in response to a change in electrolyte pH was monitored. Changes in bulk pH were controlled by the drop-wise addition of dilute HCl or NaOH, and the bulk electrolyte pH was monitored using a standard glass pH electrode (sec 3.4.3).

This technique was deliberately chosen over the cyclic voltammetric technique employed previously. The main concern with the cyclic voltammetry technique is that it actually leads to large local changes in pH. During a CV the redox cycling leads to complete conversion of the coat on the electrode surface as it is oxidised and reduced; in this case the reaction produces and consumes protons

$$Tr_{RED} \rightleftharpoons Tr_{OX} + ne^- + mH^+$$

since for 5CnI m=n=1. With approximately 2 M of redox centres within an average film (section 5.5.2) the effect on local pH is considerable. This swamps the buffering capacity of the solution, especially around pH=7, and leads to substantial local changes in pH, which affects the film response. In the case of reduction protons are required from the solution to balance the charge within the film hence there are pH increases in solution local to the film / electrolyte interface as protons are taken in from the electrolyte by the film. Similarly, in the case of oxidation protons are expelled from the

film into the electrolyte causing large decreases in the pH local to the film surface. Using potentiometric techniques no current is drawn therefore there is no overall reaction; hence no such effects are seen and the film response as a function of local pH can be assessed. Additionally, in real life a pH sensor would have to be straightforward to use, and, as this technique enables a direct, linear correlation between voltage and bulk electrolyte pH its practical simplicity is evident.

5.2.3. Response Time Experiments

For a useable pH sensor it is important to know the fundamental response time to changes in electrolyte pH for thick and thin films, as this may determine the overall rate of sensor response. 0.1 M NaCl electrolytes were prepared at acidic and neutral pHs, *i.e.* pH $\approx$ 3 and pH $\approx$ 7, and between experiments the electrolytes were bubbled with N_2 to minimise CO_2 influx and the amount of dissolved CO_2. The thick and thin CMEs were prepared and transferred to the NaCl electrolyte as outlined in section 5.2.1. For each coated electrode the potentiometric response was initially measured at the starting pH (neutral or acidic) whilst rotating to ensure equilibration of the film for 10 minutes. Data logging was then commenced, whereupon the electrode was removed and inserted into an electrolyte solution of the final pH (acidic or neutral as appropriate). The voltage change was logged against time using an in-house PC logging program written using Visual Designer software (Burr Brown) (sec 3.3.1). The bulk electrolyte pH was also monitored using a standard glass pH electrode (3.4.3). The process was repeated for

each film, going from acidic to neutral and from neutral to acidic electrolyte, and at different rotation speeds.

5.3. Response of Bare Pt Electrodes to Electrolyte pH Change

Although polymers of substituted indoles respond to pH change, it is crucial that the monitored response is characteristic of the polymer film. Platinum electrodes are known to respond potentiometrically to changes in pH[8,9,10,11,12]. It has been reported that the pH response of bare Pt is linear over the pH range 3 to 11, with the gradient ranging from -47 $mVpH^{-1}$ to -53 $mVpH^{-1}$ dependent on the surface treatment[8]. For comparison with the CMEs the pH response of a Pt RDE was measured (figure 5.1). Prior to the experiment the electrode was polished as outlined in section 3.2, and rinsed thoroughly in water.

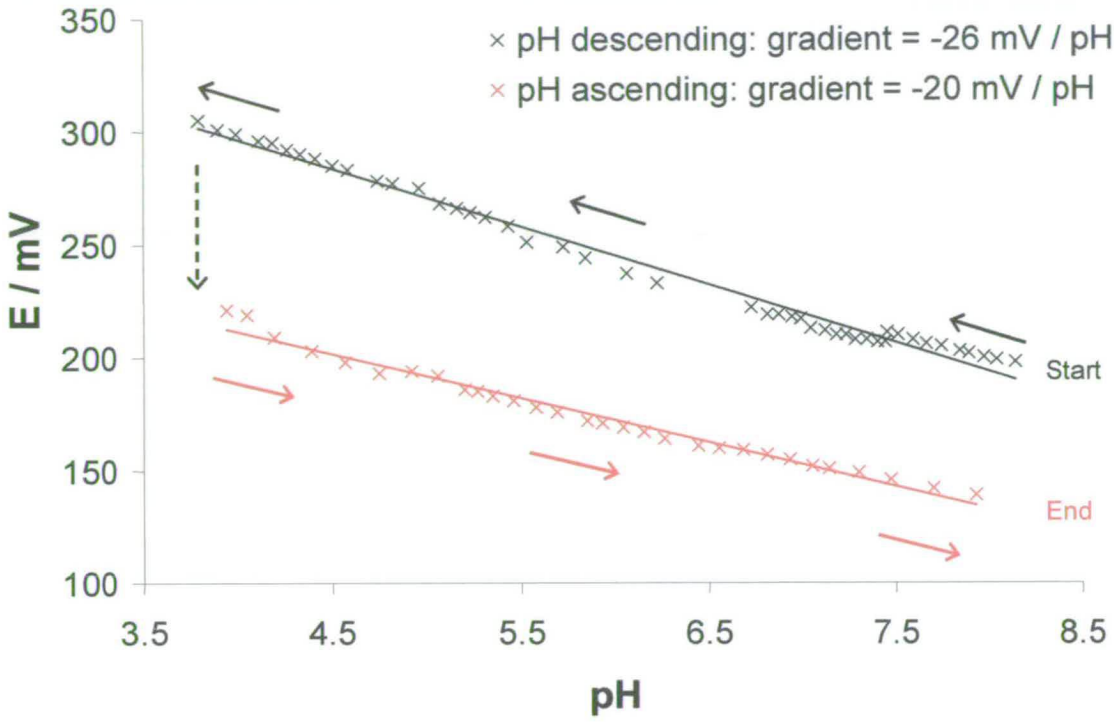

Figure 5.1: *pH response of the bare platinum electrode in 0.1 M NaCl electrolyte for descending and ascending pH*

Figure 5.1 shows the response is essentially linear but does not display a Nernstian slope, its gradient being -20 $mVpH^{-1}$ for ascending and -26 $mVpH^{-1}$ for descending pH. This gradient is in contrast with results for previous work, where the E / pH gradient of a polished Pt electrode was found to be -47 $mVpH^{-1}$.[8] In addition there is a considerable change in intercept at low pH, which leads to a marked difference in E values for ascending and descending measurements. It is known that the bare Pt electrode is susceptible to oxidation, and a layer of platinum oxide forms upon the electrode surface, the protonation and deprotonation of which has been suggested as the origin of the pH effect[8].

However, it is also possible that redox active species in solution whose reaction involves H^+ may also contribute to the pH response. These results demonstrate that the protonation / deprotonation reaction is not well defined, and that Pt electrodes are not good pH sensors under these conditions.

5.4. 5-Cyanoindole CMEs

As has been discussed in chapter 1, the structure of poly 5CnI is known to be a conjugated chain of trimer units. It has been suggested that these are linked via 2 of the N atoms, leaving one unlinked NH group per trimer unit. One possible structure for this linked species is shown in figure 5.2.

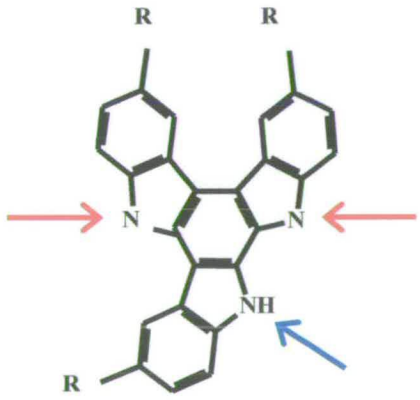

Figure 5.2: *One possible structure of 5-substituted indole linked trimer. Red arrows indicate possible linkage positions, blue arrow indicates site for protonation / deprotonation*

In this case, the remaining NH is the most labile group and can be assumed to be the 'active' site, where the deprotonation, or protonation, occurs with increase, or decrease, respectively, in environmental pH. Thin and thick films of poly-5CnI were prepared (chapter 4) on bare, polished Pt passing charges of 32 and 89 mC respectively. A

reasonable estimate of the volume occupied by the indole trimer molecule can be obtained from the crystal structure of 5-bromoindole trimer[13]. This is 860 $Å^3$ $molecule^{-1}$. Assuming complete formation of the poly-5CnI film, 9 electrons are required to form each trimer centre in the polymer film. In the case of the thin film, 32 mC corresponds to $\frac{32x10^{-3}}{9x96,485}=3.69x10^{-8}$ moles. Using the literature value of 860 $Å^3$molecule^{-1} as an estimate of the volume of the trimer unit, the volume of the film can be calculated as

$$860\ Å^3x(3.69x10^{-8})x(6.023x10^{23}) = 1.91x10^{-11}\ m^3$$

Given that the area of the electrode is 0.387 cm^2, *i.e.* $0.387x10^{-4}$ m^2, the thickness of the film can be calculated as

$$\frac{1.91x10^{-11}}{0.387x10^{-4}} = 0.49\ \mu m.$$

Similarly for the thick film, where 89 mC were passed, the thickness can be calculated as

$$\frac{0.49}{32}x89 = 1.37\ \mu m$$

It must be emphasised that the trimer volume is taken from a Bromoindole crystal, and hence this is an estimate of the film thickness. However, this gives a reasonable approximation of the film's thickness, and any error will be systematic, so the relative thickness of the thick and thin films will be accurate.

CME washings and transfers were then carried out as described in section 5.2.1; pH response experiments were performed straight after transfer and were repeated after 1 week. It was found that there was little difference between these experiments, indicating the stability of the indole pH sensor system.

5.4.1. Change in E with Electrolyte pH

The change in electrode potential was measured for increasing and decreasing pH over the range pH≈3 to pH≈10 for a stationary electrode coated with poly-5-cyanoindole. Typically a linear plot was obtained (figure 5.3) with a slope of 57 $mVpH^{-1}$, which is the Nernstian slope expected for the 1 proton, 1 electron reaction, showing that $\beta=1$ for the coat (chapter 2). The gradient remained the same irrespective of both the length of time the CME had been immersed in the NaCl electrolyte, and the direction of change of pH. Thick and thin films also exhibited the same gradient in these experiments. The time to equilibration of the film in these experiments appeared to be comparable with that of the glass electrode. Additionally, little or no shift in intercept with time was observed.

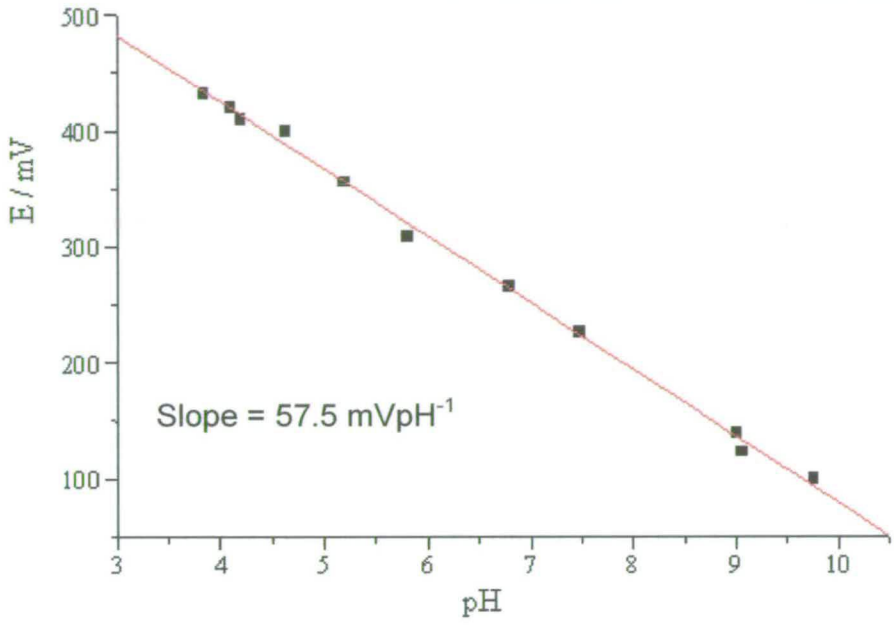

Figure 5.3: *pH response of a thin poly-5CnI – coated Pt electrode*

That the 5CnI CMEs give a linear voltage response to bulk electrolyte pH change is consistent with the hypothesis that during the redox reaction

$$\mathrm{Tr}(s) + \mathrm{e}^- + \mathrm{H}^+(aq) \rightleftharpoons \mathrm{TrH}(s)$$

there is exchange of 1 proton and 1 electron at the protonation site. Recalling equation 2.19

$$E = E' + \frac{mRT}{nF} pH$$

and if m=n then $\frac{RT}{F} = 59 \ \ mV$ at 298 K. As the redox reaction of the trimer involves 1-electron, *i.e.* n=1, the Nernstian behaviour of this system indicates that m/n =1, hence m=1. This is consistent with the supposition that the trimers link via two of the ring nitrogens, with one remaining unlinked and available for protonation / deprotonation.

5.5. Time of 5CnI Response

5.5.1. Results

A vital criterion for a reliable, workable pH sensor is its rapidity of response to change in the concentration of H^+, or OH^-, ions in the bulk electrolyte. A good pH sensor must respond rapidly to the changes in the surroundings to be of practical use. Hence, once the linear response of the poly-5CnI CMEs to changes in electrolyte pH was established, the rapidity of this response was investigated. The responses of poly-5CnI CMEs were tested at different disc rotation speeds, changing from both acidic to neutral and neutral to acidic media. The electrode was transferred from one electrolyte to the other while still rotating to enable the fastest possible transient. The time taken for the potential of the film to respond to the change in electrolyte pH was monitored until a steady-state potential value, which was characteristic of the final bulk electrolyte pH, was obtained. Figures 5.4 and 5.5 show typical voltage *vs.* time transients for the thick and thin films at rotation speeds W=0, 1, 2, 4 and 9 Hz. The experiments were carried out as described in section 3.4.3.

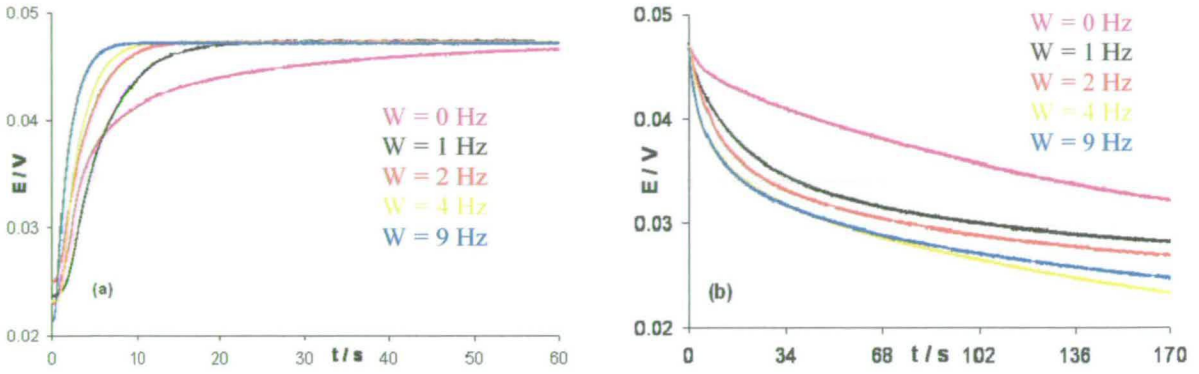

Figure 5.4 *E vs. t transients for thin 5CnI CME: (a) Neutral to acidic electrolyte; (b) Acidic to neutral electrolyte*

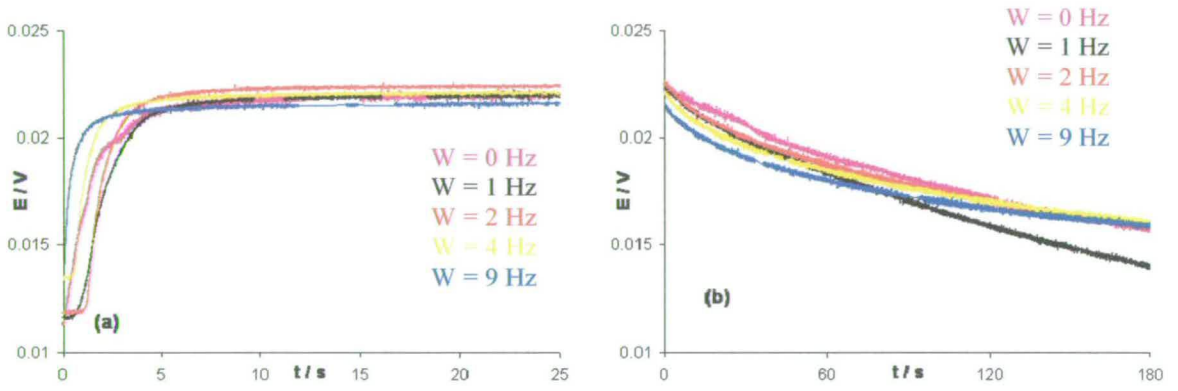

Figure 5.5 *E vs. t transients for thick 5CnI CME: (a) Neutral to acidic electrolyte; (b) Acidic to neutral electrolyte*

It is clear that the response time to the pH change decreases for both films as the rotation speed increases. This demonstrates that mass transport to and from the modified electrode is important in determining the response time. As the rotation speed, and hence proton flux, increases the mass transport of protons to and from the film increases, and the response becomes more likely to give the actual rate of response of the coat.

Another observation, which also holds true for both films, is that transfer from a neutral to an acidic medium the CME yields a faster response than going from an acidic to a neutral solution. Although true for both films, these observations are more apparent for the thin films than the thick. However, as pH is a logarithmic scale, the concentration of protons in the acidic (pH≈3) solution is very much greater than in the neutral (pH≈7) solution. Therefore in order to assess the true rate of response of the film, quantitative analysis of the data is important.

5.5.2. Quantitative Analysis of pH Data

Figure 5.3 has established that at equilibrium poly-5CnI CMEs respond linearly and reproducibly to changes in pH, showing Nernstian response. Additionally, it can be seen from the E *vs.* t transients in figures 5.4 and 5.5 that increasing the rotation speed of the CME, hence increasing proton flux to the electrode surface, decreases response time. The simplest quantitative treatment assumes a fast 5CnI coat response to the local pH at the electrode surface. In this case, to treat these observations quantitatively, the following must be considered. The linear response, gradient g (-57 $mVpH^{-1}$ in this case), of the potential, E, to the change in the surface electrolyte pH can be represented thus (figure 5.6).

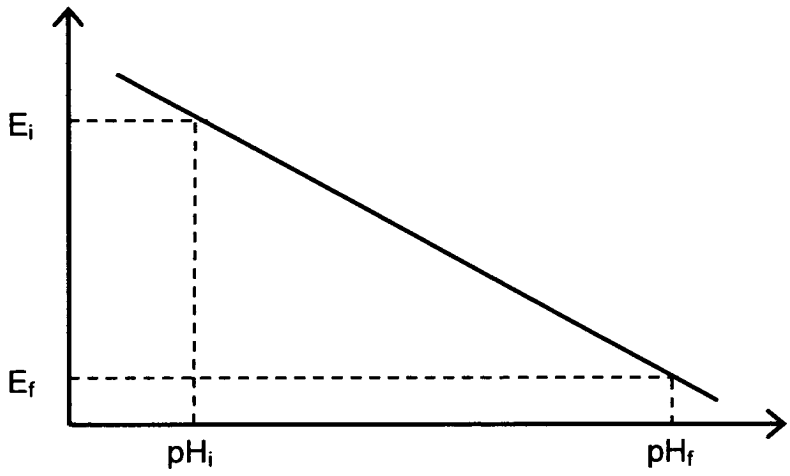

Figure 5.6: *Representation of any linear response in voltage to change in electrolyte pH*

where E_i, pH_i are the initial potential and pH respectively, that is the potential and pH before the response experiment, and E_f, pH_f are the final potential and pH respectively, that is the potential and pH at the end of the experiment where $t \rightarrow \infty$. In this case the fundamental expression that relates the local pH of the electrolyte at the electrode surface to the potential is, therefore,

$$E = E' - mpH \qquad \textbf{5.1}$$

where E' is a constant. The initial and final voltages can be expressed in terms of the corresponding pHs

$$E_i = E' - mpH_i \qquad \textbf{5.2}$$

$$E_f = E' - mpH_f \qquad \textbf{5.3}$$

Subtracting the expression 5.2 from expression 5.3 eliminates the constant E′, and an expression for the gradient, m, can be derived in terms of the potentials and pHs

$$E_f - E_i = m(pH_i - pH_f) \qquad \textbf{5.4}$$

$$m = (E_f - E_i) / (pH_i - pH_f) \qquad \textbf{5.5}$$

Assuming a fast coat response, at any time, t, equation 5.4 still holds and gives the pH at time t, pH_t; therefore if E_t and pH_t are the values of the voltages and pHs at time t, substituting $E_f \equiv E_t$ and $pH_f \equiv pH_t$ in equations 5.4 and 5.5 gives

$$E_t - E_i = ((E_f - E_i) / (pH_i - pH_f))(pH_i - pH_t) \qquad \textbf{5.6}$$

This can be rearranged to obtain an expression that can be used to calculate a value of local pH, pH_t, for any value of E, E_t, at any time, t

$$\Rightarrow pH_t = pH_i - \frac{(E_t - E_i)\,(pH_i - pH_f)}{(E_f - E_i)} \qquad \textbf{5.7}$$

From the E *vs.* t transients for 5CnI CMEs (figure 5.4 and 5.5), and using equation 5.7, the initial and final pH values recorded on the glass electrode, the initial voltage E_i, and each voltage measured, values of pH_t can be calculated from the E_t values recorded, hence plots of pH_t *vs.* t can be generated from the E *vs.* t data. It should be that these pH values correspond to the local pH measured by the CME at the electrode surface.

Values for pH_t corresponding to the measured data in figures 5.4 and 5.5 are shown in figures 5.7 and 5.8.

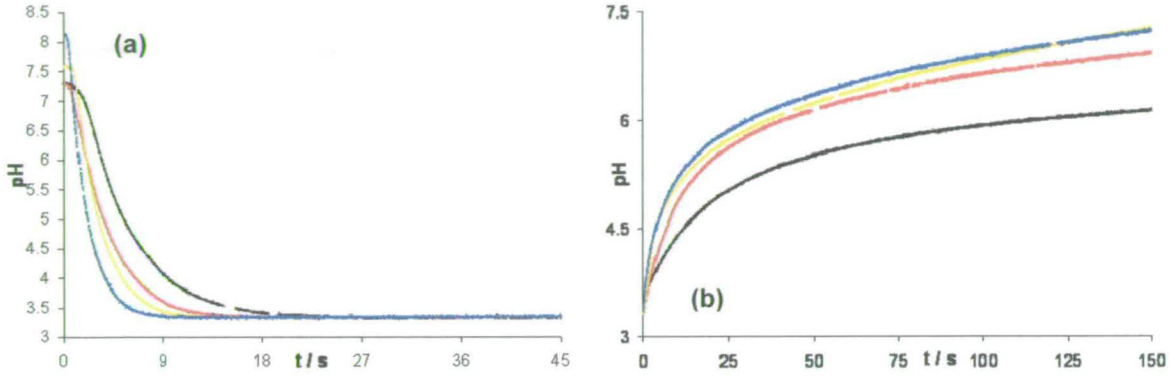

Figure 5.7: *pH vs. t plots for thin 5CnI CME. (a) Neutral to acid (b) Acid to neutral All W: W=1 Hz black plot, W=2 Hz red plot, W=4 Hz yellow plot, W=9 Hz blue plot*

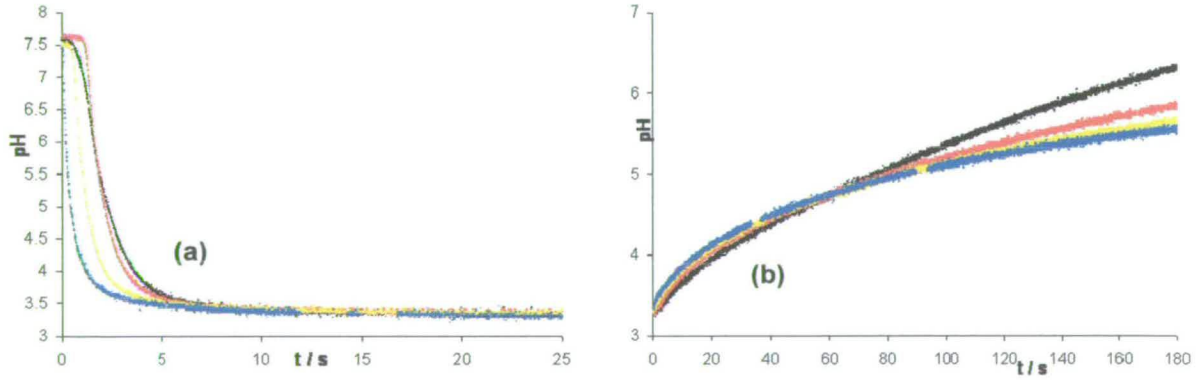

Figure 5.8: *pH vs. t plots for thick 5CnI CME. (a) Neutral to acid (b) Acid to neutral All W: W=1 Hz black plot, W=2 Hz red plot, W=4 Hz yellow plot, W=9 Hz blue plot*

At any time, t, the H^+ flux to the rotating disc electrode can then be calculated from the Levich equation[14]

$$j(t) = \frac{D}{x_D}(c_{H^+,\infty} - c_{H^+,0})$$

$$= 1.554 D^{2/3} \nu^{-1/6} W^{1/2} (c_{H^+,\infty} - c_{H^+,0}) \qquad \textbf{5.8}$$

where j = proton flux to the electrode surface ($molcm^{-2}s^{-1}$), D = diffusion coefficient of protons = 9.0×10^{-5} cm^2s^{-1}, ν = kinematic viscosity = 0.01 cm^2s^{-1}, W = rotation speed (Hz), $c_{H^+,\infty}$ is the concentration ($molcm^{-3}$) of H^+ in the bulk at any time t, $c_{H^+,0}$ is the concentration ($molcm^{-3}$) of H^+ at the electrode surface at any time, t. The concentrations of protons in the bulk and at the electrode surface, at any time, t, can be determined from

$$c_{H^+,\infty} = 10^{-(pH_f)} \qquad \textbf{5.9}$$

$$c_{H^+,0} = 10^{-(pH_t)} \qquad \textbf{5.10}$$

Hence at each time t a j(t) value for the flux can be calculated and plotted against t, giving a j vs. t transient for each experiment (figures 5.9 and 5.10). These data, calculated for the data in figures 5.4, 5.5, 5.7 and 5.8 are shown in figures 5.9 and 5.10.

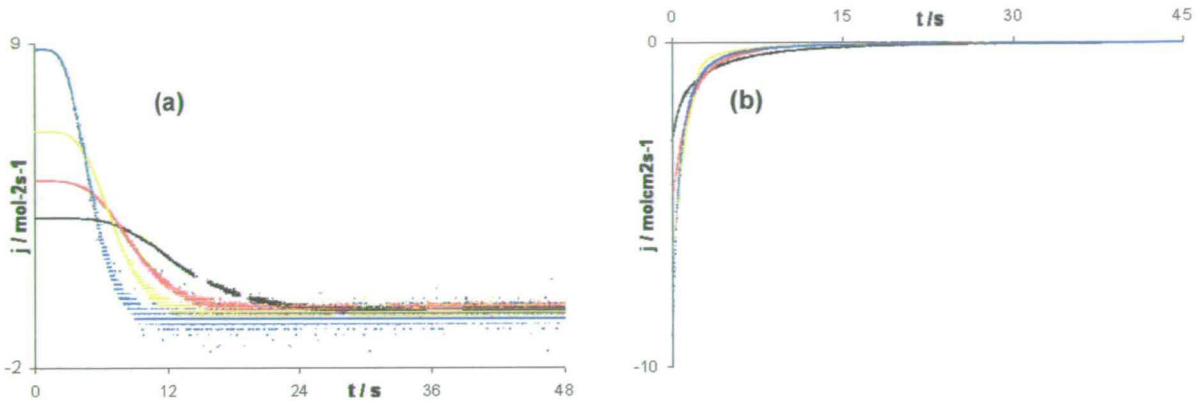

Figure 5.9: *Flux vs. time plots for thin 5CnI CME (j scale 1x10^{-9}). (a) Neutral to acid (b) Acid to neutral All W: W=1 Hz black plot, W=2 Hz red plot, W=4 Hz yellow plot, W=9 Hz blue plot*

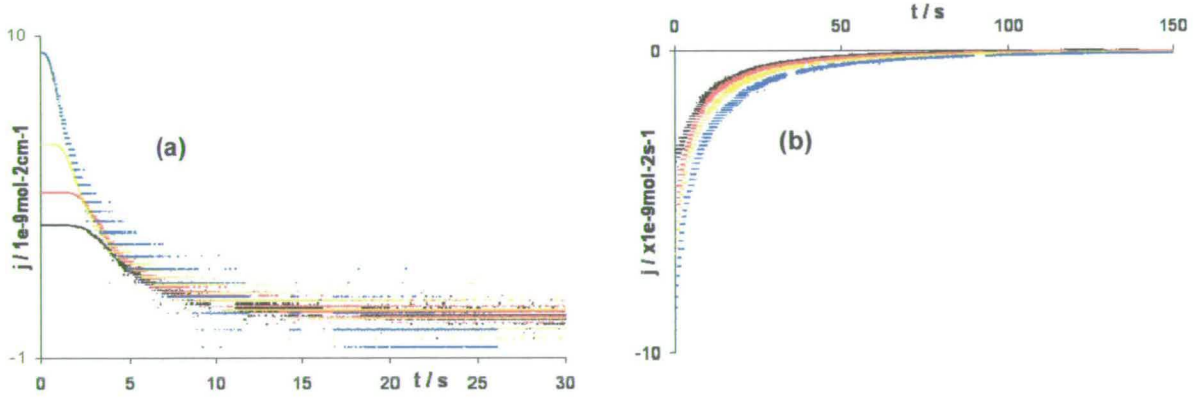

Figure 5.10: *Flux vs. time plots for thick 5CnI CME (j scale 1x10^{-9}). (a) Neutral to acid (b) Acid to neutral All W: W=1 Hz black plot, W=2 Hz red plot, W=4 Hz yellow plot, W=9 Hz blue plot*

From these data it is clear that, as expected, faster rotation speeds give rise to larger proton fluxes and faster coat protonation / deprotonation reactions. If the coat protonation / deprotonation rate was simply controlled by mass transfer of protons in

solution then it would be expected that $j \propto W^{1/2}$ through equation 5.8. Since protonation and deprotonation of each film should involve a fixed number of sites in the film, the total area under the j / t transients, which corresponds to the number of moles of protonatable sites in the film / cm^2, ought to be constant. Therefore $t \propto W^{1/2}$; hence, in this case, normalised plots of $jW^{-1/2}$ *vs.* $tW^{1/2}$ should lie on a common curve for each film.

It is clear for the data for the thin coat that this is the case for both acid to neutral and neutral to acid data (figure 5.11).

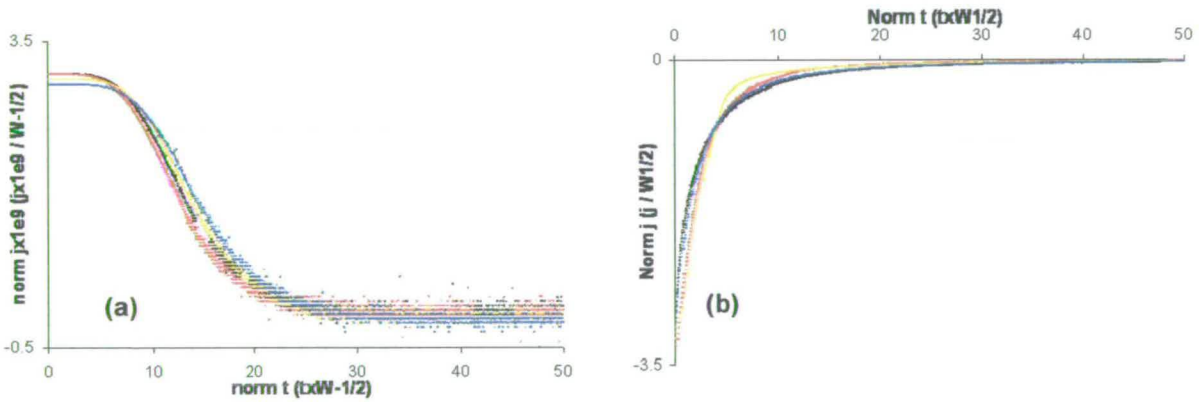

Figure 5.11: *Normalised j (x1e-9) vs. normalised t plots for thin 5CnI CME.*
(a) Neutral to acid (b) Acid to neutral
W=1 Hz black, W=2 Hz red, W=4 Hz yellow, W=9 Hz blue

This is strongly suggestive that the analysis assumptions are valid, and that coat protonation / deprotonation is fast, and that the rate determining step is simply mass

transport of protons to and from the film in solution. Therefore a thin (0.49 μm) film exhibits relatively fast switching kinetics.

When considering the thick (1.37 μm) film, however, it can be seen from the $jW^{-1/2}$ *vs.* $tW^{1/2}$ transients that at faster rotation speeds the normalised transients do not fall on a common curve, and are becoming progressively longer for both the acid to neutral and neutral to acid experiments (figure 5.12).

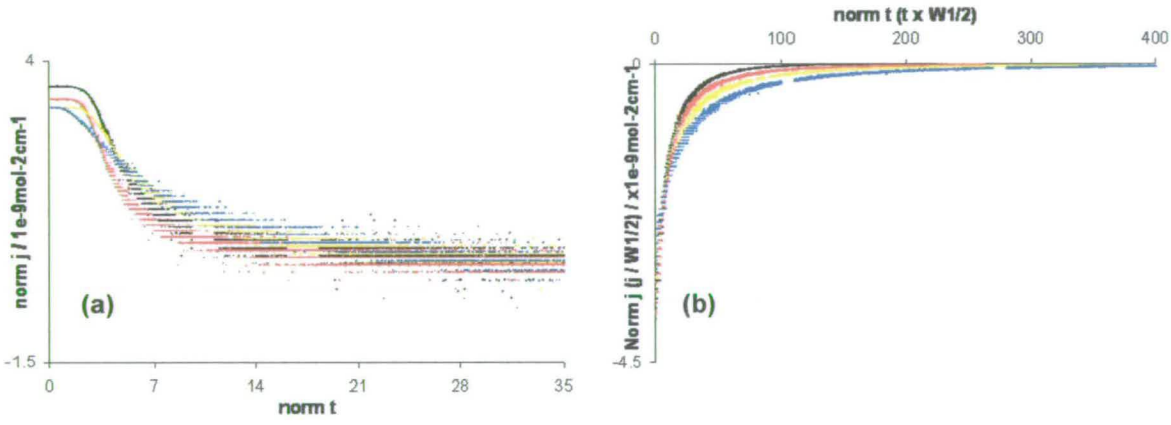

Figure 5.12: *Normalised j (x1e-9) vs. normalised t plots for thin 5CnI CME.*
(a) Neutral to acid (b) Acid to neutral
W=1 Hz black, W=2 Hz red, W=4 Hz yellow, W=9 Hz blue

This indicates that coat protonation / deprotonation rate is becoming significant at faster rotation speeds under these conditions.

Given that the thin film data is consistent with fast protonation / deprotonation of the film controlled by mass transport of H^+ to and from the film, a quantitative analysis of

the film response is possible. In this case the H^+ concentrations in the electrolyte solution and the 5CnI layer, thickness l, can be represented as in figure 5.13.

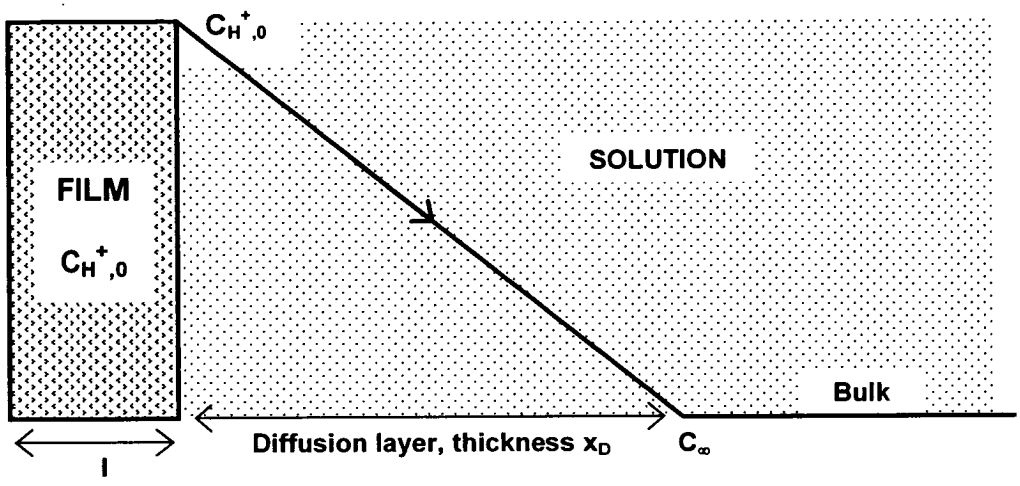

Figure 5.13: *Concentration of protons in CME and electrolyte solution*

In this case, a concentration gradient becomes established in the solution, $C_{H^+,0}$ being the concentration of H^+ at the electrode surface at any time t, and $C_{H^+,\infty}$ being the bulk concentration of H^+. As the coat response is fast, the concentration at the electrode surface can be assumed to be the same as the H^+ concentration within the film. Here there are indole trimer units, Tr (which are predominantly in their oxidised form because of the way in which the coat was made) that are in equilibrium with their protonated form TrH^+ through an equilibrium

$$TrH^+ \underset{}{\overset{K}{\rightleftharpoons}} Tr + H^+$$

The flux of the protons to / from the electrode causes a change in the film H^+ concentration, $C_{H^+,0}$. Given that most of these protons are removed from solution in the film by the back reaction above, it will generally require α protons to cause a change in the H^+ concentration in the coat (α=1 where there is no buffering; α>1 where buffering occurs). Here the change in $[H^+]$ in the film with time, $\frac{dC_{H^+,0}}{dt}$, can be related to the $[H^+]$ flux arriving at the electrode surface by the following equation, which relates the change in the total number of moles of free H^+ that appear in the film (LHS) to those that arrive due to j (RHS) (equation 5.8)

$$\alpha A l \frac{dC_{H^+,0}}{dt} = \frac{AD}{x_D}\left(C_{H^+,0} - C_{H^+,\infty}\right) \quad \textbf{5.11}$$

where A is the area of the electrode and l is the film thickness. Cancelling A and rearranging **5.11**gives equation **5.12,**

$$\frac{1}{\left(C_{H^+,\infty} - C_{H^+,0}\right)} dC_{H^+,0} = \frac{D}{\alpha l x_D} dt \quad \textbf{5.12}$$

which can be integrated with respect to $C_{H^+,0}$ and t to give

$$-\ln\left(C_{H^+,\infty} - C_{H^+,0}\right) = \frac{D}{\alpha l x_D} t + const \quad \textbf{5.13}$$

When t=0 then $C_{H^+,0}$ can be defined as $(C_{H^+,0})_{t=0}$, and hence

$$const = -\ln\left(C_{H^+,\infty} - \left(C_{H^+,0}\right)_{t=0}\right) \quad \textbf{5.14}$$

Substituting **5.14**into **5.13** and rearranging gives equation **5.15**

$$\ln\left(\frac{\left(C_{H^+,\infty} - (C_{H^+,0})_{t=0}\right)}{\left(C_{H^+,\infty} - C_{H^+,0}\right)}\right) = \frac{D}{\alpha l x_D} t \quad \textbf{5.15}$$

or

$$\left(\frac{C_{H^+,\infty} - C_{H^+,0}}{C_{H^+,\infty} - (C_{H^+,0})_{t=0}}\right) = \exp\left(\frac{-D}{\alpha l x_D} t\right) \quad \textbf{5.16}$$

From equation 5.8 the left hand side of this equation is given by $\frac{j}{j_0}$, where j_0 is the flux at t=0, hence

$$\left(\frac{j}{j_0}\right) = \exp\left(\frac{-D}{\alpha l x_D} t\right) \quad \textbf{5.17}$$

As j and j_0 are proportional to $W^{1/2}$ and $x_D \propto W^{1/2}$, this equation shows quantitatively that normalised plots of $\frac{j}{W^{1/2}}$ *vs.* $tW^{1/2}$ should lie on a common curve, as is observed for the thin film (figure 5.8). Integrating equation 5.17 gives

$$\int_0^\infty \frac{j}{j_0} dt = \frac{\alpha l x_D}{D} \qquad \textbf{5.18}$$

Now, as from equation 5.8

$$j_0 = \frac{D}{x_D}\left(C_\infty - \left(C_{H^+,0}\right)_{t=0}\right)$$

therefore

$$\int_0^\infty j dt = \left(C_\infty - \left(C_{H^+,0}\right)_{t=0}\right)\alpha l \qquad \textbf{5.19}$$

Thus integrating the area beneath the j / t plots (figures 5.9, 5.10) yields the number of moles per cm^2 of protonatable sites in the film, giving a value of αl. This should be the same in the case of the acid to neutral as it is for the neutral to acid transfer for any particular film, as the number of available sites will not change. The same is true for a particular film at different rotation speeds. For the acid to neutral transfer of the thin film, at all rotation speeds, the integration was found to be constant at a value of $1.1 \pm 0.1 \times 10^{-8}$ molcm^{-2} (table 5.1)

W / Hz	$\int_0^\infty j dt$ / x10^{-8} molcm^{-2}
1	-1.0
2	-1.1
4	-1.2
9	-1.2

Table 5.1: *Integrated j vs. t (x10^{-8} molcm)*

Therefore $\int_0^\infty jdt = \left(C_\infty - \left(C_{H^+,0}\right)_{t=0}\right)\alpha l$ = -1.1±0.1x10^{-8} molcm^{-2} = -1.1x10^{-6} moldm^2. C_∞ is the final concentration of H^+, which, in this case, is $10^{-6.39}$, and $(C_{H^+,0})_{t=0}$ is the initial concentration of H^+=$10^{-3.35}$. Therefore

$$\alpha l = \frac{1.1x10^{-6}}{4.5x10^{-4}}$$

$$= 2.4x10^{-3}\ \text{dm}$$

$$=2.4x10^{-4}\ \text{m}$$

now, l = 0.49 μm=0.49x10^{-6} m, therefore α=490.

From equation **5.17**, a plot of lnj *vs.* t should give a straight line with a gradient of $\frac{-D}{\alpha l x_D}$. Using the value of αl calculated above, if this theoretical analysis applies, it should be possible to fit a theoretical gradient to the data with good correlation. Hence

$$\alpha l = 2.4x10^{-4}\ \text{m}$$

$$=2.4x10^{-2}\ \text{cm}$$

Therefore the theoretical gradient can be calculated for the 1 Hz thin acid to neutral transient

$$\text{Gradient} = -1.554D^{2/3}\nu^{-1/6}W^{1/2}\alpha l$$

$$=-0.280\ s^{-1}$$

The data for the thin film at W=1Hz are shown in figure 5.14. Also shown is the line of theoretical gradient of -0.280 s^{-1} produced for this analysis. This relatively close correspondence of theory and experiment demonstrates the applicability of this general analysis of these data. There is, however, some deviation in linearity of the data: This is to be expected, as the theoretical treatment assumes steady-state conditions at all times; however, using the early time part of the transient, there will be an appreciable time, of the order of a second, for the diffusion layer to be established, during which time an enhanced j would be expected.

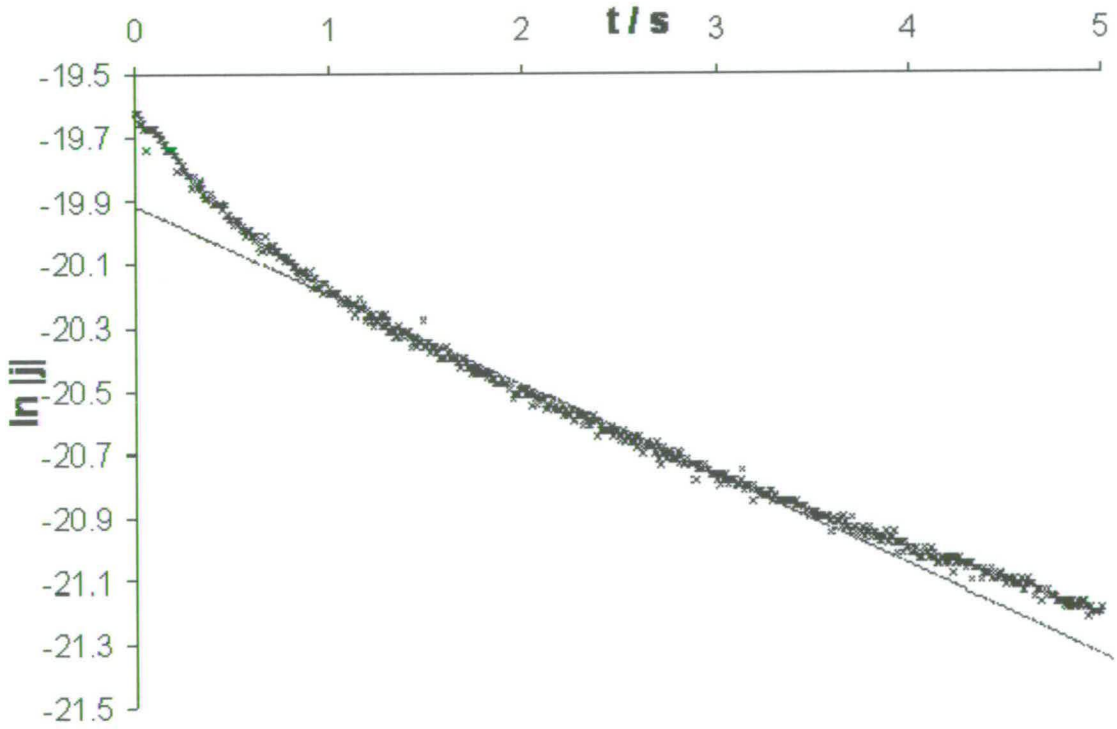

Figure 5.14: *ln –j vs. t plots for thin film, W=1 Hz, acid to neutral, first 5 seconds of the transient. Theoretical gradient = -0.280 s^{-1}*

The results from the integration with respect to time beneath the j / t plot for the acid to neutral transfer of the thin film, at all rotation speeds (table 5.1) gave a value of $1.1\pm1\times10^{-8}$ molcm^{-2} protonatable sites. For the thin (0.49 μm) film the number of moles of trimer redox centres in the film can be calculated as 3.7×10^{-7} molcm^{-2}. This corresponds to ~3% of the redox centres being protonated / deprotonated during the transient for a pH change from 3 to 7. This is a sensible value, consistent with protonation / deprotonation of the redox centres being the origin of the pH response. Thus for the thin coat the data is consistent with fast protonation / deprotonation of the film with the rate limited by the mass transport of H^+ in solution.

If the assumptions held true for the thick film, which is approximately 3 times the thickness of the thin film (1.4 μm *cf.* 0.5 μm) it would be expected that the integrated j/t plots would show that there are 3 times as many protonated sites as the thin film. For the thick film acid-base transfer at slow rotation speed, *i.e.* W= 1 Hz, this holds essentially true (table 5.2), the number of protonatable sites being calculated as $3.9\pm0.3\times10^{-8}$ molcm^{-2}.

W / Hz	$\int_0^\infty jdt$ / x10^{-8} molcm^{-2}
1	-3.9
2	-4.8
4	-6.3
9	-9.4

Table 5.2: *Integrated j vs. t (x10^{-8} molcm^{-2}) for thick film, acid to base transfer*

From equation 5.17, when $\frac{D}{x_D}$ is constant, *i.e.* when W is the same, then a common plot of $\frac{j}{j_0}$ against $\frac{t}{l}$ should be observed. The data is shown for the thick and thin films, acid to neutral, at W=1 Hz (figure 5.15).

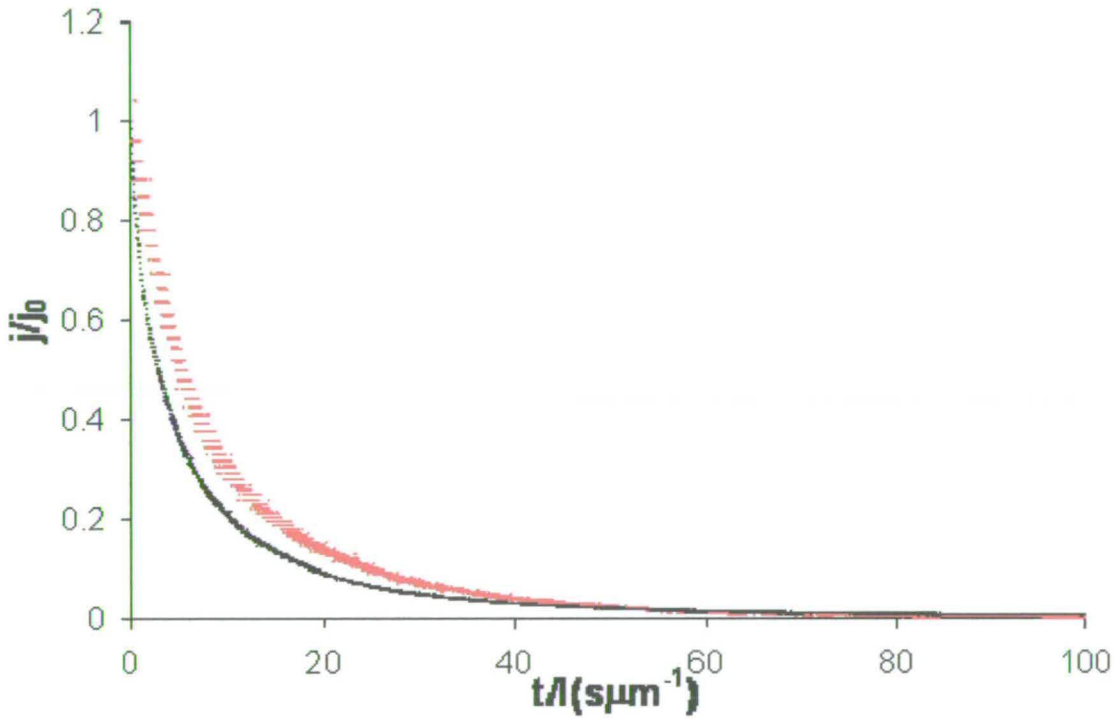

Figure 5.15: $\frac{j}{j_0}$ *vs.* $\frac{t}{l}$ *($s\mu m^{-1}$) for thin (black) and thick (red) films, acid to base, W=1Hz*

The close correspondence for these data shows that for the thick film at low rotation speed the quantitative treatment still applies and the coat protonation and deprotonation is fast. However, for the thick film at higher rotation speeds, it is clear that the data from

integration of the j/t data are no longer constant (table 5.2). This is consistent with the observation that the normalised j/t data do not lie on a common curve (figure 5.16). In this case proton diffusion through the coat is becoming rate limiting, and the assumption of a constant coat concentration $C_{H^+,0}$ throughout the coat cannot hold.

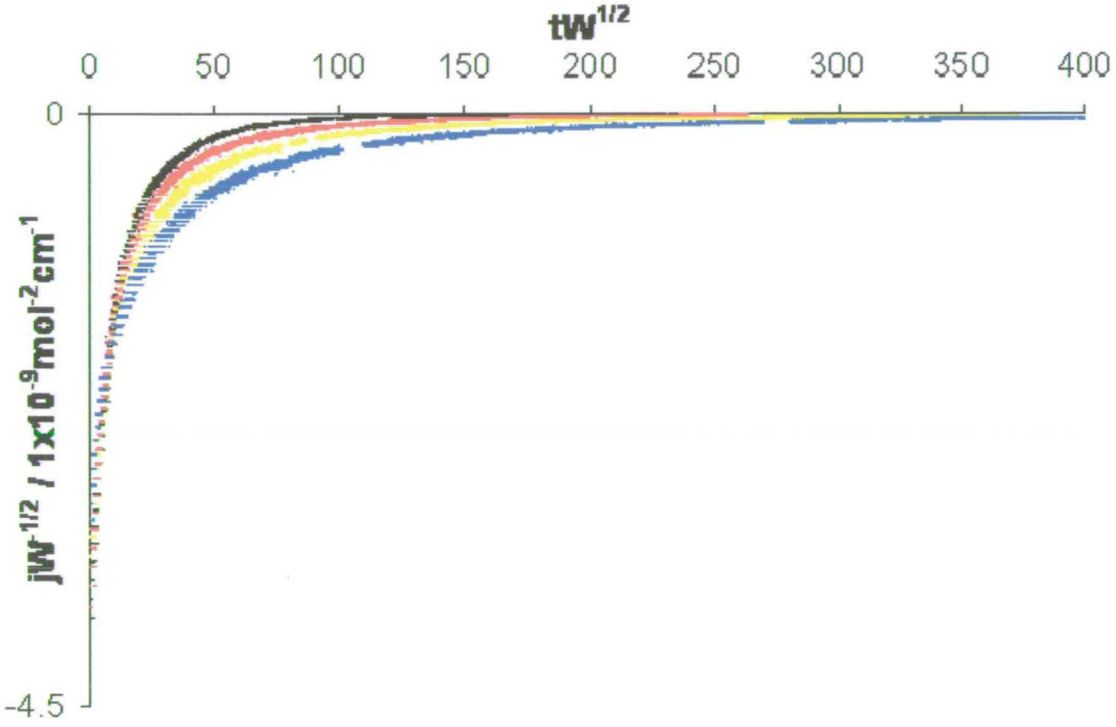

Figure 5.16: *Normalised j vs. t plots for thick film, acid to neutral, all rotation speeds. All W: W=1 Hz black plot, W=2 Hz red plot, W=4 Hz yellow plot, W=9 Hz blue plot.*

The assumptions made when performing the quantitative treatment break down and the coat kinetics are becoming relatively slow. In this case it cannot be assumed that the pH is the same throughout the coat because the average proton concentration (measured by the coat potential) and that at the interface with the electrolyte will be different. The potential of the coat is actually determined by some average pH of the film, and there is

therefore a loss of a direct relationship between E and $C_H^+{}_{,0}$. This would be expected to lead to an overestimation of the flux (as $C_H^+{}_{,0}$ would be expected to change faster than the average proton concentration in the film) and hence an overestimation of the total number of protonatable sites when integrating j with respect to t, as is observed; therefore the quantitative relationships, such as the integrated j/t transients, are lost, as the calculated number of available sites obtained by this method increases with increasing W (table 5.2).

In the case of the neutral to acidic transfer, for the thin film it can be seen from the normalised j/t data (figure 5.17), that the curves lie on top of one other; therefore the coat kinetics are still relatively fast. However an exponential j/t relationship is no longer seen.

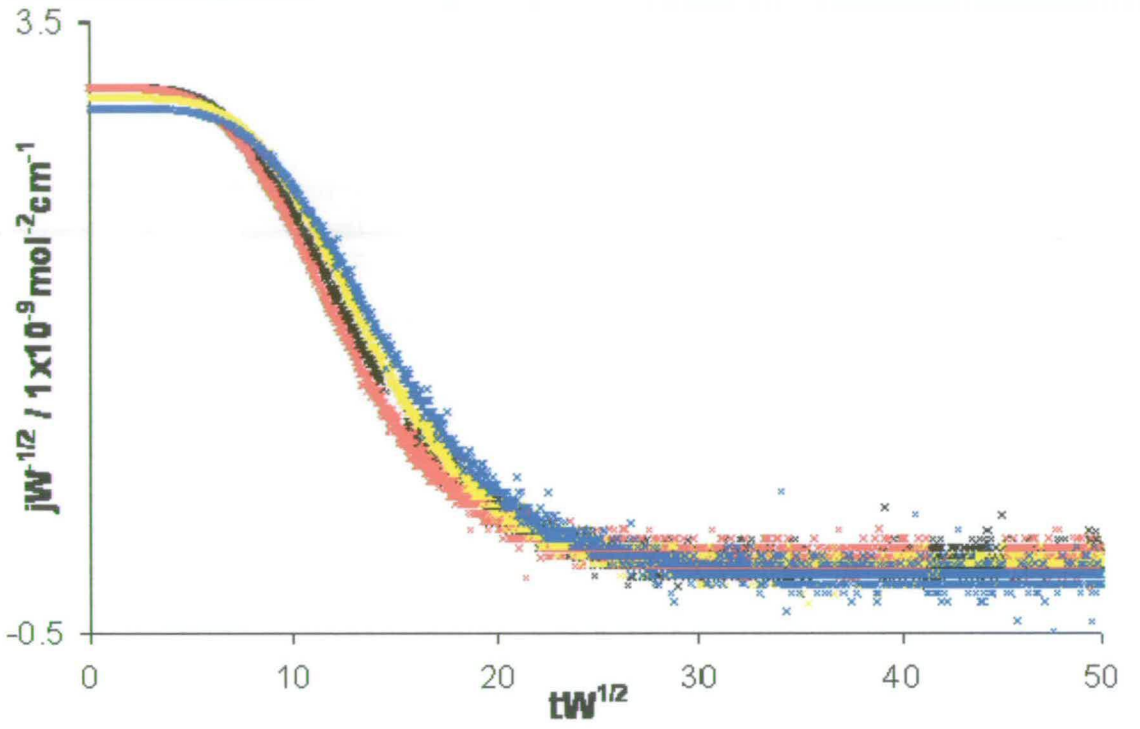

Figure 5.17: *Normalised j vs. t plots for thin film, neutral to acid, all rotation speeds*

It is clear from these data that the value of j stays constant initially, *i.e.* the pH of the coat stays constant. This can also be seen in figure 5.7. Integration of j with respect to t also shows that in this case the number of available protonatable sites is significantly greater than for the acid to neutral transfer (table 5.3).

W / Hz	$\int_0^\infty jdt$ / x10^{-8} molcm^{-2}
1	4.5
2	4.2
4	3.9
9	2.7

Table 5.3: *Integrated j vs. t (x10^{-8} molcm^{-2}) for thin film, neutral to acid transfer*

The most likely explanation for this is that there is buffer present in the coat in the neutral solution that is not present in the acidic coat. It has been suggested previously that such buffering occurs in aqueous solution owing to the presence of CO_2[5]. CO_2 dissolves readily in aqueous solutions; in acid solution hydrated CO_2 is present as H_2CO_3 and is likely to be able to be removed from the solution by degassing with N_2. The pK_a of H_2CO_3 is 6.4, so in neutral solution it would dissociate

$$H_2CO_3 \rightleftharpoons H^+ + HCO_3^-$$

Therefore at pH 7 HCO_3^- is expected to be present. This can be incorporated in the film as a counterion and can buffer incoming H^+, causing the measured pH change in the coat. From table 5.3 it is apparent that comparable amounts of buffer and protonatable trimer sites are present in the film. Consistent with this explanation, the coat pH appears to be buffered in the appropriate region of pH7 for HCO_3^- (figure 5.6).

For the thick film this delay in response due to buffering is seen; additionally the normalisation of the j/t plots does not result in a common curve (figure 5.18);

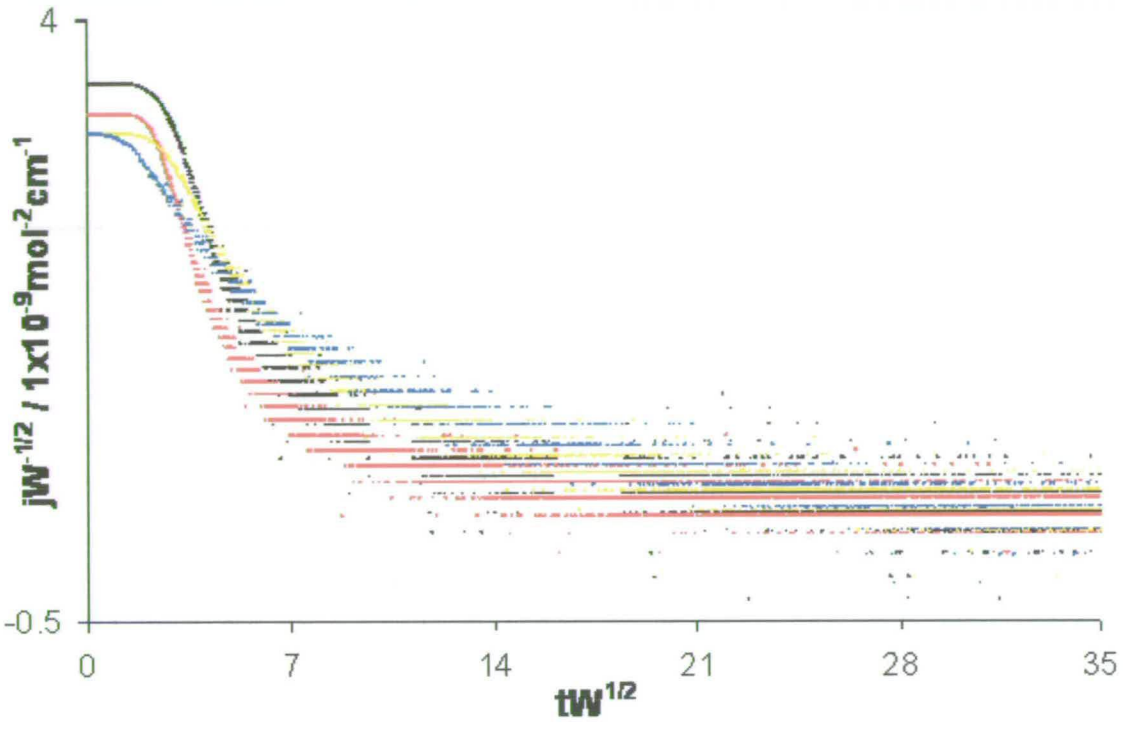

Figure 5.18: *Normalised j vs. t plots for thick film, neutral to acid, all rotation speeds. All W: W=1 Hz black plot, W=2 Hz red plot, W=4 Hz yellow plot, W=9 Hz blue plot.*

Integration under the j/t plots does not give a constant value of protonation sites over the rotation speeds (table 5.4); hence in this case there is a combination of both effects seen to date, with buffering attributable to HCO_3^- and the effects of the relatively slow coat kinetics for this film.

W / Hz	$\int_0^\infty jdt$ / x10^{-8} molcm^{-2}
1	3.3
2	3.4
4	4.0
9	4.6

Table 5.4: *Integrated j vs. t (x10^{-8} molcm^{-2}) for thick film, neutral to acid transfer.*

5.6. Conclusion

Thick and thin poly-5CnI films have a linear potential response with a Nernstian gradient of -59 $mVpH^{-1}$ to changes in electrolyte pH; this is reproducible and sustainable over a time scale of at least a week. The response seen is characteristic of the film and not the underlying Pt electrode.

The thin film of poly-5CnI, which is 0.49 μm thick, shows relatively rapid protonation and deprotonation in response to pH change. When switching from the acid to the neutral electrolyte quantitative characterisation shows the response to be consistent with a simple coat deprotonation reaction with relatively fast kinetics. It was determined that ~3% of the potential protonation sites in the coat were involved. When switching from the neutral to the acid electrolyte there is extra proton ingress into the coat and there is a marked change in the j/t transient consistent with the presence of carbonate buffer in the coat.

The thick film, 1.37 μm, as the rotation speed increases, exhibits increasing coat effects due to protonation kinetics regardless of the direction of transfer; *i.e.* from acidic to neutral or neutral to acidic solution. For the acid to neutral transfer it was found that the quantitative analysis that was successful for the thin film acid to neutral transfer held true at the low rotation speed of W=1 Hz. For this case, as predicted, the thick film being 3 times the thickness of the thin film, the number of protonatable sites obtained for the thick film acid to neutral transfer was 3 times that of the thin film.

In all the cases studied the response is of the order of seconds. The pH response is comparable to that previously observed for polypyrrole for these film thicknesses, but unlike polypyrrole appears to originate from direct coat protonation and deprotonation. This implies that poly-5CnI has potential as a practical pH sensor.

5.7. References

1. Q. Pei and R. Qian, *Synthetic Metals*, 1991, **45**, 35-48
2. K.K. Shiu, F.Y. Song, K.W. Lau, *J. Electroanal. Chem.*, 1999, **476**, 109-117
3. A. Michalska and K. Maksymiuk, *Electroanal.*, 1998, **10(3)**, 177-180
4. K. Maksymiuk, J. Bobacka, A. Ivaska and A. Lewenstam, *Anal. Lett.*, 2000, **33(7)**, 1339-1360
5. P.N. Bartlett and J. Farrington, *Bull. Electrochem.*, 1992, **8(5)**, 208-211
6. M.T. Robertson, *PhD Thesis*, 1998, University of Edinburgh
7. J.G. Mackintosh, *PhD Thesis*, 1995, University of Edinburgh
8. G. Cheek, *Anal. Chem.*, 1983, **55**, 380-381
9. P.A. van der Meulen, F. Wilcoxon, *Ind. Eng. Chem.*, 1923, **15**, 62
10. J.C. Brunnich, *Ind. Eng. Chem.*, 1925, **17**, 631
11. G.A. Harlow, C.M. Noble, G.E.A. Wyld, *Anal. Chem.*, 1956, **28**, 784
12. W.J. Albery and A.R. Mount, *J. Chem. Soc., Faraday Trans. 1*, 1989, **85(5)**, 1181-1188
13. N. Robertson, S. Parsons, E.J. MacLean, R.A. Coxall and A.R. Mount, *J. Mater. Chem.*, 2000, **10**, 2043-2047
14. A.J. Bard and L.R. Faulkner, *Electrochemical Methods – Fundamentals and Applications*, *John Wiley & Sons*, 1980

Chapter 6

Fluorescence of Poly-5-Cyanoindole

6.1. Introduction

As discussed in chapter 1, 5-substituted-indole polymers have been the subject of extensive electrochemical and photophysical investigation. Mount *et al* have made considerable progress in the characterisation of their polymerisation mechanism[1,2,3], which is outlined in section 1.5. Poly-5-cyanoindole (poly-5CnI) can be synthesised quickly, easily, cheaply and reproducibly from a solution of the 5CnI monomer using electrochemical techniques[1,2,3] (section 1.5). The system employed, a non-aqueous three-electrode set up with a rotating disc working electrode, is described in detail in sections 2.1.4 and 3.2. The 5CnI monomer is oxidised initially, forming asymmetric trimer units (Figure 6.1(b),). As described in chapter 1, the potential is held constant, and the oxidation potential of the trimer is lower than that of the monomer, these units then become oxidised and undergo linkage to form conjugated polymers consisting of linked trimer units[1,2,3].

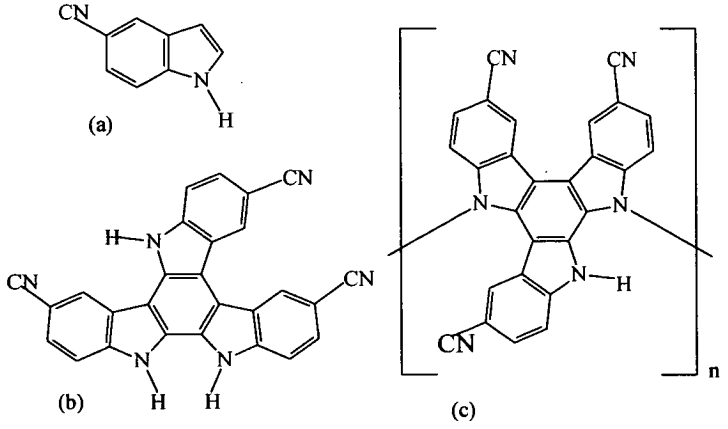

Figure 6.1: *(a) 5-cyanoindole monomer (b) Asymmetric trimer (c) Trimer showing supposed linkage positions*

The degree to which the trimer units become linked can be controlled by altering the conditions of polymerisation. Using a high concentration of monomer and a high disc rotation speed yields a high proportion of trimer, whereas using a low monomer concentration and a low disc rotation speed leads to more extensive linkage of the trimer units that have been formed. Generally the differences in the degree of linkage are manifested as differences in fluorescence[4,5]. A sample that is rich in trimer will exhibit fluorescence at shorter emission wavelengths, whereas a sample comprising more linked units will fluoresce at longer emission wavelengths. However, the fluorescence of the 5-cyanoindole trimer is so intense[4,5] that emission at longer wavelengths can be masked. Hence excitation energies must be chosen carefully.

As described in section 1.7.1, 'conjugated polymers' actually consist of many strands, each of which comprises segments of different conjugation length[6]. Although the degree to which the trimer units become linked can be controlled, the degree of conjugation cannot. The lengths of conjugation vary within one sample, as represented in figure 6.2, from effectively a single trimer unit to conjugated lengths of many trimer units, due to defects along the conjugated carbon backbone[6]. Additionally there may also be trimer units trapped within the film that have remained unlinked altogether.

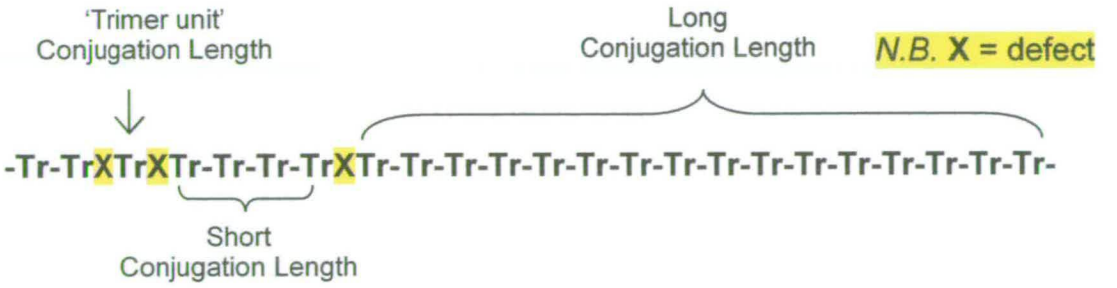

Figure 6.2: *Representation of a conjugated carbon backbone, with defects breaking the conjugation into shorter segments.*

The fluorescence of the samples differs according to the nature and proportions of the different conjugation lengths of the fluorophores present. A very short conjugation length species, *e.g.* a 'trimer unit' conjugation length, will have a higher excitation energy than a chain with extensive conjugation, which is stabilised as a result of delocalisation. Therefore, the shorter the conjugation length of the species, the shorter the excitation wavelength, λ_{ex}, and the emission wavelength, λ_{em}. Conversely, longer conjugation length species emit at longer emission wavelengths[6].

To probe the differences between the very short conjugation length species and the longer species different excitation energies are required. Using an excitation energy that is sufficiently high to excite the shortest conjugation length species, trimer fluorescence will dominate the emission spectrum[4]. Hence a longer wavelength, lower energy excitation source is required to allow excitation of the longer conjugation length, 'polymeric' species, but to minimise the excitation of the very shortest, trimer conjugation length species.

6.1.1. Experimental Details

Different films of 5-cyanoindole (5CnI) were synthesised electrochemically on a polished Pt Rotating Disc Electrode (RDE) and were dissolved completely into EtOH. Steady-State Fluorescence (SS) and Time-Correlated Single Photon Counting (TCSPC) experiments were performed on the samples to investigate differences between samples of different polymer content *i.e.* samples of higher and lower polymer content (termed higher polymer (HP) and lower polymer (LP) respectively).

Samples were polymerised from the same monomer solution but at different rotation speeds (W), the LP sample being synthesised at higher W to encourage trimer formation and the HP sample being produced at lower W to yield more extensive linkage. The conditions employed for all the polymerisations are shown in table 6.1.

Sample	Concentration / mM	W / Hz
Higher trimer	20	9
Higher polymer	20	1

Table 6.1: *The conditions used for sample preparation showing concentration of the original monomer solution used and disc rotation speed (W)*

During polymerisation the oxidation was controlled to ensure that similar charges were passed, hence similar film thicknesses produced, and the samples were removed entirely into the same volume of EtOH (10 ml) to give similar concentrations in solution.

SS fluorescence spectra were obtained for both samples at λ_{ex}=360 nm and at λ_{ex}=450 nm (section 3.4.3.1). Excitation wavelength λ_{ex}=450 nm is expected to be of sufficiently low energy to minimise direct trimer, or short conjugation length, excitation, whilst still exciting the lower energy lower conjugation length ('polymer') species, hence emission observed will be characteristic of the longer conjugated, 'polymeric' species. Emission acquired at λ_{ex}=360 nm, where the trimer is excited directly, would be expected to show predominantly trimer and short conjugation length emission. Excitation spectra were obtained at λ_{em}=435 nm to coincide with the trimer emission maximum, and λ_{em}=560 nm to coincide with the polymer emission maximum. TCSPC decays were recorded at λ_{ex}=360 nm and λ_{ex}=450 nm, at λ_{em} between 435 nm and 600 nm. (section 3.4.3.2).

6.2. Monomer Fluorescence

A typical fluorescence emission spectrum of the 5-cyanoindole monomer in EtOH solution is shown (figure 6.4). This is a single peak with a maximum at 364 nm. These results are consistent with previous work[3,4,5].

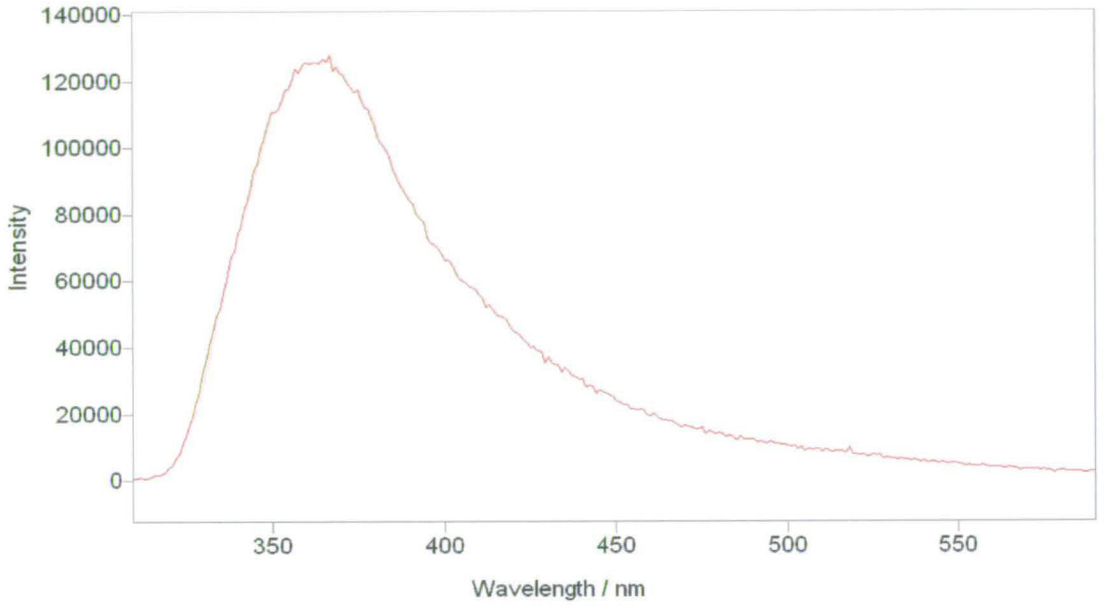

Figure 6.4: *SS fluorescence spectra of 5-CnI monomer in EtOH. (a) Excitation spectrum acquired at λ_{em}=360 nm; (b) Emission spectrum acquired at λ_{ex}=326 nm.*

The fluorescence lifetime of the 5-cyanoindole monomer in EtOH has previously been found to be 4.3 ns. [5]

6.3. Comparison of Higher Polymer and Lower Polymer Samples

6.3.1. Fluorescence at λ_{ex}=360 nm

The emission and excitation spectra of the 'higher polymer' (HP) and 'lower polymer' (LP) samples (table 6.1) were recorded (figure 6.5). The fluorescence maxima of these samples are considerably shifted to lower energy from that of the

monomer (Figure 6.4, emission maximum 364 nm). When exciting at 360 nm the emission spectra for both HP and LP are dominated by intense fluorescence between 400 and 500 nm, with emission maxima at 414 nm and 434 nm, and a shoulder at 450 nm. The excitation maxima for these samples are also shifted compared to the monomer, to 380 nm and 400 nm from 280 nm[7]. It is clear that the shapes of the HP and LP spectra are identical and the intensities comparable. These spectra have been observed previously and are known to be characteristic of the trimer species[7].

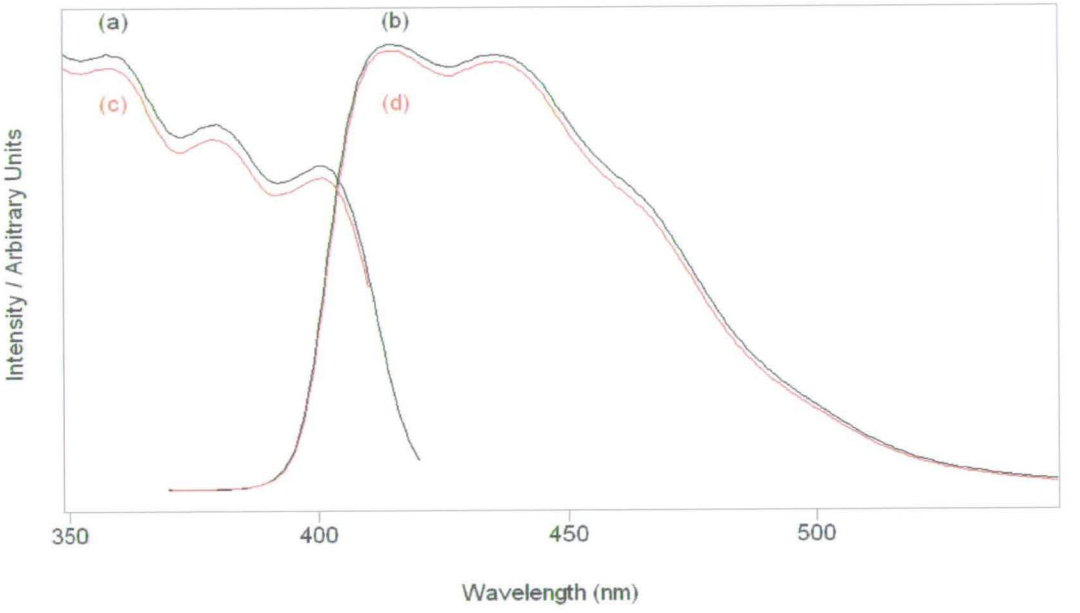

Figure 6.5: *Steady State emission and excitation spectra for HP and LP 5-CnI samples: (a) 'Higher polymer' excitation, λ_{em}=435 nm; (b) 'Higher polymer' emission λ_{ex}=360 nm; (c) 'Lower polymer' excitation λ_{em}=435 nm; (d) 'Lower polymer' emission λ_{ex}=360 nm.*

TCSPC experiments were carried out exciting at 360 nm, decays being recorded over the emission wavelength range 434-550 nm (figure 6.6). Measurements at the emission maximum, 414 nm, were not made because, at this excitation wavelength, this maximum coincides with a Raman band.

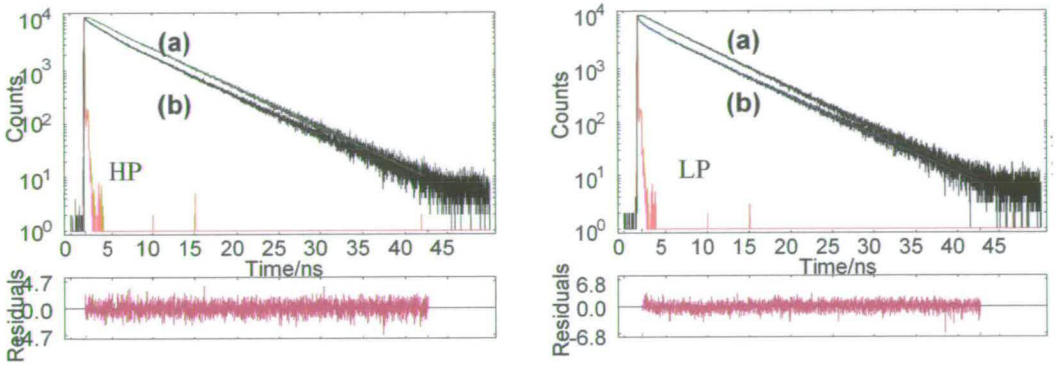

Figure 6.6: *Decays of HP and LP (log y-scale), λ_{ex}=360 nm. (a) λ_{em}=435 nm (green line is corresponding fitted curve), (b) λ_{em}=550 nm (blue line is corresponding fitted curve).*

The fluorescence lifetimes were determined by fitting the decays using expression 2.36; to recap this is

$$I(t) = \sum_{i=1}^{n} A_i \exp(-t/\tau_i)$$

where t is the time, I(t) is intensity at time=t, τ_i are the decay times, n is the number of decay times and A_i = A-factors. The lifetimes, A-factors and percentage of each component contributing to the steady-state emission obtained for the fitting are presented in tables 6.2, 6.3 and 6.4.

λ_{em} / nm		τ_1	τ_2	τ_3	χ^2
435	τ / ns	5.83	-	-	1.01
	A	1	-	-	
	%	100	-	-	
450	τ / ns	5.83	-	-	1.04
	A	1	-	-	
	%	100	-	-	
500	τ / ns	5.84	-	-	1.08
	A	1	-	-	
	%	100	-	-	
550	τ / ns	5.90	2.48	0.23	1.03
	A	0.61	0.16	0.23	
	%	89	10	1	

Table 6.2: *Lifetimes, A-factor (as fraction of 1) and % contribution to SS for HP 5CnI sample, λ_{ex}=360 nm. SD in: τ ≈0.003; A ≈ 0.001*

λ_{em} / nm		τ_1	τ_2	τ_3	χ^2
435	τ / ns	5.70	-	-	1.07
	A	1	-	-	
	%	100	-	-	
450	τ / ns	5.77	-	-	1.07
	A	1	-	-	
	%	100	-	-	
500	τ / ns	5.78	-	-	1.15
	A	1	-	-	
	%	100	-	-	
550	τ / ns	5.86	2.01	0.20	1.08
	A	0.53	0.09	0.38	
	%	92	6	2	

Table 6.3: *Lifetimes, A-factor (as fraction of 1) and % contribution to SS for LP 5CnI sample, λ_{ex}=360 nm. SD in: τ ≈0.003; A ≈ 0.001*

Sample	τ / ns	χ^2_g	χ^2_{435}	χ^2_{450}	χ^2_{500}
HP	5.82	1.10	1.05	1.12	1.12
LP	5.73	1.21	1.15	1.14	1.35

Table 6.4: *Globally fitted lifetimes, λ_{em}=435-500 nm , of the HP and LP 5CnI samples, λ_{ex}=360 nm*

As shown in tables 6.2, 6.3 and 6.4, lifetimes obtained for both HP and LP were similar across the whole emission range 435-550 nm, the standard deviation (SD) and χ^2 values indicating good fits. From tables 6.2 and 6.3 it is clear that over the range 435-500 nm a single lifetime of 5.8±0.1 ns is obtained for both of the samples, showing that only one species is emitting. Consistent with this, it was found that the decays of each sample could be fitted to one global lifetime of 5.8±0.1 ns across the emission region (table 6.4).

At the longer emission wavelength, λ_{em}=550 nm, further lifetimes were obtained. A tri-exponential function was required, the lifetimes obtained being τ_1=5.9±0.1 ns, τ_2=2±0.5 ns τ_3=200±30 ps for both of the samples. The lifetime of the longest component, τ_1=5.9±0.1 ns, is comparable to the single lifetime obtained for λ_{em}=435-500 nm. This component constitutes the majority of both the emitting population (indicated by the A-factor; 0.61 for the HP sample and 0.53 for the LP sample) and the SS emission intensity (approximately 90% for both samples). The component constituting the next highest proportion of the emitting population for both samples is the shortest component, τ_3=200 ps (0.38 for LP, 0.23 for HP). The component with the intermediate lifetime, τ_2=2 ns, constitutes 0.16 of the total emitting population for the HP sample and 0.09 of the LP sample.

Exciting at λ_{ex}=360 nm, the emission is dominated by the trimer species. Even at longer emission wavelengths, *i.e.* $\lambda_{em}\geq$550 nm, the tail of the trimer emission overlaps with any emission that may arise from the polymeric species. Additionally, excitation of the lower energy, polymeric species could very well occur indirectly,

through energy transfer from higher energy excited species (outlined in section 1.7.1). To investigate the nature of the longer, more conjugated species it was necessary to excite the sample with a lower energy source that was sufficient to excite the species in question but not the trimer, hence experiments were conducted at λ_{ex}=450 nm.

Work carried out by Samuel *et al* on PPV showed that excitation at short wavelengths gives complicated decays and multiple lifetimes[8,9]. This is clearly not the case here. The trimer is the only emitting species observed at 435-500 nm. It is not, unlike the systems studied by Samuel *et al*, a conjugated species or a single linked trimer unit making up part of a polymer strand, but is a free entity in solution.

6.3.2. Fluorescence at λ_{ex}=450 nm

SS fluorescence emission spectra for both the HP and the LP sample were recorded at λ_{ex}=450 nm (figure 6.7). The HP sample has a definite maximum at λ_{em}=560 nm, but for the LP sample the emission is less distinct with no clear maximum. Both samples exhibit a tail, rising steeply at the blue edge of the emission (≤ 510 nm), due to overlap with the trimer emission. Owing to this trimer tail it was not deemed sensible to record decays at the shortest emission wavelengths for either sample, hence the shortest λ_{em} chosen was 560 nm. Decays for both samples were recorded at λ_{em}=560 nm, 580 nm and for the HP sample at λ_{em}=600 nm (figure 6.8).

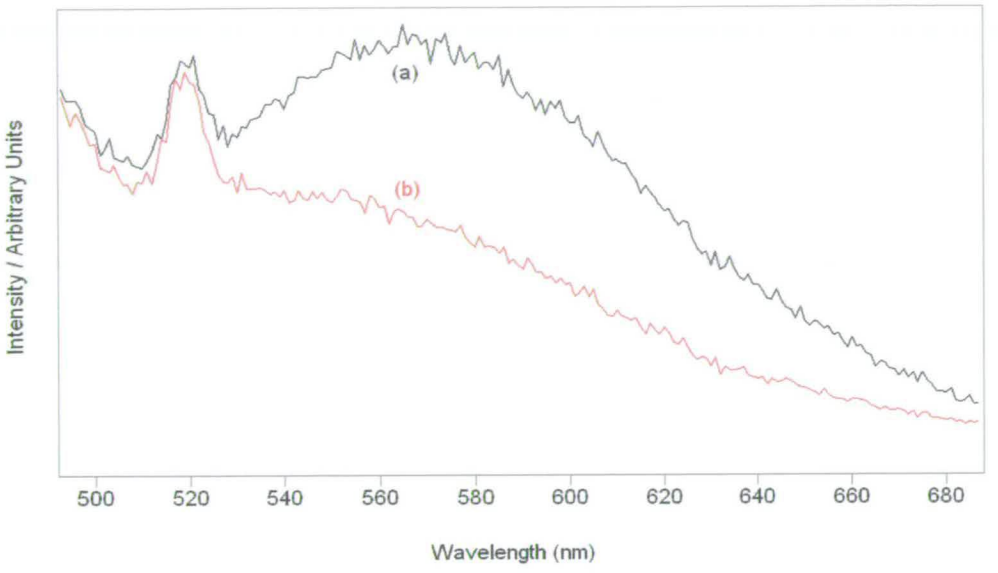

Figure 6.7: *Steady State emission spectra for HP and LP 5CnI samples (a) 'Higher Polymer' emission λ_{ex}=450 nm; (b) 'Lower Polymer' emission λ_{ex}=450 nm*

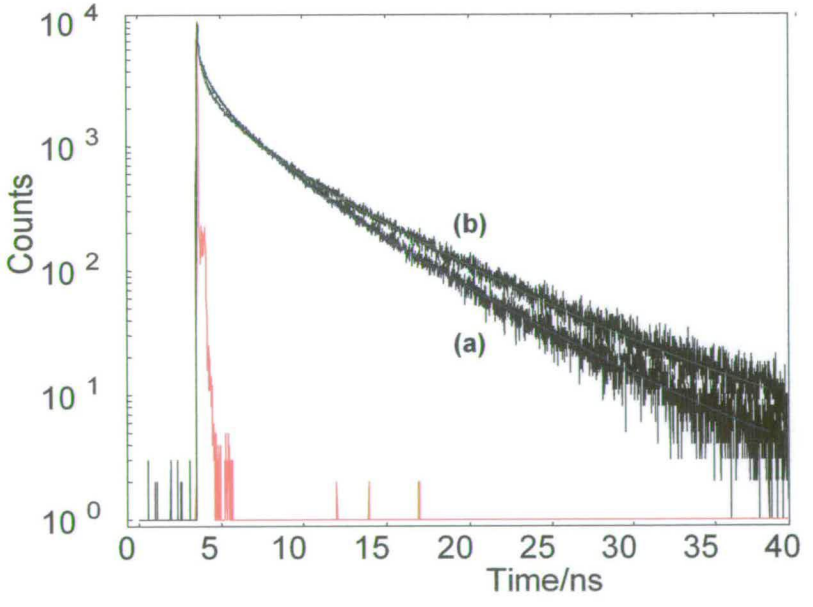

Figure 6.8: *Decays at λ_{ex}=450 nm, λ_{em}=560 nm. (a) HP (blue line is corresponding fitted curve); (b) LP (green line is corresponding fitted curve)*

6.3.2.1. HP Sample

Using λ_{ex}=450 nm, fluorescence decays were obtained across the emission region λ_{em}=560-600 nm, and were fitted globally to 3 lifetimes (table 6.5).

Global lifetime / ns	τ_1 / ns 4.80	τ_2 / ns 1.51	τ_3 / ns 0.14	χ^2_g 1.38
λ_{em} / nm	**A_1** **%**	**A_2** **%**	**A_3** **%**	**χ^2**
560	0.14 64.42	0.18 26.10	0.68 9.48	1.46
580	0.15 62.18	0.24 30.51	0.61 7.31	1.32
600	0.16 60.67	0.29 33.32	0.55 6.01	1.34

Table 6.5: *Lifetimes, A-factors and % contributions to SS emission for HP sample. Major emitting constituent of sample is highlighted. χ^2 values are comparable to those for the individually fitted decays*

This indicates the same three emitting species are present over the wavelength region λ_{em}=560-600 nm, albeit in different proportions of the excited state population, and contributing different amounts to the SS emission at each emission wavelength.

The global set of components contains a long lifetime τ_1=4.8±0.1 ns, an intermediate lifetime τ_2=1.5±0.1 ns and a short lifetime τ_3=140±10 ps. The majority of the emitting species show a short lifetime, τ_3=140 ps. The contribution of this species to the emitting population is 0.68 at λ_{em}=560 nm, decreasing to 0.55 at λ_{em}=600 nm. The intermediate lifetime component, τ_2=1.5±0.1 ns, and longest lifetime

component, τ_1=4.8±0.1 ns contribute approximately equally to the emitting population at λ_{em}=560 nm (0.18 and 0.14 respectively); these increase to 0.29 and marginally to 0.16 respectively at λ_{em}=600 nm.

Although the 140 ps component constitutes the majority of the emitting species over this emission wavelength region, it has the lowest contribution to the SS emission, 9.5% at λ_{em}=560 nm, decreasing to 6.0% at λ_{em}=600 nm. The SS emission is dominated by the 4.8 ns component, 64.4% at λ_{em}=560 nm and 60.7% at λ_{em}=600 nm. The 1.5 ns component contributes 26.1% to the SS emission at λ_{em}=560 nm, rising to 33.3% at λ_{em}=600 nm.

6.3.2.2 LP sample

The fluorescence decays of the LP sample can be fitted globally to three lifetimes over the emission region λ_{em}=560-580 nm (table 6.6).

Global lifetime / ns	τ_1 / ns 5.79	τ_2 / ns 1.46	τ_3 / ns 0.12	χ^2_g 1.27
λ_{em} / nm	**A_1** **%**	**A_2** **%**	**A_3** **%**	**χ^2**
560	0.11 68.55	0.15 22.04	0.74 9.41	1.34
580	0.12 66.54	0.18 25.31	0.70 8.14	1.19

Table 6.6: *Lifetimes, A-factors and % contributions to SS emission for LP sample. The major emitting constituent of the sample is highlighted. The χ^2 values are comparable to those for the individually fitted decays, indicating the applicability of global fitting.*

The 3 lifetimes are a long lifetime τ_1=5.8±0.1 ns, an intermediate lifetime τ_2=1.5±0.1 ns and a short lifetime τ_3=120±10 ps. The component that constitutes the majority of the excited state population at λ_{ex}=360 nm is that with the shortest lifetime, τ_3=120 ps; the A-factor is 0.74 at λ_{em}=560 nm, and 0.70 at λ_{em}=580 nm. The intermediate lifetime component, τ_2=1.5 ns constitutes 0.15 at λ_{em}=560 nm, increasing to 0.18 at λ_{em}=580 nm, and the longest lifetime component, τ_1=5.8 ns makes up 0.11 at λ_{em}=560 nm and 0.12 at λ_{em}=580 nm. This increase is very slight and is likely to be within experimental error.

The SS emission arises principally from the 5.8 ns component, 68.6% at λ_{em}=560 nm decreasing to 66.5% at λ_{em}=580 nm. The 1.5 ns component contributes 22.0% at

λ_{em}=560 nm, increasing to 25.3% at λ_{em}=580 nm, with the contribution from the 120 ps component being less than 10%.

6.3.3 Discussion

6.3.3.1. λ_{ex}=360 nm

The lifetime of the 5-cyanoindole monomer in EtOH has previously been found to be τ=4.3 ns[5]. The SS emission spectrum shows nothing characteristic of monomer fluorescence; additionally none of the emission from the samples has the monomer lifetime; therefore none of the emission from these polymerised samples can arise from the monomer.

The polymerised samples showed different decay characteristics depending on the emission wavelength. Exciting at λ_{ex}=360 nm, in the emission region λ_{em}=435-500 nm, both samples have a single lifetime, τ=5.8±0.1 ns, with negligible difference between HP and LP. It has been shown previously that this is the region in which the trimer species fluoresces[7], hence this lifetime can be attributed to trimer. This lifetime is slightly longer than that of the monomer (τ=4.3 ns[5]), consistent with a slightly greater degree of delocalisation, and hence lower energy and greater stability of the excited state. The results are in very good agreement so it can be inferred that the trimer of 5CnI has a lifetime of 5.8 ns.

At emission wavelength λ_{em}=550 nm two further lifetimes are seen in addition to that of the trimer. At this wavelength, the trimer is dominant in terms of the A-factor (0.6 for both samples) and the contribution to the SS emission (90% for both samples).

The intermediate and shortest lifetime components, τ_2=2 ns and τ_3=0.2 ns, are not seen in the short wavelength, *i.e.* trimer, emission region, and must be characteristic of lower excitation energy, longer conjugation length species. Being longer conjugation length species one might predict that their lifetimes should be longer than that of the trimer; however, since these species have shorter fluorescence decay lifetimes they must be subject to more efficient non-radiative (NR) decay mechanisms than the trimer.

6.3.3.2. λ_{ex}=450 nm

Using λ_{ex}=360 nm fluorescence emission is dominated by the trimer, with emission from longer conjugation length species being concealed. However, using λ_{ex}=450 nm, the longer conjugation length species are being excited selectively, resulting in minimal contribution of the trimer to the initial excited state population.

At λ_{ex}=450 nm both HP and LP systems exhibit 3 emitting species, ostensibly similar to the results seen at λ_{ex}=360 nm, λ_{em}=550 nm. The values of τ_2 and τ_3 using λ_{ex}=450 nm are similar for both HP (τ_2=1.5±0.1 ns, τ_3=140±10 ps) and LP (τ_2=1.5±0.1 ns, τ_3=120±10 ps) and are comparable in magnitude to those obtained at λ_{ex}=360 nm, λ_{em}=550 nm, where τ_2=2±0.1 ns, τ_3=200±10 ps for both samples. In addition to the values of the intermediate and short lifetime components, τ_2=2 ns and τ_3=200 ps respectively, being similar for both HP and LP, so are the A-factors and contributions to the SS emission.

The component with the shortest lifetime, τ_3=100±10 ps is the major constituent of the excited state population for both samples across the emission region studied. For HP the A-factor decreases from 0.68-0.55 as λ_{em} increases from 560 nm to 600 nm and for LP the contribution decreases from 0.74 to 0.70 as λ_{em} increases from 560 nm-580 nm. These decreases in A-factor with increasing emission wavelength indicate that these are relatively short conjugation length species, similar in nature in both the HP and LP samples, which have an efficient NR pathway.

Comparing these values and trends with those seen at λ_{ex}=360 nm, λ_{em}=550 nm, the actual lifetimes show slight discrepancy, but certainly they are comparable. This discrepancy arises because for polymer species each lifetime is likely to represent a distribution of species with lifetimes of similar magnitude. The slightly different lifetime values obtained for each sample at the long emission wavelengths, or the difference in the lifetimes obtained for the two different excitation wavelengths, implies that slightly different distributions of emitting species are produced. The difference between the A-factors at the two excitation wavelengths is much more pronounced than the difference in lifetimes. At λ_{ex}=360 nm, the shortest component is a less significant contributor to the emitting population than at λ_{ex}=450 nm (A-factor of 0.23 and 0.38 for HP and LP respectively at λ_{ex}=360 nm). This reflects the dominance of the trimer emission when exciting at 360 nm.

The components with the intermediate lifetimes, τ_2=1.51±0.1 ns for both HP and LP, contribute the second highest proportion of the three components to the excited state population. The A-factors of these species increase as λ_{em} increases, an observation

that is more apparent for the HP sample (0.18 at 560 nm; 0.24 at 580 nm; 0.29 at 600 nm) than for the LP sample (0.15 at 560 nm; 0.18 at 580 nm). Hence it can be inferred that this is a species with a longer conjugation length, and a less efficient NR pathway, than that giving rise to τ_3=100 ps.

The value of the lifetime of the longest component, τ_1, is different in HP (4.8±0.1 ns) from that in LP (5.8±0.1 ns). In the case of LP the value is the same as the trimer lifetime acquired at λ_{ex}=360 nm, λ_{em}=435-550 nm, ergo it is the trimer emitting species. Although trimer excitation would be expected to be minimal at λ_{ex}=450 nm, the SS emission spectrum (figure 6.7) shows that it is occurring; overlap between the weaker, longer wavelength emission from the longer conjugation length species (the peak) and the tail of the trimer emission spectrum is evident. This component constitutes the least of the emitting population of the sample, and can be said, within experimental error, to remain constant over the emission wavelength range (A-factors of 0.11 at 560 nm and 0.12 at 580 nm).

The lifetime of the corresponding component in the HP sample is 4.8±0.1 ns, which is significantly shorter than that of LP (τ_1=5.8±0.1 ns). The A-factor for this component increases marginally from 0.14 at 560 nm to 0.16 at 580 nm, an increase slight enough to be assumed to be within experimental error, such that the A-factors can be said to remain constant over this emission wavelength region. The SS emission of the HP sample shows more intense 'polymeric' emission than the LP sample. The longest lifetime, 4.8±0.1 ns, for the HP sample may be attributable to the overlap of the trimer lifetime and a relatively long-lived polymer species with a

similar lifetime. For both samples emission from the long τ component dominates the SS fluorescence spectrum. Conversely, for both samples, the major contributor to the excited state population is the shortest-emitting species, τ_3. Work carried out on PPV by Samuel *et al* shows that exciting at longer wavelength results in a single lifetime being observed, which was proposed to be the longest possible conjugation length species[8,9]. This is not the case here, where multiple fluorophores are apparently being observed.

6.4. Conclusion

The fluorescence decay lifetimes obtained could not be attributed to the 5CnI monomer, whose lifetime has been determined as τ= 4.3 ns[5], for any of the cases studied . The lifetime of 5CnI free trimer was determined as 5.8 ns. Exciting at λ_{ex}=360 nm, the major emitting species of both the HP and the LP samples at all emission wavelengths is the free trimer. Components attributed to conjugated polymer had shorter lifetimes than the free trimer, indicating more efficient non-radiative decay pathways, likely to be intramolecular energy transfer.

Excitation at the long wavelength, 450 nm, resulted in emission that is characteristic of lower excitation energy polymer species. A distribution of lifetimes averaging to 3 distinct polymer lifetimes was observed. The polymer species with the dominant contribution to the emitting population had the short decay time 130±10 ps for both samples, and appeared to have a relatively short conjugation length. This implies that a major channel for NR decay is energy transfer to surrounding longer conjugation length, lower excitation energy segments of polymer. This short lifetime

component accounts for less than 10% of the long wavelength SS emission for both samples because of its low quantum yield.

The fluorescence properties of the HP and LP samples are very similar. The nature of the conjugation lengths of the emitting species seems to be the same in each sample, with only slightly more polymer apparent in the HP sample. It is known that the extent of conjugation in these systems is difficult to determine electrochemically, but fluorescence lifetime measurements can be used to characterise this. Considering electrochemical measurements, Koutecky-Levich analysis (chapters 2 and 4) has shown[1] that these films have a constant slope, if allowances are made for the concentrations. From the slope of the Koutecky-Levich plots, the number of electrons, n, transferred per indole monomer was calculated as 2.7±0.4, which is consistent with polymerisation reactions that produce a high proportion of trimer[1]. Here, for the first time, the fluorescence data confirms that, at short excitation and emission wavelengths, emission can be attributed solely to the trimer fluorophore. Therefore, it has now been shown that it is possible to make films of poly-5CnI under a variety of W and C conditions, which contain essentially only one fluorescent species. The intrinsic fluorescence of all the molecules in the poly-5CnI coat are essentially the same, and it is now possible to study the fluorescence of as-deposited films, and probe the effects of inter-species energy transfer on the fluorescence lifetimes.

6.5. References

1. J.G. Mackintosh, C.R. Redpath, A.C. Jones, P.R.R. Langridge-Smith, A.R. Mount, *J. Electroanal. Chem*, 1995, **388**, 179-185
2. J.G. Mackintosh, C.R. Redpath, A.C. Jones, P.R.R. Langridge-Smith, D.R. Reed, A.R. Mount, *J. Electroanal. Chem.*, 1994, **375**, 163
3. P. Jennings, A.C. Jones, A.R. Mount and A.D. Thomson, *J. Chem. Soc., Faraday Trans.*, 1997, **93(21)**, 3791-3797
4. P. Jennings, A.C. Jones and A.R. Mount, *J. Chem. Soc., Faraday Trans.*, 1998, **94**, 3619-3624
5. P. Jennings, *PhD Thesis*, 1999, University of Edinburgh
6. .J. Schwartz, *Annual Review of Phys. Chem.*, 2003, 141-172
7. J.G. Mackintosh, *PhD Thesis*, 1996, The University of Edinburgh
8. I.D.W. Samuel, B. Crystall, G. Rumbles, P.L. Burn, A.B. Holmes, R.H. Friend, *Synth. Met.*, 1993, **54**, 281
9. I.D.W. Samuel, B. Crystall, G. Rumbles, P.L. Burn, A.B. Holmes, R.H. Friend, *Chem. Phys. Letts.*, 1993, **213(5,6)**, 472

Chapter 7

Fluorescence of 5-bromoindole trimer

7.1. Introduction

Like 5CnI, 5-bromoindole (5BrI) is known to polymerise to form an asymmetric trimer unit (figure 7.1), which further polymerises to form films of linked trimer units of various conjugation length.

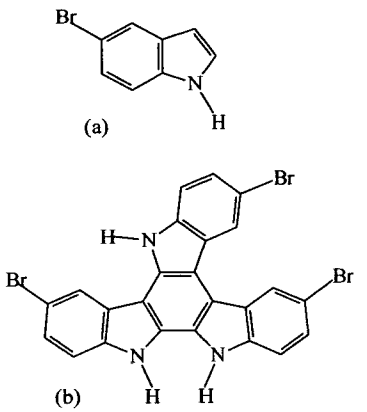

Figure 7.1: *(a) 5-Bromoindole Monomer (b) 5-Bromoindole asymmetric trimer*

Samples of poly-5CnI, when excited at λ_{ex}=360 nm, showed emission from the trimer exclusively at λ_{em}=435-500 nm, and the lifetimes obtained for each sample show that the trimer is the only species emitting (section 6.3.1). 5BrI trimer is not as easy to isolate. Using λ_{ex}=360 nm, and at λ_{em}=435-500 nm, in previous work, multiple components have been seen. Hence a subtle method for sample preparation had to be devised to obtain as pure a sample of 5BrI trimer as possible. The procedure for this is described in section 7.2.

In previous work a sample that appeared to contain free trimer had been studied[1], the lifetime of this free trimer species being 5.5 ns, but other decay components were also present. A sample of pure free trimer with a monoexponential fluorescence decay, τ, had not been produced; hence a definitive 5BrI free trimer lifetime had not been obtained. Having determined the 5CnI free trimer lifetime to be 5.8 ns (chapter 6) the logical next step is to determine the 5BrI free trimer lifetime.

7.2. Sample preparation

Even when synthesised under conditions that favour lower polymer, *i.e.* higher trimer content, polymer emission at λ_{em} >500 nm is evident; therefore a method of preparation of a purely trimer sample had to be devised. It is known that the solubilities of the different components within the films, *i.e.* free trimer units and polymer of different trimer conjugation lengths, are different in a given solvent[2]. This attribute, coupled with the facile control of composition of the film, enabled development of a 'linkage-and-extraction' technique.

A sample was prepared on polished Pt under conditions selected to generate a low trimer content film (c=10 mM, W=1 Hz). Then, after the standard wash-in-MeCN routine, the resulting film was cycled between -0.1 V and 1.1 V in electrolyte to encourage extensive linkage to trap the trimer components within. It would seem very likely that, in addition to the linked trimer chains, there would be isolated trimer units (fig 7.2) and the

difference in solubility between the free and linked trimer would enable selective sample solvation.

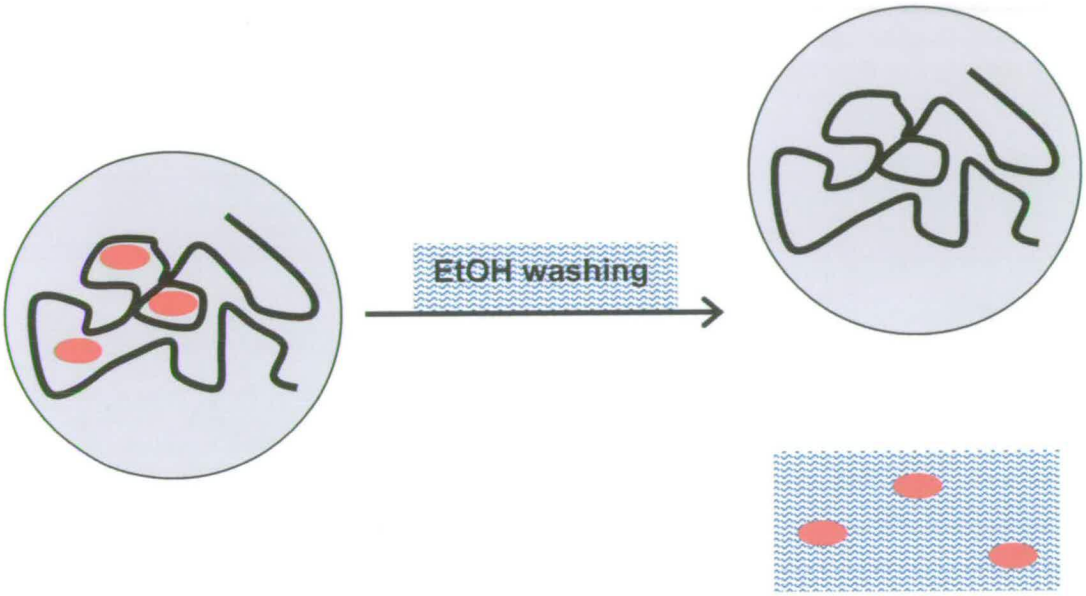

Figure 7.2: ***(a)*** *Representation of isolated, unlinked trimer units (red ellipses) within a long, tangled chain of linked trimers (black line) on the Pt electrode surface (grey background circle).* ***(b)*** *After washing with EtOH the more soluble isolated trimer units form a trimer solution, with the less soluble, highly linked chains of trimer remaining attached to the electrode surface.*

Removal of the film into the solvent, EtOH, occurred via successive washings of the sample, the intent being to remove components of different solubility at different stages of washing. Ideally, the free trimer chromophore solubility would be suitably different from that of the extensively linked polymer that a pure trimer sample might be obtained. Each washing was studied by SS fluorescence and TCSPC, and one yielded a single emitting species decay.

7.3. Monomer Fluorescence Lifetime

The SS emission spectrum of the 5BrIn monomer in EtOH was recorded at excitation wavelength of 275 nm and was found to comprise a single peak, emission maximum λ_{em}=338 nm. These results are consistent with previous work[1,3].The fluorescence lifetime of the 5-bromoindole monomer in EtOH has previously been found to be τ= 4.5 ns[3].

7.4. 5-BrI Trimer Fluorescence Lifetime

The SS fluorescence emission spectrum of the 5BrI trimer sample was recorded at λ_{ex}=360 nm (fig 7.3) and λ_{ex}=400 nm. The emission spectrum at λ_{ex}=360 nm is presented as it shows the entire emission profile.

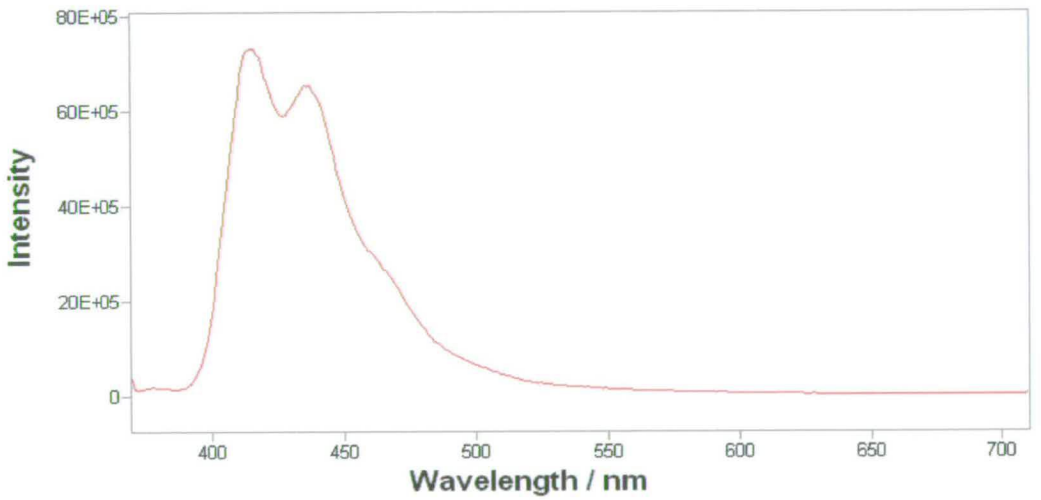

Figure 7.3: *SS emission spectra of the 5BrI trimer sample in EtOH. λ_{ex}=360 nm.*

The emission spectrum obtained is characteristic of trimer emission, with nothing that could be attributed to monomer fluorescence being observed. There is no significant

emission above λ_{em}=500 nm, which would indicate emission from polymeric species. Additionally, using λ_{ex}=400 nm no emission from polymeric species is observed.

TCSPC experiments were performed using λ_{ex}=400 nm, λ_{em}=435 nm, giving a single exponential decay indicating the presence of one emitting species (fig 7.4).

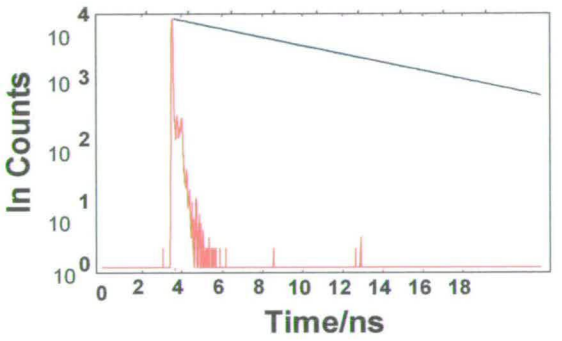

Figure 7.4. *TCSPC decay of free trimer sample showing one emitting species. Black line is experimental data, blue line is the fitted function, red line is the IRF.*

The lifetime obtained for the decay was τ=5.5 ns, with χ^2=1.1. This indicates the high quality of the fitting.

7.4.1. Discussion

The conditions employed for synthesis of this sample were chosen to produce the maximum amount of free trimer possible. The SS emission spectrum verifies that this is the case, with no evident emission at longer wavelengths (λ_{em}>500 nm), *i.e.* no emission from the longer conjugated polymeric species. At the excitation wavelength λ_{ex}=400 nm, the emission at λ_{em}=435 nm is where the trimer fluoresces, hence the lifetime obtained, τ=5.5 ns, must be the lifetime of the trimer

The lifetime of the trimer, τ=5.5 ns, is of similar magnitude, but slightly longer than that of the monomer, 4.5 ns. This is expected for a system of greater electronic delocalisation. The 5BrI trimer lifetime is very similar to that of the 5CnI trimer, τ=5.8 ns. The presence of the Br atom in 5BrI trimer seems to have made no significant difference to the lifetime compared to the 5CnI trimer. This is also the case with the monomer. Often, the presence of such an atom causes an appreciable reduction in lifetime through the heavy atom effect (HAE). However, this is not the case here.

7.5. Conclusions

Using the 'linkage-and-extraction' technique described in section 7.2 it was possible to produce a sample of pure free 5BrI trimer in solution. The fluorescence decay of this sample was a single exponential with a lifetime of 5.5 ns, which is therefore defined as the characteristic lifetime of the free 5BrI trimer molecule.

7.6. References

1. P. Jennings, *PhD Thesis*, 1999, The University of Edinburgh
2. J.H. Burroughes, D.D.C. Bradley, A.R. Brown, R.N. Marks, K. Mackay, R.H. Friend, P.L. Burns and A.B. Holmes, *Nature*, 1990, **347**, 539
3. P. Jennings, A.C. Jones, A.R. Mount, *J. Chem. Soc., Faraday Trans.*, 1998, **94**, 3619-3624

Chapter 8

Fluorescence of Poly-5-Bromoindole Prepared on a Bare Pt Electrode

8.1. Introduction

Solutions of poly-5-Bromoindole (poly-5BrI) are, like those of poly-5CnI, highly luminescent[1,2]. The most notable difference between poly-5-BrI and polymers of many other luminescent poly-5-substituted indoles is that solutions of poly-5-BrI exhibit intense steady state (SS) emission at long emission wavelengths, even at relatively high excitation energies, *i.e.* the emission is not dominated by that arising from the trimer species.

Like 5CnI, 5-bromoindole (5BrI) is known to polymerise to form films of linked trimer units (figure 8.1) of various conjugation length.

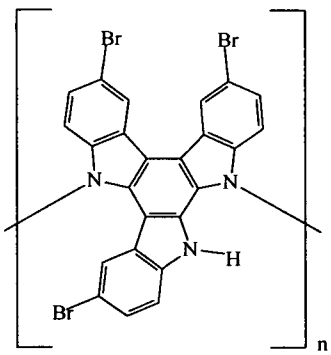

Figure 8.1: *5-Bromoindole asymmetric trimer showing linkage sites.*

At λ_{ex}=360 nm the 5BrI trimer species emits in the region λ_{em}=400-500 nm, a characteristic shared with the 5CnI trimer. However, unlike 5CnI, 5BrI samples show SS emission of significant intensity at wavelengths greater than 500 nm, and there is a clear difference between the SS emission of films prepared to give higher proportions of polymer and trimer. Therefore, 5BrI offers the opportunity of probing the photophysics of polymer species further.

8.2. Sample Preparation

Films of poly-5BrI were synthesised on bare polished Pt electrodes. Conditions were chosen so that films of relatively higher and lower polymer content were produced. The polymerisation conditions employed are presented in table 8.1. The films were washed thoroughly in MeCN to remove any monomer, and then were dissolved entirely into EtOH. Each sample was studied by Steady State Fluorescence Spectroscopy (SS) and Time Correlated Single Photon Counting (TCSPC).

Sample	C / mM	W / Hz
Higher polymer	10	1
Lower polymer	200	9

Table 8.1: *The conditions used for sample preparation showing concentration of the original monomer solution used and disc rotation speed (W)*

8.3. Steady State Fluorescence

Steady State emission spectra were recorded for both HP and LP samples at λ_{ex}=360 nm as shown in figure 8.2.

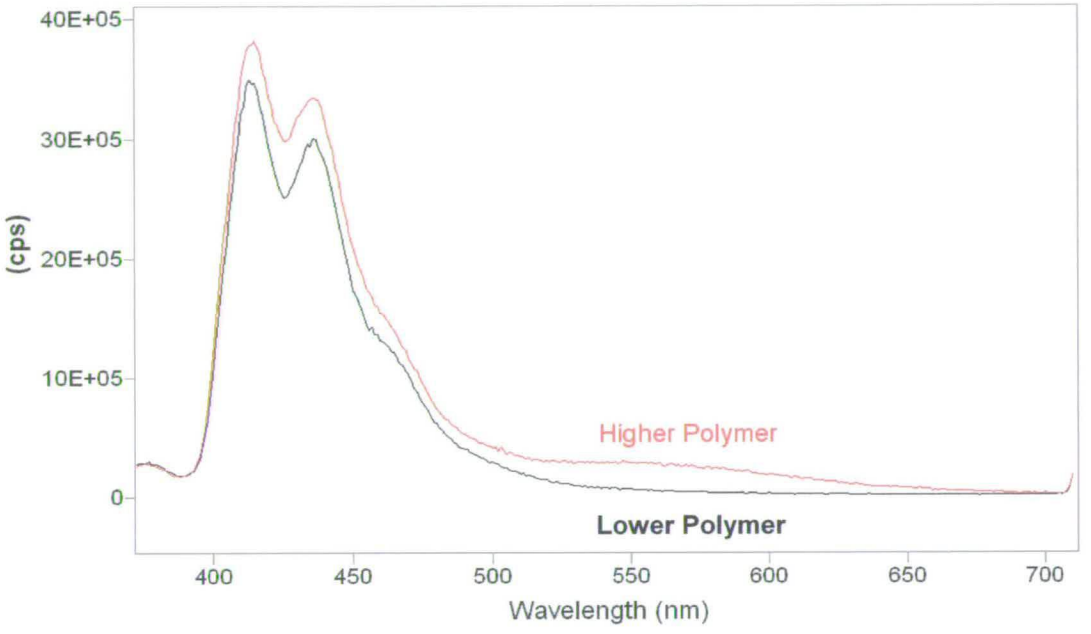

Figure 8.2: *SS emission spectra for HP and LP poly-5BrI in EtOH at λ_{ex}=360 nm*

The emission spectra of both samples at λ_{ex}=360 nm show nothing that could be attributed to the monomer[2], with the spectra shifted considerably to lower energy. The emission spectra for both HP and LP are dominated by intense fluorescence between λ_{em}=400-500 nm, attributed to trimer, with maxima at 414 nm and 434 nm, and a shoulder at 450 nm. The excitation maxima for these samples are also shifted compared to the monomer, 380 nm and 400 nm rather than 275 nm[2]. In contrast with the 5CnI

samples, those from 5BrI show a peak at longer λ_{em}, which is attributed to the polymeric emitting species.

SS emission spectra of the HP and LP samples were also recorded using λ_{ex}=450 nm (figure 8.3)

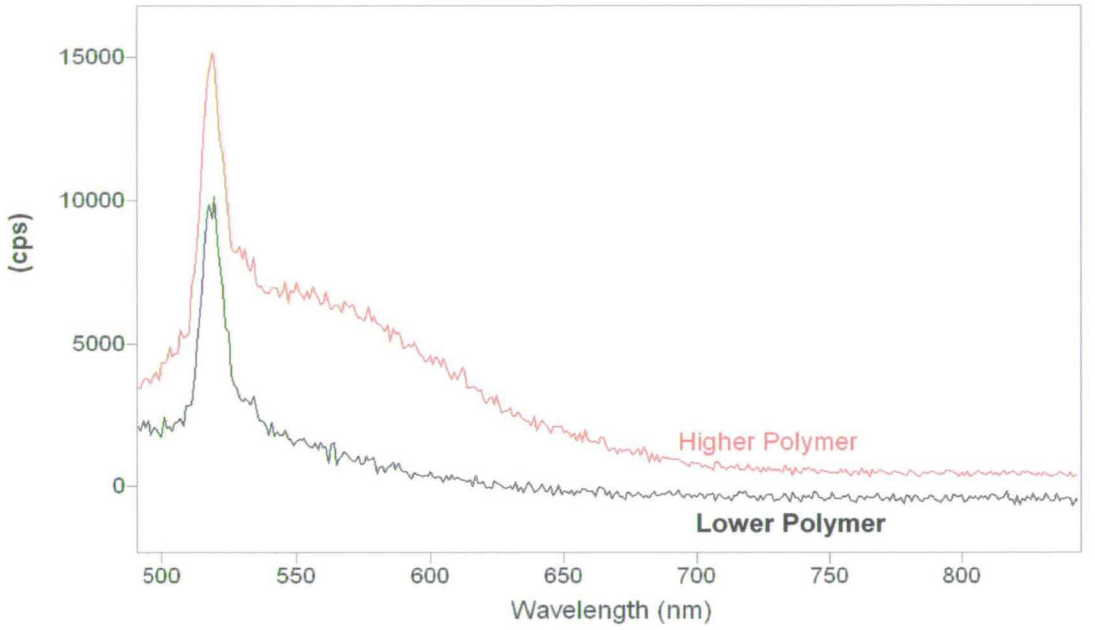

Figure 8.3: *SS emission spectra for HP and LP poly-5BrI in EtOH at λ_{ex}=450 nm*

Although there is evidently emission from the HP sample at λ_{ex}=450 nm, it is low in intensity. There is a clear difference between the HP and LP samples: the LP does not have any significant emission intensity in this wavelength region. Owing to the low intensity, It was not practical to record fluorescence decays of these samples at λ_{ex}=450 nm.

8.4. Time Correlated Single Photon Counting at λ_{ex}=360nm

TCSPC experiments were carried out at λ_{ex}=360 nm over the range λ_{em}=400-450 nm. Although there is clearly intense emission at 414 nm, it was found that this peak coincided with a Raman band; hence obtaining meaningful lifetimes was not possible. The decays could not be fitted to a set of global lifetimes for either HP or LP; therefore the lifetimes obtained from individual fits are presented in tables 8.2 and 8.3.

8.4.1. LP Sample: Results and Discussion

The lifetimes obtained for the decays of the LP sample obtained at λ_{ex}=360 nm, λ_{em}=435 nm and 450 nm are presented in table 8.2.

Lifetime / ns	τ_1 A_1 %	τ_2 A_2 %	τ_3 A_3 %	χ^2
λ_{em}=435 nm	2.50 <0.01 4.0	0.35 0.04 7.0	0.17 0.96 89	1.17
λ_{em}=450 nm	2.80 <0.01 5.0	0.47 0.02 4.0	0.17 0.98 91	1.14

Figure 8.2: *Individual lifetimes, A-factors (fraction of 1), % contribution to SS fluorescence emission and χ^2 for LP, λ_{em} range 435-450 nm. Major component of sample highlighted.*

The decay of the LP sample could be fitted to 3 lifetimes at both of the emission wavelengths, the values of the lifetimes at both wavelengths being comparable. The lifetimes obtained are τ_1=2.6±0.2 ns, τ_2=0.4±1 ns and τ_3=170 ps. The 170 ps component forms virtually all of the excited state population at both of the emission wavelengths studied, the A-factors being 0.96 at 435 nm and 0.98 at 450 nm. This component also constitutes 90±1% of the SS emission at both wavelengths. The τ_1=2.6 ns component is almost negligible in terms of its A-factor, and the τ_2=0.4 ns component has an A-factor of only 0.03; combined the 0.4 ns and 2.6 ns components constitute only 10±1% of the SS emission.

The SS emission spectrum of the LP sample is characteristic of the trimer; therefore the 170 ps component must be a trimer species. The SS emission spectra of the LP sample and the free trimer sample appear to be identical over the emission region 435-450 nm. However, this lifetime is dramatically different from the free trimer lifetime of 5.5 ns (chapter 7). The 170 ps component must be a trimer species that is subject to very efficient non-radiative decay. This lifetime can be attributed to a highly quenched trimer species within a polymer chain. Such a species would constitute the shortest possible conjugation length unit within the polymer chain and would be subject to facile energy transfer to lower excitation energy, longer conjugation length segments. The components with the longer lifetimes could be short conjugation length oligomers; that is species of only a few trimer units, which are longer lived than the single quenched trimer unit but still emit with relatively short wavelength emission. Alternatively, the

2 ns and 0.4 ns components could be single trimer-conjugation-length units within different intrachain environments such as different length oligomers.

8.4.2. HP Sample: Results and Discussion

The decays of the HP sample obtained could be fitted to 4 lifetime components at each λ_{em}. The parameters obtained are presented in table 8.3.

Lifetime / ns	τ_1 A_1 %	τ_2 A_2 %	τ_3 A_3 %	τ_4 A_4 %	χ^2
λ_{em}=435 nm	5.70 0.03 62	1.10 0.05 15	0.21 0.25 16	0.03 0.67 6.95	1.06
λ_{em}=450 nm	5.80 0.04 58	1.20 0.06 17	0.25 0.25 16	0.06 0.65 9	1.03

Figure 8.3: *Individual lifetimes, A-factors (as a fraction of 1), % contribution to SS fluorescence emission and χ^2 for HP, λ_{em} range 435-450 nm. Major component of sample highlighted.*

The lifetimes, A-factors and percentage contributions to the SS emission are similar for both emission wavelengths. The lifetimes obtained are τ_1=5.7±0.1 ns, τ_2=1.1±0.1 ns, τ_3=0.23±0.02 ns and τ_4<100 ps. The highest constituent of the excited state population is the shortest component with the sub-100 ps lifetime, A-factor 0.66±0.01 of the emitting population at both emission wavelengths. The τ_3=210 ps component constitutes

the next highest proportion (A-factor 0.25), with the τ_1=5.7 ns and τ_2=1.1 ns making up less than 0.10 between them. The τ_1=5.7 ns component contributes the most to the SS emission, (60±2%). The τ_2=1.1 ns and τ_3=210 ps components each make up 16±1% at each wavelength, and the sub-100 ps components constitute less than 10% of the total SS emission.

In chapter 9 it will be shown that the sub-100 ps component is characteristic of the poly-5BrI polymer emission. In the present sample, although this component constitutes the majority of the emitting population, it contributes less than 10% to the SS emission, and can be attributed to the short wavelength tail of the polymer emission spectrum, which overlaps with the trimer emission region.

60% of the SS emission comes from the 5.7 ns component. This, as shown in chapter 7, corresponds to the free trimer in solution. This component is the smallest constituent of the excited state population; however, there is more of this species present in this sample than the LP sample, where no free trimer was detected. It is likely that during polymerisation of the HP sample, free trimer units are trapped within the polymer strands, as discussed in chapter 7. When the film is dissolved these are released as free trimers in the solution.

The 230 ps component can be assumed to be the same type of emitting species as the 170 ps component in the LP sample; that is, it is a highly quenched intra-chain trimer

unit. The 1 ns component could be either a short conjugation length species or a trimer unit in a different intra-chain environment from the 170 ps trimer component.

The LP sample exhibits 3 fluorescent components, the overwhelmingly major contributor to the emitting population being the 170 ps component. The A-factor for this is 0.97±0.01 at both emission wavelengths. Having been prepared under conditions that encourage trimer formation, the initial thought might be that high free trimer content would be observed. From the lifetimes and A-factors, this is clearly not the case. The reason for this is that the 5BrI trimer is a fairly soluble product of the electropolymerisation reaction; under polymerisation conditions that produce trimer-rich films little linkage of the trimers is occurring, so the newly formed trimer units will tend to be swept into the bulk solution. In contrast, under conditions that produce polymer-rich films, a great deal of linkage of the trimers is occurring, and unlinked trimer units become trapped in the polymer that is forming; when the polymer film is dissolved into EtOH these trimer units are freed. Thus the lifetime of the free trimer is seen in the fluorescence decay of the HP sample.

In clear contrast to the HP and LP samples of 5CnI, which exhibit a single fluorophore, τ=5.8 ns at λ_{ex}=360 nm in the range λ_{em}=435-500 nm, and the sample of selectively extracted 5BrI trimer, which exhibits a single fluorophore τ=5.5 ns at λ_{em}=435 nm, these 5BrI samples show multiple emitting species in the region λ_{em}=435-450 nm. Moreover,

there are considerable differences between the HP and LP samples in this region, which were not observed for the poly-5CnI HP and LP samples when exciting at λ_{ex}=360 nm.

The present results may be compared with the work carried out by Samuel *et al* on PPV systems[3]. In the latter work, as in the present case, when exciting at short wavelengths a multi-component decay was observed. This is evidence for intra-chain excitation, as explained in section 1.7.1. This phenomenon will be discussed further in relation to the results in chapter 9.

8.5. Conclusions

Both LP and HP samples have a component with a lifetime of around 200 ps, which corresponds to a heavily quenched intrachain trimer moiety. The HP sample also exhibits emission from a short conjugation length polymer species, which has a sub-100 ps lifetime, and from free-trimer. The latter two species are not apparent in the LP sample. In fact the emission from the LP sample is almost entirely due to the highly quenched intrachain trimer species.

This study of poly-5-BrI produced on a bare Pt electrode proved valuable in revealing the existence of an intrachain trimer species that is spectroscopically identical to the free trimer, but whose fluorescence lifetime is over two orders of magnitude shorter. However, the polymerisation process of 5BrI on bare Pt does not yield predictable results, as the polymerisation is not as controlled as for other indole systems. The

polymerisation of 5BrI on bare Pt in chapter 4 shows variability due to the difficulty in making the first film on the surface and changing current with t. This difficulty in initial film formation causes there to be different surface conditions upon which polymerisation may occur. Using a template of a substance that polymerises relatively easily means that there is a completely even surface upon which polymerisation may occur.

8.6. References

1. P. Jennings, A.C. Jones, A.R. Mount, *J. Chem. Soc., Faraday Trans.*, 1998, **94**, 3619-3624
2. P. Jennings, *PhD Thesis*, 1999, The University of Edinburgh
3. I.D.W. Samuel, G. Rumbles and C.J. Collison, *Am Phys. Soc. Phys Rev. B, Rapid Comm.*, 1995, **52(16)**, 573-576

Chapter 9

Fluorescence of Poly-5-Bromoindole Prepared on a Poly-5-Nitroindole Template

9.1. Introduction

9.1.1. Intrachain and Interchain Interactions in Conjugated Polymer Systems

In earlier chapters (chapter 1, 6 and 8) the concept of intrachain energy transfer was mentioned as the reason for the shorter-than-trimer polymer lifetimes in chapter 6 and the quenched trimer lifetimes in chapter 7. However, for the systems reported in chapters 6 and 8 there was not much fluorescence intensity from the polymer species. The phenomenon of intrachain excitation and energy transfer becomes more apparent for the longer emission wavelength polymer species in this chapter.

As described in chapter 1, studies of photoluminescence in PPV and MEH-PPV systems have shown that the sample consists of regions with a range of conjugation lengths and excitations migrate to lower energy regions before photons are emitted[1,2]. Additionally it was found that the luminescence decay is slower in solid films than in solutions; these results were attributed to the formation of interchain species[3,4]. Interchain species can only be formed if the polymer species are in close proximity to one another[2], for example in a solid film. For a dilute solution, such as those studied in this thesis, the likelihood of two distinct species coming into close enough proximity with one another to allow this to happen is very small. The degree of coiling of the polymer species also is a factor in the likelihood of a polymer chromophore encountering another species, the

likelihood being greater for an open, uncoiled chain than a tightly coiled one[2]. However, as described in section 1.7.1, even for a tightly coiled polymer chain a kind of pseudo-interchain energy transfer may occur between two sections of a long, coiled or tangled polymer strand.

Although 5-bromoindole (5BrI) oxidises to form the asymmetric trimer, which subsequently oxidises further to give the polymer of linked trimers commonly seen for such indole monomers[5,6,7,8,9,10,11,12], its polymerisation does not occur as reproducibly as for other systems, such as 5-cyanoindole (5CnI), thus less precise control of the polymerisation procedure is possible. It has been shown that the use of a template film improves the reproducibility of polymerisation in the case of such monomers[13], therefore a template layer of 5-nitroindole was used. This was found to improve the control and reproducibility of the polymerisation process greatly, as seen in chapter 4.

Particular care was to be taken when investigating the fluorescence of the samples that were prepared in this manner. At the interface between the 5NI and the 5BrI layers, there may be co-polymerisation between the 5NI and 5BrI species. The outer layers, however, are films of pure poly-5BrI. Hence the 5BrI samples were to be removed by method washing as carried out when attempting to obtain pure 5BrI trimer, illustrated in chapter 7.

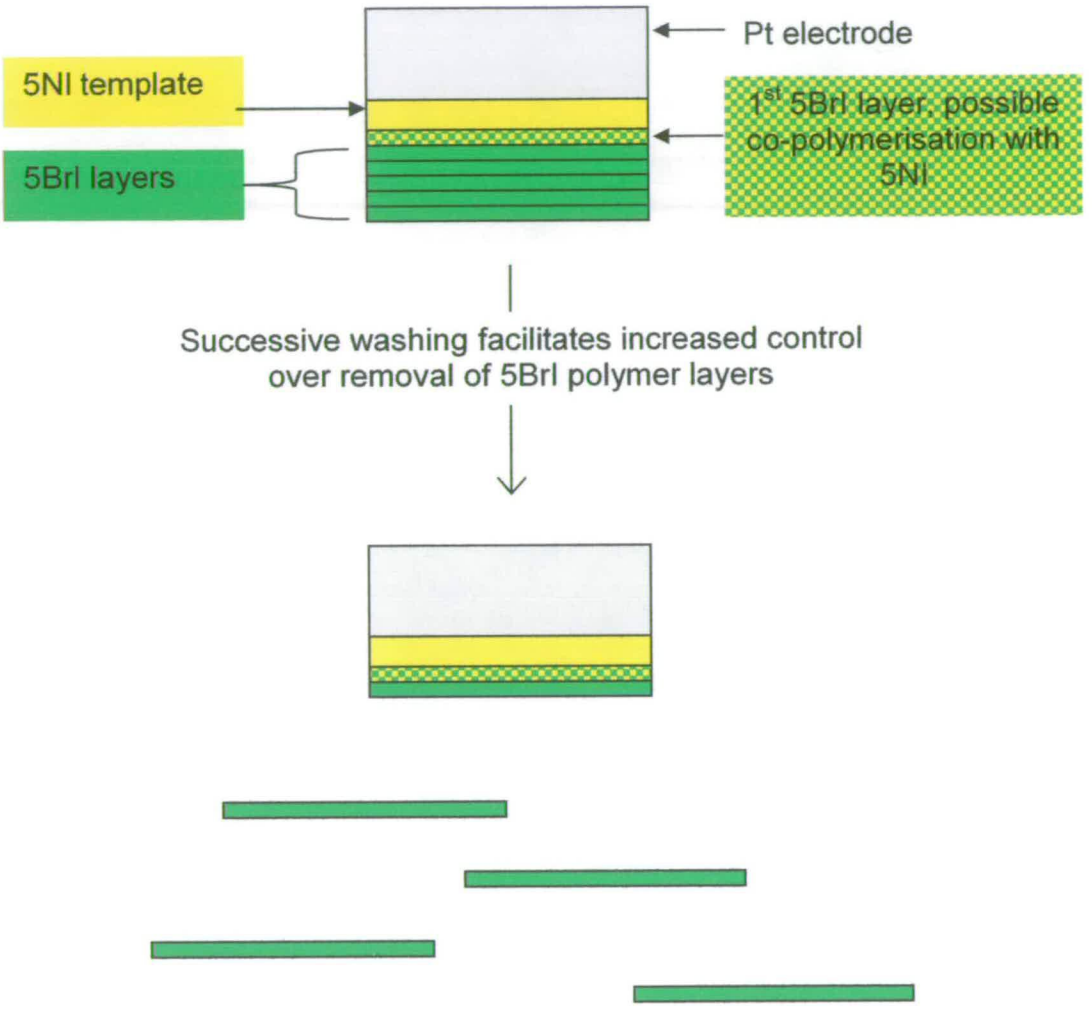

Figure 9.1: *Representation of 'successive washing' method of polymer removal*

9.1.2. Sample Preparation

Preparation of poly-5-BrI was achieved using the standard technique that is outlined in chapter 3. Samples were prepared to enable comparison of fluorescence characteristics between 'higher polymer' (HP) and 'lower polymer' (LP) film samples. The films were prepared from monomer solutions of different concentrations and at different rotation speeds, chosen to optimise trimer formation or linkage as necessary. The 5NI template was prepared using the standard electro-polymerisation technique, on a polished Pt electrode, from a 50 mM solution with a rotation speed of 2 Hz. This template was rinsed thoroughly in background electrolyte prior to the polymerisation of 5BrI on top of it. The conditions for the polymerisations of 5BrI are given in table 9.1.

Sample	Concentration / mM	W / Hz
Lower polymer, LP	200	9
Higher polymer, HP	10	1

Table 9.1: *Conditions for the polymerisation of the HP and LP 5BrI samples on 5NI. All polymerisations were carried out for 60 seconds*

The 5BrI films were rinsed in MeCN to remove any monomer, and were subjected to successive washings, each in 10 ml EtOH for 10 s.

SS fluorescence emission spectra were obtained for both samples HP and LP at λ_{ex}=360 nm and λ_{ex}=450 nm. Excitation information was obtained at emission wavelengths chosen to coincide with the trimer and polymer emission maxima. For comparison TCSPC experiments were performed on a sample of poly-5NI in solution. This was found to be non-fluorescent, as expected.

9.2. Steady State Fluorescence Spectra

Using λ_{ex}=360 nm excites all emitting species in the sample, resulting in a SS fluorescence spectrum (figure 9.2) showing emission from all fluorophores. To generalize, the 'trimer' emission lies in the region λ_{em}=400-500 nm, the 'polymer' $\lambda_{em}\geq$550 nm[14]. At λ_{ex}=450 nm, the longer conjugation length species are excited directly but this wavelength is of sufficiently low energy to preclude trimer excitation, hence the only emission observed is from the longer conjugation length species. The SS fluorescence emission spectra for the HP and LP samples were recorded at λ_{ex}=360 nm and λ_{ex}=450 nm (figures 9.2 and 9.3), and exhibit markedly different emission profiles.

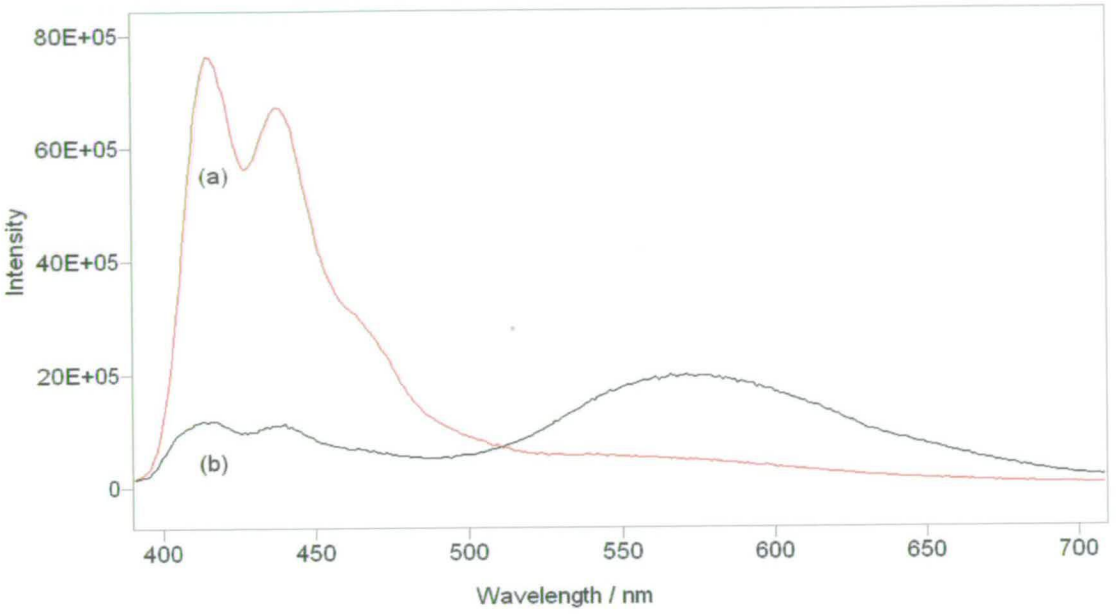

Figure 9.2: *SS emission spectra of 5BrI films in EtOH, λ_{ex}=360 nm. (a) LP, (b) HP.*

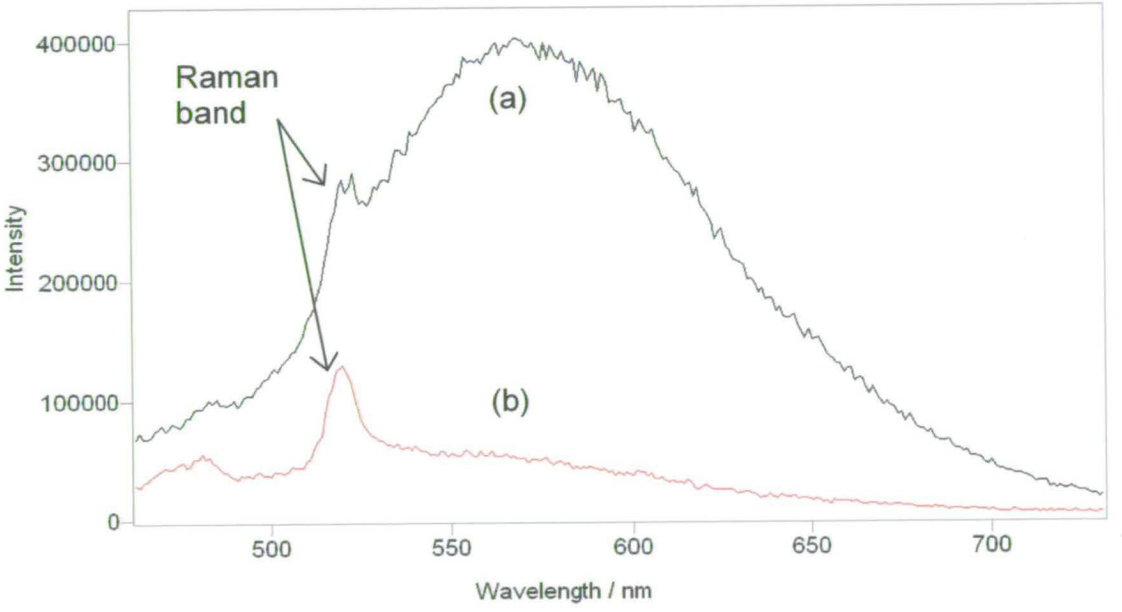

Figure 9.3: *SS emission spectra of 5BrI films in EtOH. (a) HP, (b) LP. λ_{ex}=450 nm.*

When exciting at λ_{ex}=360 nm, the emission of the LP sample is significantly higher in intensity in the region λ_{em}=400-500 nm than that of the HP sample, whereas the HP sample has much higher intensity emission in the λ_{em}>500 nm region than the LP sample. The maximum intensity of the emission from the HP sample in the λ_{em}>500 nm region is almost double that of the maximum intensity of its emission in the region λ_{em}=400-500 nm whereas the maximum intensity of the emission of the LP sample in the region λ_{em}=400-500 nm is almost ten times the maximum intensity at λ_{em}>500 nm.

Exciting at λ_{ex}=450 nm, the HP sample shows relatively intense emission across the region λ_{em}=500-650 nm, with a clear maximum at 560 nm. The LP sample shows some emission, but its emission maximum is less well defined, and is almost 10 times less intense, than the HP sample. Neither sample exhibits the overlap from the trimer emission that was seen for the poly-5CnI sample using λ_{ex}=450 nm (chapter 6).

9.3. Time–resolved fluorescence at λ_{ex}=450 nm

Fluorescence decays were recorded using λ_{ex}=450 nm so that the lifetimes of the low energy, long conjugation length species, which emit at longer wavelength, could be determined with minimal interference from the trimer.

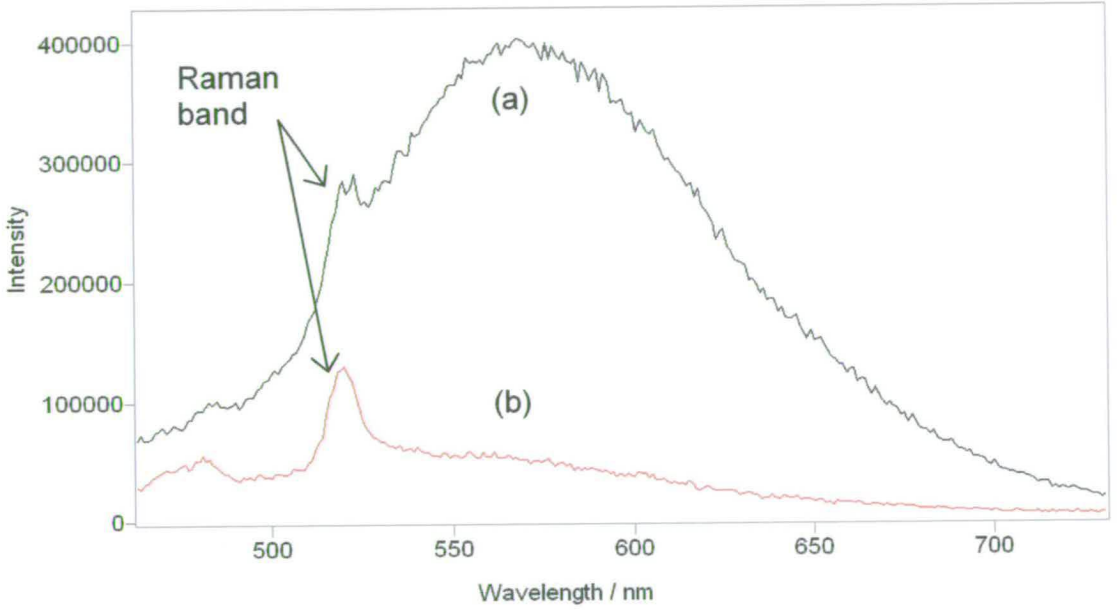

Figure 9.4: *SS emission spectra of 5BrI films in EtOH. (a) HP, (b) LP. λ_{ex}=450 nm.*

Decays for the HP sample were recorded over the whole emission region λ_{em}=500-600 nm, avoiding the Raman band at 520 nm. The decays of the LP sample were recorded at 550 nm and 600 nm.

9.3.1. HP Sample

9.3.1.1. Results

The fluorescence decays for the HP sample across the emission region λ_{em}=500-600 nm could be fitted to one set of 4 global lifetimes (table 9.2). This implies that similar species are contributing to the emitting population over the emission wavelength range λ_{em}=500-600 nm. None of the lifetimes obtained can be attributed to the monomer (4.5 ns)[12] or the trimer (5.5 ns).

Global lifetime / ns	τ_1 **7.50**	τ_2 **2.90**	τ_3 **0.60**	τ_4 **0.07**	χ^2_g **1.23**
λ_{em} / nm	A_1 %	A_2 %	A_3 %	A_4 %	χ^2
500	0.05 40	0.16 48	0.13 8.1	0.66 4.7	1.26
550	0.04 28	0.21 58	0.15 8.4	0.61 4.1	1.21
560	0.04 25	0.22 62	0.15 8.5	0.60 3.9	1.22
570	0.03 23	0.23 64	0.16 6.1	0.58 3.7	1.22
600	0.03 18	0.24 67	0.19 11	0.55 3.6	1.24

Table 9.2: *Global lifetimes, A-factors (as a fraction of 1), % contribution to SS fluorescence emission and global χ^2 for HP, λ_{em} range 500-600 nm. Global χ^2 values for each λ_{em} are comparable to those obtained for individual fits. Emitting species with highest A-factor, i.e. component constituting highest proportion of excited state population, is highlighted.*

The lifetimes obtained for the emission region λ_{em}=500-600 nm span 2 orders of magnitude, the longest lifetime component τ_1=7.5±0.1 ns and the shortest lifetime component τ_4=70±10 ps. The intermediate lifetime components are τ_2=2.9±0.1 ns and τ_3=600±10 ps. To facilitate comparison of the trends across the emission region, the A-factors and percentage contributions to the SS emission were plotted against the corresponding λ_{em} (figures 9.5 and 9.6).

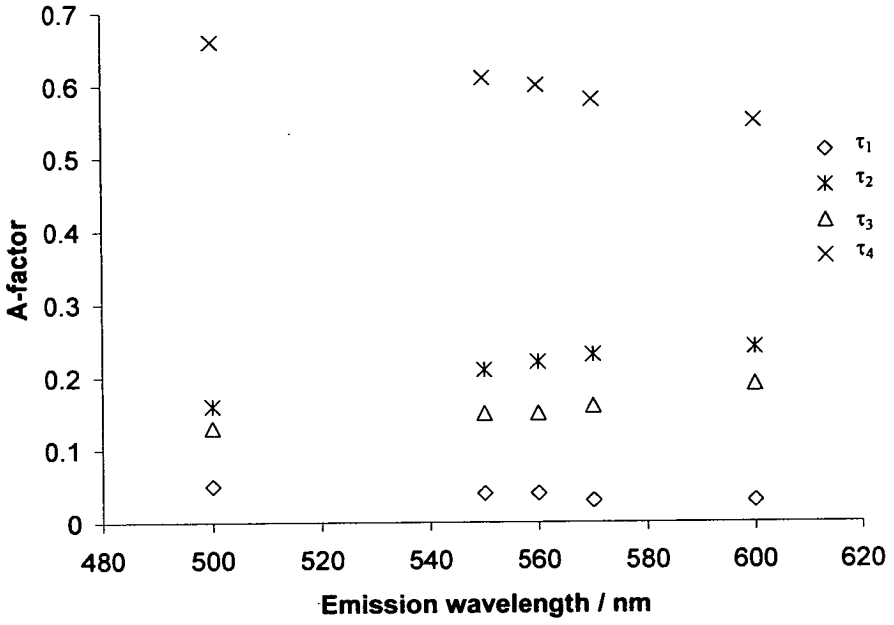

Figure 9.5: *A-factor vs. emission wavelength, λ_{ex}=450 nm, HP sample, λ_{em}=500-600 nm. τ_1=7.5 ns, τ_2=2.9 ns, τ_3=0.6 ns, τ_4=70 ps.*

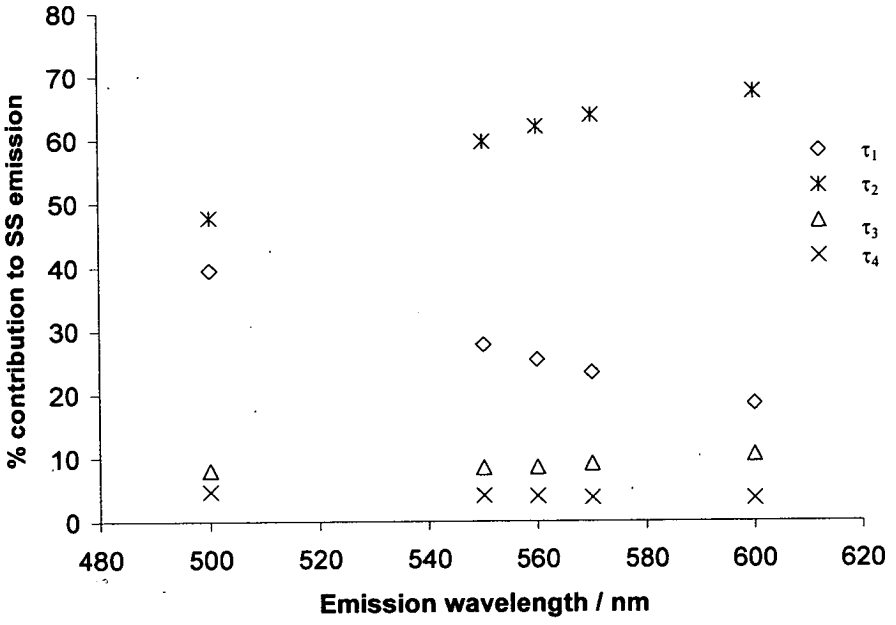

Figure 9.6: *% contribution vs. emission wavelength, λ_{ex}=450 nm, HP sample, λ_{em}=500-600 nm. τ_1=7.5 ns, τ_2=2.9 ns, τ_3=0.6 ns, τ_4=70 ps.*

The A-factors indicate that the majority of the excited state population can be attributed to the 70 ps component across the whole emission region, and this contribution decreases from 0.66 at 500 nm to 0.55 at 600 nm. Owing to the very short lifetime, this component contributes the least to the overall SS emission, 5% at 500 nm and 4% at 600 nm. The longest lifetime component τ_1=7.5 ns constitutes the lowest proportion of the excited state population, 0.05 at λ_{em}=500 nm and 0.03 at λ_{em}=600 nm. This component's contribution to the SS emission is considerable, 40% at 500 nm decreasing to 18% at 600 nm. The intermediate component with the lifetime 2.9 ns constitutes 0.16 of the excited state population at 500 nm, increasing to 0.24 at 600 nm, and it has the greatest contribution to the SS emission, increasing from 48% to 68% as emission wavelength increases from λ_{em}=550-600 nm. The shorter intermediate component with lifetime 580 ps constitutes 0.13 of the excited state population at 500 nm and 0.19 at 600 nm, and its percentage contribution to the SS emission is 8% at 550 nm and 11% at 600 nm.

9.3.1.2. Discussion

The components emitting when excited at λ_{ex}=450 nm will be conjugated lengths of polymer. As the emission wavelength increases from λ_{em}=560-650 nm, the A-factor of the 70 ps component decreases from 0.66 to 0.55. It constitutes the majority of the excited state population at t=0, and must be a conjugated species with an efficient non-radiative pathway; however, as its contribution decreases with decreasing emission energy it must be a component with a relatively short conjugation length *i.e.* higher

excitation energy than the other emitting polymer species. As the sample consists of polymer species of varying degrees of conjugation this relatively high-energy polymer species will donate energy to surrounding polymer species of longer conjugation length (figure 9.7) thus shortening its lifetime.

Figure 9.7: *Representation of the energy transfer (ET) mechanism from the relatively short conjugation length species to a longer conjugation length, lower energy species. (✓=ET)*

The intensity of both the 2.9 ns and 600 ps components increases over λ_{em}=500-600 nm, indicating that they are species with longer conjugation lengths, *i.e.* they have lower excitation energy) than the 70 ps component, the 2.9 ns component (0.16 at 550 nm; 0.24 at 600 nm) being the slightly higher contributor to the excited state population than the 600 ps component (0.13 at 550 nm; 0.19 at 600 nm). The lifetimes are shorter than that of the free trimer (5.5 ns, chapter 7), indicating that there is a non-radiative energy transfer pathway available to this species that was not available to the free trimer.

The 7.5 ns component constitutes only a very small fraction of the total initial excited state population of the sample (0.03±0.01), the A-factor being very small but decreasing from 0.05 to 0.03 with increasing wavelength. This lifetime is considerably longer than the free trimer lifetime of 5.5 ns. The other components in the HP sample, which have been attributed to polymer strands of different conjugation length, are much more abundant than the 7.5 ns component in the initial excited stated when λ_{ex}=450 nm.

Although it may be assumed that everything emitting in the λ_{em}=500-600 nm region must be attributable to conjugated species, it is possible that there is a small overlap from the tail of the trimer emission; hence the 7.5 ns component could be attributed to a mixture of the trimer emission and long-lifetime, low-abundance polymeric species.

9.3.2. Lower Polymer Sample

9.3.2.1. Results and Discussion

For the LP sample, decays were recorded at emission wavelengths λ_{em}=550 nm and 600 nm. The decays fitted globally to one set comprising three lifetimes (table 9.3), indicating that the nature of the emitting species does not vary significantly over the emission wavelength range λ_{em}=550-600 nm. The values of χ^2 indicate that the fitting is reasonably good, although not so good as for the HP sample.

Global lifetime / ns	τ_1 5.70	τ_2 3.00	τ_3 0.80	χ^2_g 1.29
λ_{em} / nm	**A_1 %**	**A_2 %**	**A_3 %**	**χ^2**
550	0.29 52	0.44 41	0.27 6.8	1.32
600	0.30 53	0.46 42	0.23 5.6	1.29

Table 9.3: *Global lifetimes, A-factors (as a fraction of 1), contribution to SS fluorescence emission and global χ^2 for LP, λ_{em} range 550-600 nm. χ^2 values are comparable to individual fits.*

None of the lifetimes obtained can be attributed to the monomer (4.5 ns)[12]. However, the longest lifetime component τ_1=5.7±0.1 ns is similar in value to the lifetime of the 5BrI trimer.

All three lifetimes obtained are reasonably long, τ_1=5.7±0.1 ns, τ_2=3.0±0.1 ns and τ_3=0.8±0.1 ns. There are no lifetimes of the sub-hundred-picosecond order, the shortest component approaching the nanosecond. The A-factors of the components do not vary significantly over the emission region λ_{em}=550-600 nm. The τ_2=3 ns component constitutes the majority of the initial excited state population, and its contribution does not change significantly over this emission region, increasing slightly from 0.44 at λ_{em}=550 nm to 0.46 at λ_{em}=600 nm. The τ_1=5.7 ns and τ_3=0.8 ns components each constitute a reasonable proportion of the excited state population, with the contribution of neither varying significantly over this emission region (0.29 at 550 nm, 0.30 at 600 nm and 0.27 at 550 nm, 0.23 at 600 nm for τ_1 and τ_2 respectively). More than 90% of the SS emission intensity arises from the components with lifetimes 5.7 ns (50±3%) and 3 ns (40±2) , the component τ_3=800 ps contributing less than 10% to the total emission seen.

The longest lifetime for the LP sample, τ_1=5.7 ns, which is, within the error boundaries, the same as the free trimer lifetime, τ=5.5 ns. This 5.7 ns component constitutes 0.30±0.01 of the excited state population at t=0. Although there is no obvious overlap with trimer emission, as there was for the poly-5CnI sample, the emission from the LP

sample is of very low intensity across the whole emission region λ_{em}=500-600 nm. Therefore it is conceivable that the tail of the trimer emission spectrum is making a significant contribution to the fluorescence observed in this wavelength range.

9.3.2.2. Higher Polymer *vs.* Lower Polymer

The SS emission spectra of the HP and LP samples (figure 9.4) show a marked difference in intensity, but from the SS spectra alone nothing can be deduced about the nature of the emitting species within each sample. The parameters obtained for the decays of each sample at λ_{em}=550 and 600 nm are presented for comparison in tables 9.4 and 9.5.

Global lifetime / ns	τ_1 7.50	τ_2 2.90	τ_3 0.60	τ_4 0.07	χ^2_g 1.23
λ_{em} / nm	A_1 %	A_2 %	A_3 %	A_4 %	χ^2
550	0.04 28	0.21 58	0.15 8.4	0.61 4.1	1.21
600	0.03 18	0.24 67	0.19 11	0.55 3.6	1.24

Table 9.4: *Global lifetimes, A-factors (as a fraction of 1), contribution to SS fluorescence emission and global χ^2 for HP, λ_{em} range 550-600 nm.*

Global lifetime / ns	τ_1 5.70	τ_2 3.00	τ_3 0.80	χ^2_g 1.29
λ_{em} / nm	A_1 %	A_2 %	A_3 %	χ^2
550	0.29 52	0.44 41	0.27 6.8	1.32
600	0.30 53	0.46 42	0.23 5.6	1.29

Table 9.5: *Global lifetimes, A-factors (as a fraction of 1), contribution to SS fluorescence emission and global χ^2 for LP, λ_{em} range 550-600 nm*

In contrast to the decays obtained for the HP sample, which fit globally to 4 lifetimes, the decays of the LP sample fitted to 3 global lifetimes across the region λ_{em}=550-600 nm. The most striking observation is the absence of the very short, sub-100 ps component in the LP sample. This indicates that the HP component with the 70 ps

lifetime is characteristic of longer chain polymer in which there is a high probability of NR decay by energy transfer from this relatively short conjugation length species to longer conjugation lengths in the polymer chain; there is no such species in the LP sample.

The HP and LP samples appear to have two common lifetimes; τ_2=3.0±0.1 ns and τ_3=700±100 ps. The contributions of these components to the emitting population are significant for both of the samples, 22±2% and 17±2% (τ_2 and τ_3 respectively) for HP and 43±1% and 25±2% (τ_2 and τ_3 respectively) for LP. It is likely that these are components of similar conjugation length in each sample.

The long lifetime, τ_1, differs between the HP and LP samples, 7.5 ns and 5.7 ns respectively, because the HP sample contains a higher proportion of longer conjugated species than the LP sample. The LP 5.7 ns lifetime can be attributed to the trimer, of which a very small amount contributes to the emitting population at these wavelengths, whereas the HP sample 7.5 ns lifetime is an average of the small amount of trimer and low-abundance long conjugation lengths of polymer. The longest conjugation lengths of polymer have longer lifetimes than shorter conjugation lengths.

9.3.3. Poly-5-bromoindole *vs.* poly-5-cyanoindole

9.3.3.1. Higher Polymer Samples

The lifetimes obtained for the fitting of the decays obtained at λ_{ex}=450 nm for the HP samples of the poly-5-BrI on pol-5NI and poly-5-CnI samples are compared in table 9.6.

Global τ / ns 5BrI 5CnI	τ_1 7.50 4.80	τ_2 2.90 1.51	τ_3 0.60 0.14	τ_4 0.07 -	χ^2_g 1.23 1.38
λ_{em} / nm	A_1 %	A_2 %	A_3 %	A_4 %	χ^2
560 5BrI	0.04 25	0.22 62	0.15 8.5	0.60 3.9	1.22
5CnI	0.14 64	0.18 26	0.68 9.5	- -	1.46
600 5BrI	0.03 18	0.24 67	0.19 11	0.55 3.6	1.24
5CnI	0.16 61	0.29 33	0.55 6.0	- -	1.34

Table 9.6: *Lifetimes obtained for the HP samples of poly-5-bromoindole and poly-5-cyanoindole.* λ_{ex}*=450 nm,* λ_{em}*=550 nm.*

The most apparent difference between the HP poly-5BrI and poly-5CnI samples is that the poly-5CnI sample lacks the characteristically polymeric 70 ps component that is dominant in the poly-5BrI HP sample when exciting at λ_{ex}=450 nm. This is evidence of the greater extent of polymerisation in the 5BrI than the 5CnI sample, and hence greater efficiencies of NR decay by energy transfer to longer conjugation lengths. Additionally, the poly-5CnI has significant contribution from the trimer emission, indicating that in this system there is less linkage of trimer units.

9.4. Excitation at λ_{ex}=360 nm

9.4.1. Higher Polymer sample, emission region λ_{em}=560-650 nm

The emission from the trimer is evident, the characteristic double peaks being seen at λ_{em}=400-450 nm. Additionally, between λ_{em}=500-700 nm a broad peak resulting from emission from conjugated polymeric species, which is of higher intensity than the trimer emission, is observed. Between 450 nm and 500 nm, it is evident that there is overlap between the trimer and the polymer emission.

9.4.1.1. Results

The fluorescence spectrum acquired upon exciting the HP sample using λ_{ex}=360 nm (figure 9.8) results in an emission profile originating from all the fluorophores present.

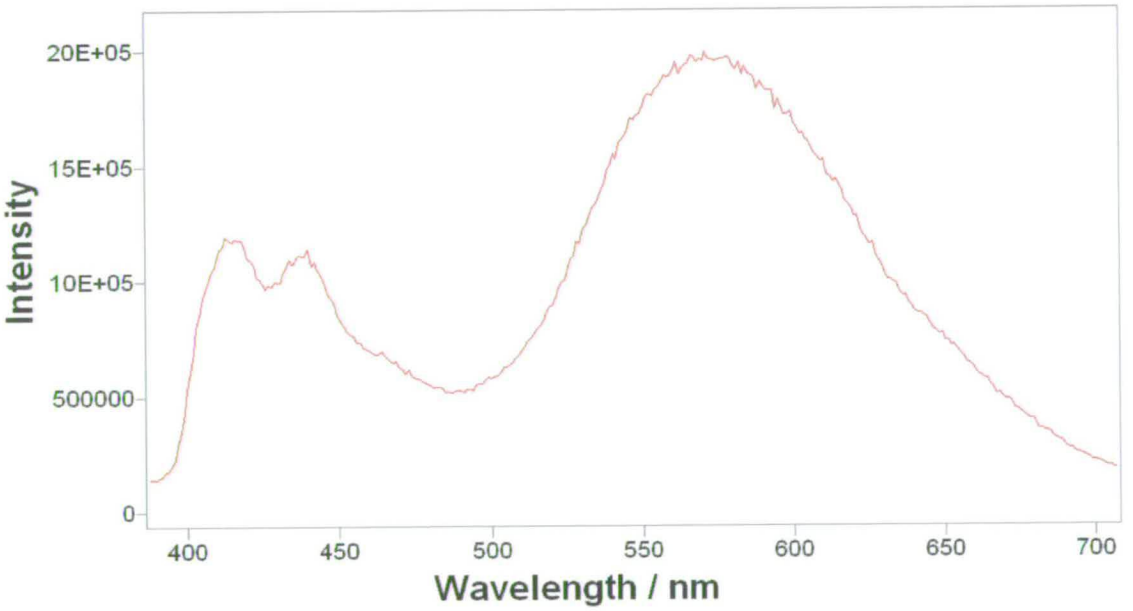

Figure 9.8: *Fluorescence emission spectrum of 5BrI HP sample, λ_{ex}=360 nm.*

Decays were recorded across the emission region λ_{em}=560-650 nm and the lifetimes were determined (table 9.7). All the decays in this emission region fitted to one set of 4 global lifetimes.

Global lifetime / ns	τ_1 **5.00**	τ_2 **2.14**	τ_3 **0.35**	τ_4 **0.06**	χ^2_g **1.39**
λ_{em} / nm	A_1 $\%_1$	A_2 $\%_2$	A_3 $\%_3$	A_4 $\%_4$	χ^2
560	0.05 40	0.12 42	0.21 12	0.61 6	1.50
570	0.05 39	0.14 44	0.22 12	0.59 5	1.37
580	0.05 38	0.15 46	0.22 11	0.58 5	1.21
600	0.05 35	0.16 49	0.21 11	0.59 5	1.30
650	0.04 30	0.15 53	0.19 11	0.62 6	1.57

Table 9.7: *Lifetimes, A-factors (as a fraction of 1), contribution to SS fluorescence emission and global χ^2 for HP, λ_{em} range 560-650 nm. χ^2 values comparable with those obtained for individual fits, within experimental error.*

The 4 lifetimes obtained span almost 2 orders of magnitude: τ_1=5.0±0.1 ns; τ_2=2.1±0.1 ns; τ_3=350±10 ps; τ_4=60±10 ps. All four components remain constant in terms of A-factor over the whole emission region, indicating that they do not differ significantly in their emission spectra. The major contributor to the initial excited population is the component that emits with a lifetime of 60 ps (0.60±0.02 at all λ_{em}).

The component with the longest lifetime, 5.0 ns, constitutes the least of the emitting species at these wavelengths, at 0.05±0.01. The components giving rise to the lifetimes τ_2=2.1 ns and τ_3=0.4 ns make up 0.14±0.0% and 0.20±0.02 of the initial excited population respectively. The majority of the intensity in the SS emission comes from the 5.0 ns and 2.1 ns components, 35±5% and 45±8% respectively.

9.4.1.2. Discussion

Comparison of the decay parameters obtained at the two different excitation wavelengths, 360 nm and 450 nm, will reveal whether different populations of emitting species are produced at the different excitation wavelengths. The lifetimes for both excitation wavelengths are presented in table 9.8.

	τ_1 / ns	τ_2 / ns	τ_3 / ns	τ_4 / ns
λ_{ex}=450 nm	7.50	2.91	0.58	0.07
λ_{ex}=360 nm	5.00	2.14	0.35	0.06
λ_{em} / nm	**A_1** **$\%_1$**	**A_2** **$\%_2$**	**A_3** **$\%_3$**	**A_4** **$\%_4$**
560	0.04	0.22	0.15	0.59
λ_{ex}=450 nm	25.46	62.07	8.33	3.94
	0.05	0.12	0.21	0.61
λ_{ex}=360 nm	40.44	41.77	11.97	5.81
600	0.03	0.24	0.19	0.55
λ_{ex}=450 nm	18.43	67.47	10.51	3.59
	0.05	0.16	0.21	0.59
λ_{ex}=360 nm	35.25	49.12	10.52	5.11

Table 9.8: *Lifetimes, A-factors and % contribution to SS emission obtained in the global emission region λ_{em}=560-600 nm for 5BrI HP sample, λ_{ex}=450 nm and λ_{ex}=360 nm.*

The lifetime values of the components τ_2-τ_4 are very similar at the two excitation wavelengths, indicating that these are emitting species of a similar type. The A-factors for these species are comparable, with the sub-100 ps component being the greatest contributor to the emitting population in this emission region for both excitation wavelengths.

The most noticeable difference between the lifetimes obtained at the two excitation wavelengths is in the value of the longest lifetime, τ_1. Exciting at λ_{ex}=450 nm, τ_1=7.50 ns, whereas using λ_{ex}=360 nm, at 5.0 ns, the lifetime is considerably shorter. The 5ns component obtained when exciting at 360 nm is similar to the value of the trimer lifetime; however, its contribution to the SS emission intensity is 40%. Examination of the emission spectrum, figure 9.8, shows that it is not possible that 40% of the emission intensity at 560 nm comes from trimer emission. Therefore this decay lifetime must be associated with a longer conjugation length species. The longest decay time can be attributed to a distribution of the lowest energy, longest conjugation length emitting species, for which the probability of energy transfer is the lowest.

Using λ_{ex}=450 nm the lower energy species are excited directly. However λ_{ex}=360 nm excites all the fluorophores within the sample, therefore the lower energy, longer conjugated species may become excited indirectly, via energy transfer from higher energy excited species, which could lead to differences in the population of the excited state.

9.4.2. Lower Polymer Sample

9.4.2.1. Results

The emission spectrum of the LP sample, when excited at λ_{ex}=360 nm, shows high intensity emission in the trimer region (λ_{em}=400-500 nm) compared to the emission arising from the longer conjugation length fluorophores (λ_{em}>500 nm) (figure 9.10; *cf.* HP sample, λ_{ex}=360 nm, figure 9.8). Nevertheless, there is some emission apparent at λ_{em}>500 nm.

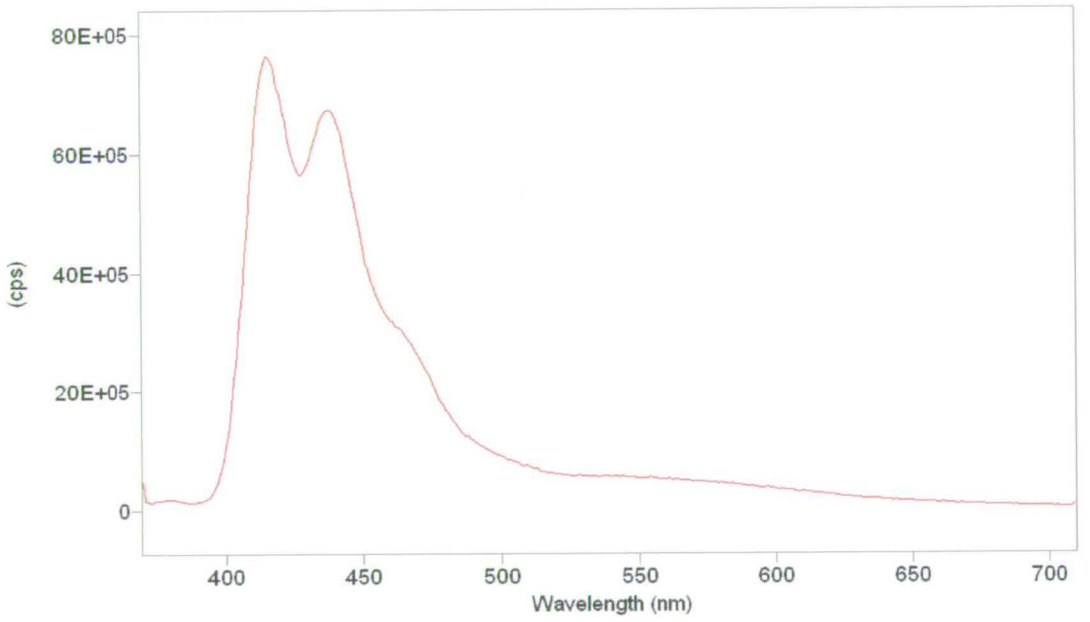

Figure 9.10: *SS fluorescence emission of LP sample at λ_{ex}=360 nm*

Decays were recorded at emission wavelengths of 550 nm and 600 nm and fitted globally to one set of 4 lifetimes (table 9.9), τ_1=6.4±0.1 nm, 3.1±0.1 ns, 0.9±0.05 ns and 0.3±0.05 ns.

Global lifetime / ns	τ_1 6.43	τ_2 3.12	τ_3 0.92	τ_4 0.26	χ^2_g
λ_{em} / nm	A_1 $\%_1$	A_2 $\%_2$	A_3 $\%_3$	A_4 $\%_4$	χ^2
550	0.04 22	0.18 47	0.26 20	0.51 11	1.30
600	0.06 24	0.30 56	0.26 14	0.38 6	1.31

Table 9.9: *Lifetimes, A-factors (as a fraction of 1), contribution to SS fluorescence emission and global χ^2 for LP, λ_{ex} λ_{em} range 550-600 nm. χ^2 values are comparable to individual fitting.*

In contrast with the HP sample, there is no sub-100 picosecond component. The component that constitutes the majority of the initial excited population is the τ_4=0.3 ns component, 0.51 at 550 nm decreasing to 0.38 at 600 nm. The τ_1=6.4 ns component constitutes the least of the excited population at these wavelengths, 0.05 but, owing to its high quantum yield, still makes a significant contribution to the SS emission (~23%).

The greatest contributor to the SS emission is the τ_2=3.1ns component, 46% at 550 nm rising to 56% at 600 nm. This component constitutes a considerable proportion of the initial excited state population, 0.18 at 550 nm, increasing to 0.30 at 600 nm, as does the 0.9 ns component, 0.26 at both wavelengths.

9.4.2.2. Discussion

Although the LP sample was synthesised to minimize the proportion of linkage within the film, the SS emission spectrum (9.10) shows definite evidence of emission from polymeric species at longer λ_{em}. The major contributor to the excited state population is the species that has the lifetime 0.3 ns. Its contribution decreases significantly as the emission wavelength increases, indicating that it is a component of relatively short conjugation length. This is very likely to be the tail of the quenched trimer emission. The τ_2=3.1 ns component increases in terms of proportion of the excited state population as λ_{em} increases, therefore it is a species of longer conjugation length than the 0.3 ns component. The τ_1=6.4 ns component, which constitutes only 0.05±0.01 of the initial excited species at these wavelengths is likely to be attributable to an average between the free trimer lifetime and some conjugated species with a lifetime similar to that of the free trimer. This is comparable with the 5 ns component obtained for the HP sample at this excitation wavelength.

9.4.2.3. Comparison between HP and LP

Global lifetime / ns	τ_1 5.00	τ_2 2.14	τ_3 0.35	τ_4 0.06	χ^2_g 1.39
λ_{em} / nm	A_1 $\%_1$	A_2 $\%_2$	A_3 $\%_3$	A_4 $\%_4$	χ^2
560	0.05 40	0.12 42	0.21 12	0.61 6	1.50
600	0.05 35	0.16 49	0.21 11	0.59 5	1.30

Figure 9.10: *Lifetimes, A-factors and % contribution to the SS emission for HP sample, λ_{ex}=360 nm, λ_{em}=560, 600 nm*

Global lifetime / ns	τ_1 6.43	τ_2 3.12	τ_3 0.92	τ_4 0.26	χ^2_g
λ_{em} / nm	A_1 $\%_1$	A_2 $\%_2$	A_3 $\%_3$	A_4 $\%_4$	χ^2
550	0.04 22	0.18 47	0.26 20	0.51 11	1.30
600	0.06 27	0.30 56	0.26 14	0.38 6	1.31

Figure 9.11 *Lifetimes, A-factors and % contribution to the SS emission for LP sample, λ_{ex}=360 nm, λ_{em}=550, 600 nm*

The striking difference between the HP and LP samples at λ_{ex}=360 nm, λ_{em}>550 nm, is the same as that observed between the samples using λ_{ex}=450 nm, which is the absence of the very short, sub-picosecond component in the LP sample. This verifies that this

very short lifetime, long wavelength component is characteristic of more extensive polymerisation.

9.4.2.4. Comparison between poly-5BrI HP and poly-5CnI HP

The lifetimes obtained for the long wavelength emission of the poly-5BrI and poly-5CnI HP samples at λ_{ex}=360 nm are presented in table 9.12.

Global τ / ns	τ_1 A_1 %	τ_2 A_2 %	τ_3 A_3 %	τ_4 A_4 %
5BrI	5.00 0.05 40	2.14 0.12 42	0.35 0.21 12	0.06 0.61 6
5CnI	5.90 0.61 89	2.48 0.16 10	0.23 0.23 1	- - -

Figure 9.12: *Lifetimes, A-factors and % contributions to the SS emission for HP poly-5BrI and poly-5CnI samples at λ_{ex}=360 nm. For poly-5BrI λ_{em}=560 nm, for poly-5CnI λ_{em}=550 nm.*

As was the case using λ_{ex}=450 nm, the major difference between the 5BrI and 5CnI samples is the absence of the polymeric sub-100 ps-lifetime component for the 5CnI sample that is dominant at these wavelengths for the 5BrI sample. The τ_2 and τ_3 components are similar for both samples, which is consistent with their being due to similar relatively long conjugation length that are present in both polymer systems. The dominant emitting species in the poly-5CnI is the free trimer, whereas this is negligible in poly-5BrI.

9.4.3. Emission region λ_{em}=400-500 nm

To examine the shorter conjugation length species, it is necessary to investigate emission from the samples at the shorter emission wavelength region of the spectra. The HP and LP samples both emit in the region λ_{em}=400-500 nm, but have markedly different emission profiles (figure 9.11).

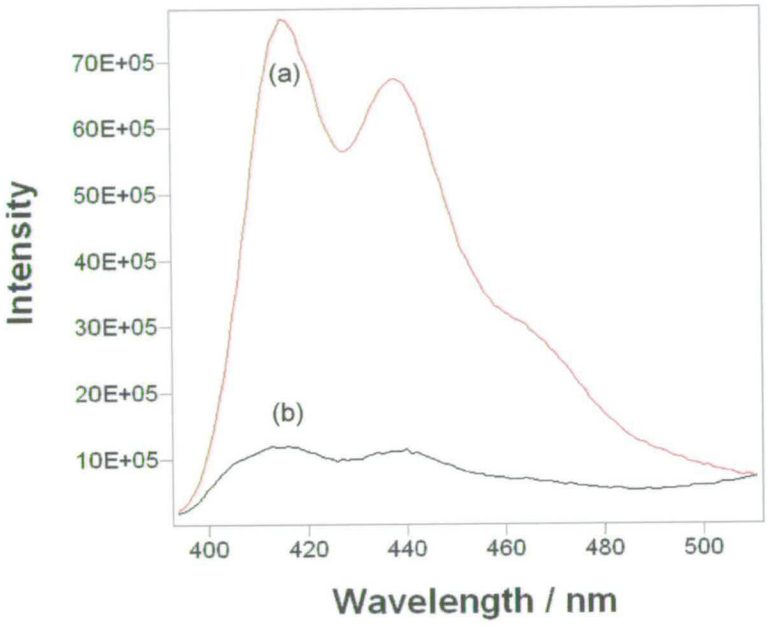

Figure 9.11: *SS emission spectra of samples, λ_{ex}=360 nm. (a) LP, (b) HP*

Between λ_{em}=400-450 nm, the emission of the LP sample is of significantly higher intensity than that of the HP sample, and tails off at longer wavelengths (>450 nm), whereas the HP emission intensity increases at these longer emission wavelengths. The HP polymer emission appears to have considerable overlap with the trimer emission,

causing the trimer peaks to be flatter and less well defined than in the LP sample, which has the classic trimer emission profile.

9.4.3.1. Higher Polymer Sample

The HP sample exhibits relatively low intensity emission in the trimer region, λ_{em}=400-500 nm (figure 9.12), compared to the longer emission wavelength region, λ_{em}>500 nm (figure 9.8).

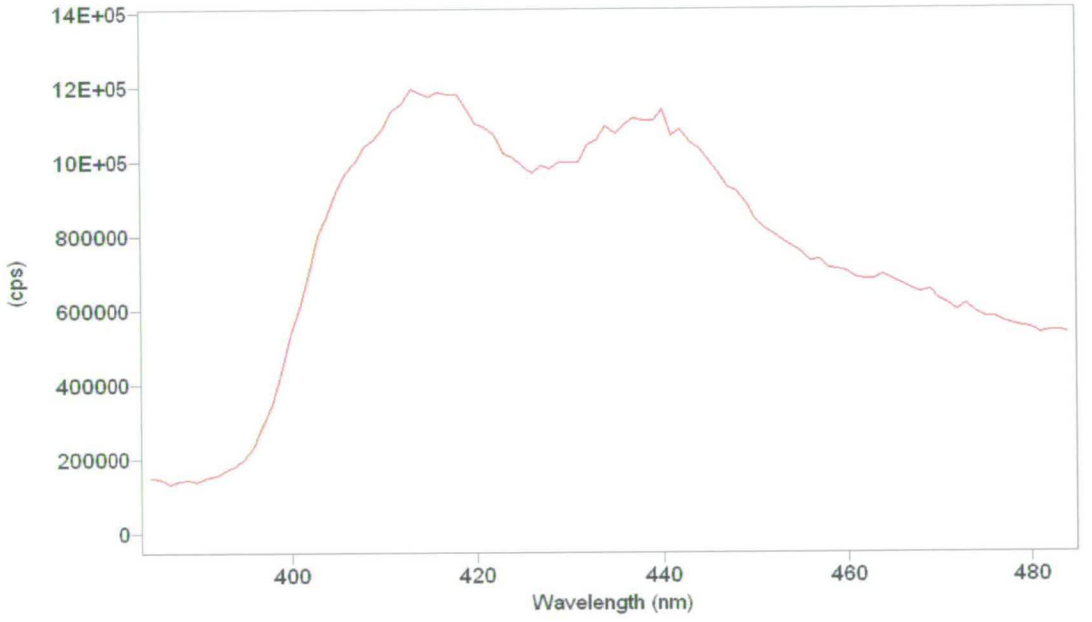

Figure 9.12: *Emission spectrum of the HP sample, λ_{ex}=360 nm, trimer emission region*

Decays were recorded at λ_{em}=435 nm and 453 nm and fitted globally to four lifetimes (table 9.13).

Global lifetime / ns	τ_1	τ_2	τ_3	τ_4	χ^2_g
	7.15	1.73	0.25	0.07	1.29
λ_{em} / nm	A_1 $\%_1$	A_2 $\%_2$	A_3 $\%_3$	A_4 $\%_4$	χ^2
435	0.02	0.04	0.36	0.59	1.36
	32	24	29	15	
453	0.02	0.06	0.38	0.55	1.26
	36	27	26	11	

Table 9.13: *Lifetimes, A-factors (as a fraction of 1), contribution to SS fluorescence emission and global χ^2 for HP, λ_{em} range 435-460 nm. χ^2 values comparable with individual fits*

The global set of lifetimes obtained comprises τ_1=7.2±0.1 ns, τ_2=1.7±0.1 ns, τ_3=250±10 ps and τ_4=70±10 ps. The initial excited state population consists of predominantly the τ_4=70 ps and τ_3=250 ps components. The 70 ps component constitutes 0.59 at 435 nm and 0.55 at 453 nm, and the 250 ps component 0.36 at 435 nm and 0.38 at 453 nm. The two longest components τ_1=7.2 ns and τ_2=1.7 ns, constitute less than 0.10 of the initial excited population altogether, the 7.1 ns component constituting 0.02 of the emitting population at both emission wavelengths and the 1.7 ns component constituting 0.04 at 435 nm and 0.06 at 453 nm.

In this sample the emission in this wavelength region is a combination of that from the trimer fluorophore and that from the short wavelength emission, short conjugation length polymer species. The 70 ps decay time has already been found to be characteristic of a short conjugation length polymer species, and its observation here is consistent with that definition. The 250 ps lifetime is similar in magnitude to that

identified previously (chapter 8) as being due to a highly quenched intrachain trimer fluorophore.

9.4.3.2. Lower Polymer sample Results and Discussion

The SS emission spectrum of the LP sample when exciting at λ_{ex}=360 nm shows relatively intense emission in the trimer region, λ_{em}=400-500 nm (figure 9.13).

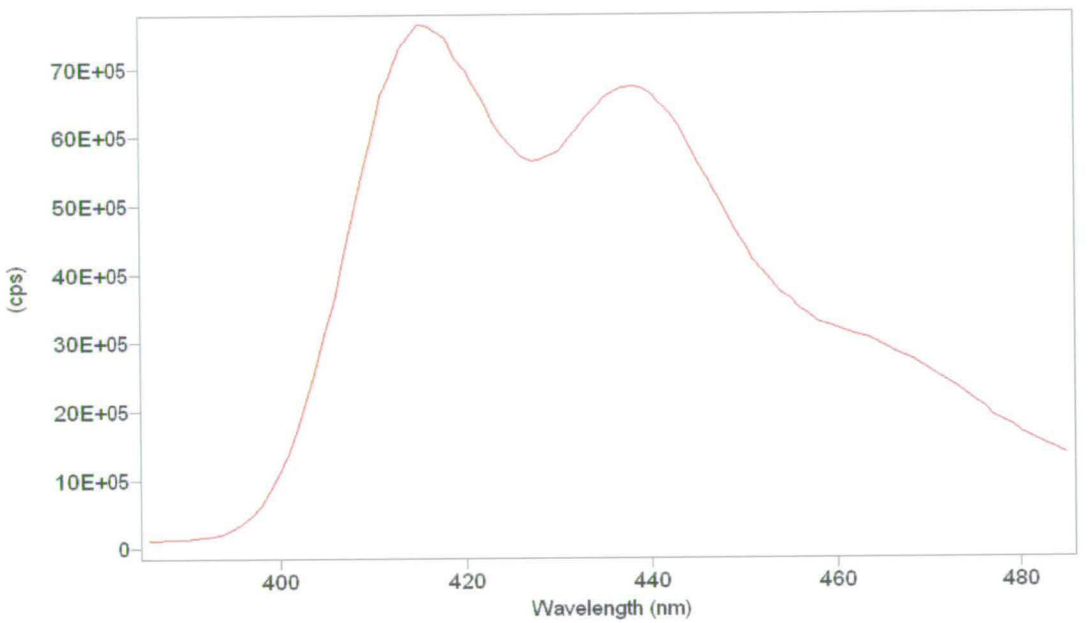

Figure 9.13: *Emission spectrum of the HP sample, λ_{ex}=360 nm, trimer emission region*

Fluorescence decays were recorded at λ_{em}=435 nm and 453 nm, and were found to fit globally to one set comprising four lifetimes (table 9.14). The lifetimes obtained are τ_1=4.9±0.1 ns, τ_2=1.2±0.1 ns, τ_3=230±10 ps and τ_4=70±10 ps. The major constituent of the initial excited state population is the component τ_3=230 ps, 0.83 at 435 nm and 0.81 at 453 nm.

Global lifetime / ns	τ_1	τ_2	τ_3	τ_4	χ^2_g
	4.89	1.17	0.23	0.07	1.09
λ_{em} / nm	A_1 $\%_1$	A_2 $\%_2$	A_3 $\%_3$	A_4 $\%_4$	χ^2
435	0.01	0.02	0.83	0.15	1.02
	12.93	8.03	75.08	3.96	1.09
453	0.01	0.03	0.81	0.18	1.15
	14.76	12.46	67.99	4.79	1.13

Table 9.14: *Lifetimes, A-factors (as a fraction of 1), contribution to SS fluorescence emission and global χ^2 for LP, λ_{em} range 435-453 nm*

The τ_4=70 ps component constitutes the next highest proportion of the excited state population, 0.15 at 435 nm and 0.18 at 453 nm. The τ_1=4.9 ns component contributes only 0.01 to the excited state population at both wavelengths, and the τ_2=1.2 ns component contributes 0.02 at 435 nm and 0.03 at 453 nm. The majority of what is seen in the SS emission spectrum is the τ_3=230 ps component, 0.75 at 435 nm and 0.68 at 453 nm.

The emission in this region is primarily due to the trimer. The τ_3=230 ps component, which makes up 0.82±0.01 of the excited state population and contributes 70±5% to what is seen in the SS emission, is due to the quenched intrachain trimer species, as previously observed in chapter 8. Similarly, the τ_4=70 ps component is due to a short conjugation length polymer species. Emission from this species makes a negligible contribution (<5%) to the observed fluorescence spectrum.

There appears to be no lifetime corresponding to that of the free trimer, the longest lifetime obtained being 4.9 ns. However, the τ_1=4.9 ns component (and the τ_2=1.2 ns component) constitute a very small proportion of the emitting population (3-4% together). Considering again the fact that each lifetime is unlikely to be representative of a single emitting species, but rather an average of a distribution of components, it is possible that the free trimer is present in a small proportion, the measured lifetime having been skewed by other components of similar lifetime.

9.4.3.3. Comparison between Higher Polymer and Lower Polymer samples

The lifetimes obtained for the HP and LP poly-5BrI samples at λ_{ex}=360 nm, λ_{em}=435 nm, are presented in table 9.15

	τ_1 / ns	τ_2 / ns	τ_3 / ns	τ_4 / ns
HP	7.15	1.73	0.25	0.07
LP	4.89	1.17	0.23	0.07
λ_{em} / nm	A_1	A_2	A_3	A_4
	$\%_1$	$\%_2$	$\%_3$	$\%_4$
435 HP	0.02	0.04	0.36	0.59
	32	24	29	15
LP	0.01	0.02	0.83	0.15
	13	8	75	4
453 HP	0.02	0.06	0.38	0.55
	36	27	26	11
LP	0.01	0.03	0.81	0.18
	15	12	68	5

Table 9.15: *Lifetimes, A-factors and % contribution to SS emission obtained poly-5BrI HP and LP samples.* λ_{ex}*=360 nm and* λ_{ex}*=435-453 nm.*

The most significant difference between the HP and the LP sample at this excitation wavelength is in the proportion of the two shortest lifetimes species in each sample. The 70 ps short conjugation length species is predominant in the HP sample, but constitutes only about 0.2 of the excited state population in the LP sample. The intrachain trimer moiety with the lifetime of ~250 ps dominates in the LP sample, where it constitutes approximately 0.8 of the excited state population, but is much less significant in the HP sample.

9.4.3.4. Comparison with λ_{ex}=360 nm, λ_{em}=435-453 nm, poly-5CnI

The poly-5CnI sample exhibited only one lifetime at the stated wavelengths, which was attributable to the free trimer. The longest lifetime of the HP and LP samples are not due to the free trimer, but are likely to be averages of the free trimer and the lifetimes of other short conjugation length species. The longest lifetime species in both HP and LP represents less than 0.05 of the excited state population; in both cases the short-lived species are dominant.

9.5. Conclusions

The work presented in this chapter has allowed the identification of different polymeric emitting species, and determination of their characteristic lifetimes. These are as follows. The 70 ps component is a short conjugation length species in a relatively long polymer chain, the 200-300 ps component is an intrachain trimer. These species both have very efficient non-radiative energy transfer pathways. The 5.7 ns component is free trimer. The components with lifetimes in the range 0.4 to 3 ns are due to relatively long conjugation length, long emission wavelength species in a range of polymer environments. The 5-8 ns lifetime is a relatively short conjugation length, short emission wavelength species, present as free oligomers or in short polymer chains. Following from this the differences in composition of the emitting species in the LP and HP samples was established.

The effects of polymer environment on the lifetime of a particular conjugation length was observed. Short conjugation length species, which have similar excitation energies, are seen in the short emission wavelength region with rather different lifetimes, indicating the existence of species in different polymer environments. A short conjugation length existing as a short oligomer, when it constitutes all or a large fraction of the total polymer chain length, will have a long lifetime, which is comparable to that of the free trimer chromophore. In contrast, the same conjugation length in a long chain polymer, where there is efficient non-radiative decay by energy transfer to longer chain length segments will have a much shorter lifetime.

9.6. References

1. I.D.W. Samuel, G. Rumbles and C.J. Collison, *Am Phys. Soc. Phys Rev. B, Rapid Comm.*, 1995, **52(16)**, 573-576
2. B.J. Schwartz, *Annual Review of Phys. Chem.*, 2003, 141-172
3. I.D.W. Samuel, G. Rumbles, C.J. Collison, R.H. Friend, S.C. Moratti and A.B. Holmes, *Synthetic Metals*, 1997, **84**, 497-500
4. L. Magnani, G. Rumbles, I.D.W. Samuel, K. murray, S.C. Moratti, A.B. Holmes, R.H. Friend, *Synth. Met.*, 1997, **84**, 899
5. J.G. Mackintosh and A.R. Mount, *J. Chem. Soc. Faraday Trans.*, 1994, **90(8)**, 1121-1125
6. J.G. Mackintosh, C.R. Redpath, A.C. Jones, P.R.R. Langridge-Smith, D.R. Reed, A.R. Mount, J. *Electroanal. Chem.*, 1994, **375**, 163
7. J.G. Mackintosh, A.R. Mount, D. Reed, *Magn. Reson. Chem.*, 1994, **32**, 559
8. J.G. Mackintosh, C.R. Redpath, A.C. Jones, P.R.R. Langridge-Smith, A.R. Mount, *J. Electroanal. Chem*, 1995, **388**, 179
9. J.G. Mackintosh, *PhD Thesis*, 1995, The University of Edinburgh
10. A.D. Thomson, *PhD Thesis*, 1997, The University of Edinburgh
11. M. Robertson, *PhD Thesis*, 1998, The University of Edinburgh
12. P. Jennings, *PhD Thesis*, 2000, The University of Edinburgh
13. P. Jennings, A.C. Jones, A.R. Mount and A.D. Thomson, *J. Chem. Soc., Faraday Trans.*, 1997, **93(21)**, 3791-3797
14. P. Jennings, A.C. Jones, A.R. Mount, *J. Chem. Soc., Faraday Trans.*, 1998, **94**, 3619-3624

Chapter 10

Conclusions

This thesis presented a comprehensive investigation into the fluorescence properties of electropolymerised 5-bromodindole (5BrI) and 5-cyanoindole (5CnI) in ethanol. The fluorescence studies carried out on each system, in particular poly-5-BrI, gave useful insight into the phenomenon of intra-chain species. For the first time, preparation of a sample of pure 5-BrI asymmetric trimer was accomplished. The fluorescence lifetime of this free 5BrI trimer was determined to be 5.5 ns, whilst that of the 5CnI trimer was found to be 5.8 ns. In addition to these free trimer species, the electropolymerised samples were found to contain other trimer species, which were, in each system, spectroscopically identical to the free trimer but possessed much shorter fluorescence lifetimes. Additionally, longer conjugated polymeric species were observed.

For short wavelength excitation (360 nm) of the poly-5CnI samples, the free trimer was found to be the major emitting species for both the higher polymer (HP) and lower polymer (LP) samples at all emission wavelengths. Components attributed to conjugated polymers were observed to have shorter lifetimes that the free trimer, indicating efficient non-radiative (NR) decay pathways. Excitation of the poly-5CnI HP and LP samples at longer wavelength, 450 nm, resulted in emission that is characteristic of lower excitation energy polymer species, the HP emission being significantly more intense than the LP emission. For both samples, a distribution of lifetimes, averaging to 3 distinct polymer lifetimes, was observed. The polymer species with the dominant

contribution to the emitting population had the shortest decay time, 130±10 ps, and appeared to have a relatively short conjugation length, indicating that a major channel for non-radiative decay is intramolecular energy transfer to surrounding, longer conjugation length, lower excitation energy segments of polymer.

Of the two samples, poly-5BrI and poly-CnI, poly-5BrI showed much more intense emission from longer conjugation length species than poly-5-CnI, revealing much information about the different types of emitting conjugated species, including intra-chain components. It was concluded that there were several types of emitting species observed in the poly-5BrI systems: Two species with very efficient non-radiative energy transfer pathways, namely, the 70 ps component, which is a short conjugation length species in a relatively long polymer chain, and the 200-300 ps component, which is an intra-chain trimer; the 5.5-5.7 ns component, which is due to free trimer molecules; components with lifetimes in the range 0.4-3 ns; which are thought to be due to relatively long conjugation length, long emission wavelength species in a range of polymer environments; the 5-8 ns lifetime species correspond to relatively short conjugation length, short emission wavelength species, which are present as free oligomers or in short polymer chains.

In addition to the determination of its fluorescence properties, the potentiometric study of poly-5CnI as a pH sensor was carried out. Thick (1.37 μm) and thin (0.49 μm) poly-5CnI films were both found to have a linear potential response to changes in electrolyte

pH, with a Nernstian gradient of -59 $mVpH^{-1}$, which was found to be reproducible and sustainable over a time scale of at least a week. The thin film displayed relatively rapid protonation and deprotonation in response to pH change. When switching from the acid to the neutral electrolyte, quantitative characterisation showed the response to be consistent with a simple coat deprotonation reaction with relatively fast kinetics. It was determined that ~10% of the potential protonation sites in the coat were involved. When switching from the neutral to the acid electrolyte there is extra proton ingress into the coat and there is a marked change in the j/t transient consistent with the presence of carbonate buffer in the coat.

The thick film exhibited increasing coat effects with increasing rotation speed. For the acid to neutral transfer it was found that the quantitative analysis that was successful for the thin film acid to neutral transfer held true at the low rotation speed of W=1 Hz. For this case, the number of protonatable sites obtained for the thick film was 3 times that of the thin film.

In all the cases studied the response is of the order of seconds. The pH response is comparable to that previously observed for polypyrrole for these film thicknesses, but unlike polypyrrole appears to originate from direct coat protonation and deprotonation.

Thus, to conclude, this thesis has shown that the analysis of the fluorescence lifetimes of the samples, particularly the electropolymerised 5-BrI system, proved to be insightful to the understanding of the effects intrachain energy transfer, through the observation that a particular conjugation length species will fluoresce with different lifetimes depending on its situation within a longer polymer strand. Additionally, the extent of polymerisation in the 5BrI system was shown to be greater than that in the 5CnI system. It was also shown that poly-5CnI has potential as a practical pH sensor.

Appendix 1

Fitting Multiple Exponential Decays

As mentioned throughout this thesis, the fitting of exponentials to the fluorescence decays had to be executed with care. Fitting began with the smallest number of exponentials possible, more being added as necessary. Outlined in this section is a brief illustration of the fitting process for multiple-exponential decays.

Poly-5CnI HP sample, λ_{ex} = 360 nm, λ_{em} = 550 nm (presented in chapter 6).

Usually the fitting procedure is started by attempting to fit the decay to one exponential. However, in this case the fitting programme did not find a suitable fit using one exponential; hence two lifetimes was the smallest number used. Lifetimes of 5.7 ns and 1 ns were obtained, but the fit was poor. This is indicated by the high χ^2 value (2.2) and the non-random residuals at the start of the fit. Adding a third exponential so that three lifetimes are obtained (5.9 ns, 2.5 ns and 0.2 ns) improves the χ^2 value (1.0) and randomises the residuals. The results of the fittings are presented in figure A1. It may be argued that this is an artificial improvement on the basis that a χ^2 value of 1.0 is too good to be real, and adding exponentials always improves fitting; however it can be seen from the results presented in table 6.2 for emission wavelengths 435-50 nm that a χ^2 value of 1.0 was obtained for a single exponential decay, indicating that a similarly good χ^2 can be obtained for the minimal number of exponentials. Additionally an improvement from 2.2 to 1.0 is significant.

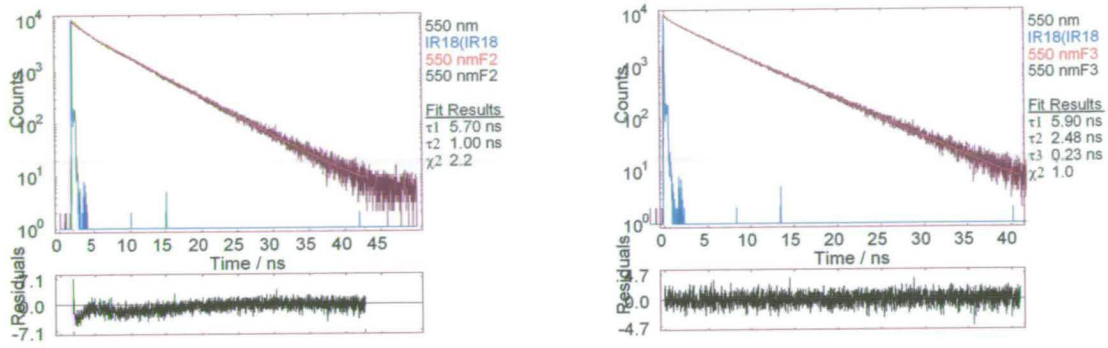

Figure A1: *Fitting HP poly-5CnI decays, recorded at λ_{ex} = 360 nm, λ_{em}=550 nm, to (a) 2 lifetimes and (b) 3 lifetimes.*

Poly-5-BrI on poly-5-NI HP sample, λ_{ex} = 450 nm, λ_{em} = 500 - 600 nm (presented in chapter 9).

Similarly the improvement of the fitting of the poly-5-BrI sample, both individually and globally, by adding a fourth exponential is illustrated in table A1 and Figure A2. Initially 1, then 2 exponentials were used, but no results were obtained. Fitting to 3 exponentials gave very poor global (3.8) and individual (2.8 – 3.8) χ^2 values, and non-random residuals especially at the start of the decay. The addition of the fourth exponential yielded a vast improvement in both, the χ^2 values being 1.23 (global) and 1.21 – 1.26 (individual).

	(a) 3 Lifetimes	(b) 4 Lifetimes
	τ_1=7.5 ns τ_2=2.8 ns τ_3=0.17 ns χ^2_g=3.80	τ_1=7.5 ns τ_2=2.9 ns τ_3=0.60 ns τ_4=0.07 ns χ^2_g=1.23
λ_{em} / nm	χ^2	χ^2
500	3.80	1.26
550	2.80	1.21
560	3.10	1.22
570	3.20	1.22
600	3.20	1.24

Table A1: *Fitting HP poly-5BrI on poly-5NI decays, recorded at λ_{ex} = 450 nm, λ_{em}=500 – 600 nm, to (a) 3 lifetimes and (b) 4 lifetimes.*

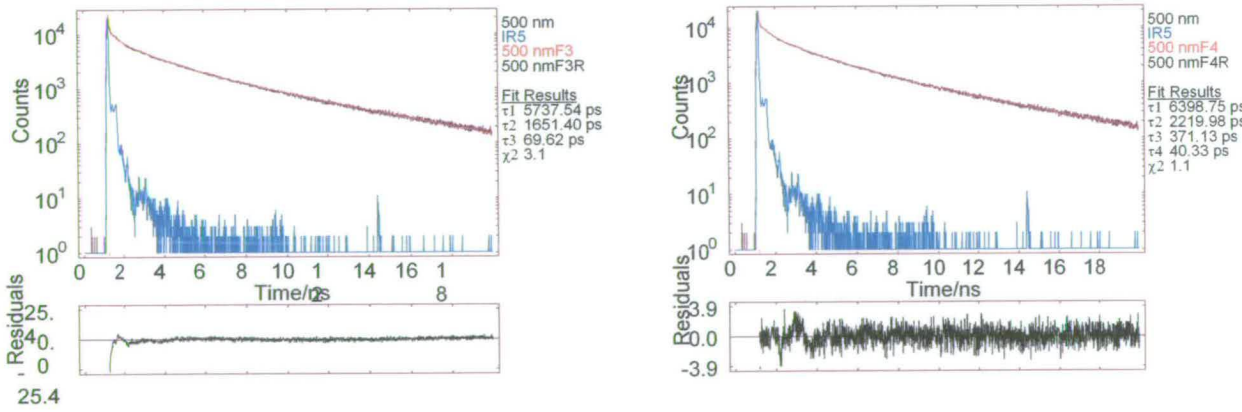

Figure A2: *Fitting HP poly-5BrI on poly-5NI decays, recorded at λ_{ex} = 450 nm, λ_{em}=500 nm, to (a) 2 lifetimes and (b) 3 lifetimes.*